11-8-2012

Switching Patterns and Steady-State Analysis of Grid-Connected and Stand-Alone Single-Stage Boost-Inverters for PV Applications

Mahdi Saghaleini
Florida International University, msagh001@fiu.edu

DOI: 10.25148/etd.FI12121001

FLORIDA INTERNATIONAL UNIVERSITY

Miami, Florida

SWITCHING PATTERNS AND STEADY-STATE ANALYSIS OF GRID-CONNECTED AND STAND-ALONE SINGLE-STAGE BOOST-INVERTERS FOR PV APPLICATIONS

A dissertation submitted in partial fulfillment of

the requirements for the degree of

DOCTOR OF PHILOSOPHY

in

ELECTRICAL ENGINEERING

by

Mahdi Saghaleini

2012

To: Dean Amir Mirmiran
College of Engineering and Computing

This dissertation, written by Mahdi Saghaleini, and entitled Switching Patterns and Steady-State Analysis of Grid-Connected and Stand-Alone Single-Stage Boost-Inverters for PV Applications, having been approved in respect to style and intellectual content, is referred to you for judgment.

We have read this dissertation and recommend that it be approved.

Nezih Pala

Jean Andrian

Wilfrido Moreno

Chris Edrington

Masoud Milani

Kang Yen, Major Professor

Date of Defense: November 8, 2012

The dissertation of Mahdi Saghaleini is approved.

Dean Amir Mirmiran
College of Engineering and Computing

Dean Lakshmi N. Reddi
University Graduate School

Florida International University, 2012

DEDICATION

To my wife Elham, thank you for your love, support, and patience. It has been a long road, but you’ve been with me the whole time. I love you.

To my parents, my sister Mahshad, and my brother Mehrdad, everything that I am, and ever will be is because of you. I love you.

ACKNOWLEDGMENTS

I wish to express my sincere gratitude to my advisor, Dr. Kang Yen, for his guidance, encouragement and support during my graduate studies. His impressive knowledge and human qualities have been a source of inspiration and a model for me to follow.

I'm also grateful to my former advisor, Dr. Behrooz Mirafzal, for his guidance during my graduate studies at FIU. I wish to thank my committee members, Dr. Masoud Milani, Dr. Nezih Pala, Dr. Chris Edrington, Dr. Jean Andrian, and Dr.Wilfrido Moreno, for encouragement and for serving on my advisory committee. At this point, I wish to specifically emphasize my gratitude for all the help and encouragement I received from Dr. Shekhar Bhansali, chairperson of the Electrical and Computer Engineering Department in FIU, whose guidance and help gave me encouragement to proceed with confidence towards the completion of this work.

I would also like to acknowledge FIU students and staff for providing an enjoyable educational atmosphere. Especially, I would like to thank Dr. Ali Kashefi Kaviani for endless discussions and sharing with me his rich practical experience, Mr. Brian Hadley for working with me on the project, and all others who made my work and my stay in FIU more enjoyable. I should also acknowledge the DEA fellowship from the FIU graduate school that helped me to work better on my dissertation.

With much love, I thank my wife Elham for her loving care and unconditional support. This dissertation is her accomplishment as much as it is mine.

ABSTRACT OF THE DISSERTATION

SWITCHING PATTERNS AND STEADY-STATE ANALYSIS OF GRID-CONNECTED AND STAND-ALONE SINGLE-STAGE BOOST-INVERTERS FOR PV APPLICATIONS

by

Mahdi Saghaleini

Florida International University, 2012

Miami, Florida

Professor Kang Yen, Major Professor

Renewable or sustainable energy (SE) sources have attracted the attention of many countries because the power generated is environmentally friendly, and the sources are not subject to the instability of price and availability. This dissertation presents new trends in the DC-AC converters (inverters) used in renewable energy sources, particularly for photovoltaic (PV) energy systems. A review of the existing technologies is performed for both single-phase and three-phase systems, and the pros and cons of the best candidates are investigated.

In many modern energy conversion systems, a DC voltage, which is provided from a SE source or energy storage device, must be boosted and converted to an AC voltage with a fixed amplitude and frequency. A novel switching pattern based on the concept of the conventional space-vector pulse-width-modulated (SVPWM) technique is developed for single-stage, boost-inverters using the topology of current source inverters (CSI). The six main switching states, and two zeros, with three switches conducting at any given instant in conventional SVPWM techniques are modified herein into three

charging states and six discharging states with only two switches conducting at any given instant. The charging states are necessary in order to boost the DC input voltage. It is demonstrated that the CSI topology in conjunction with the developed switching pattern is capable of providing the required residential AC voltage from a low DC voltage of one PV panel at its rated power for both linear and nonlinear loads.

In a micro-grid, the active and reactive power control and consequently voltage regulation is one of the main requirements. Therefore, the capability of the single-stage boost-inverter in controlling the active power and providing the reactive power is investigated. It is demonstrated that the injected active and reactive power can be independently controlled through two modulation indices introduced in the proposed switching algorithm. The system is capable of injecting a desirable level of reactive power, while the maximum power point tracking (MPPT) dictates the desirable active power.

The developed switching pattern is experimentally verified through a laboratory scaled three-phase 200W boost-inverter for both grid-connected and stand-alone cases and the results are presented.

TABLE OF CONTENTS

LIST OF TABLES

LIST OF FIGURES

FIGURE PAGE

CHAPTER 1

INTRODUCTION

This introductory chapter contains four sections. The first section describes the background of the problem. The second section presents a summary of the literature search of the problem. The third section articulates objectives and contributions of this research in advancing a new inverter system for renewable energy systems. Meanwhile, the fourth and final section introduces the general organization of this dissertation.

1.1 Background of the Problem

Since the last decade, the world has encountered a very serious issue that has effects on every aspects of modern life. The energy from the fossil fuels is not a good resource to address all the needs of today's human beings. This is why so much effort has been put forward researching possibilities for substitution energy resources. So far, renewable or sustainable energy (SE) sources have attracted the attention of many countries because the power generated is environmentally friendly, and the sources are not subject to the instability of price and availability that are typical of conventional energy sources such as oil. SE sources make use of high-power and high-speed solid-state technology in order to efficiently convert the energy to useful power and connect to a power network (the grid and/or local loads). For example, solar modules are variable DC voltage sources, and the output voltage of wind generators can be either DC or AC depending on the type of the wind generator. However, regardless of the type of generator, it is also a variable voltage source. In order to make these SE sources useful, especially when considering the generation of a line-frequency AC voltage, a single-stage or multiple-stage power conversion is necessary.

A multiple-stage power conversion system typically involves a DC-DC converter which is used to isolate and/or boost the variable low-voltage input to a constant DC output, and a DC-AC converter (inverter) which produces the sinusoidal output for either the stand-alone or the grid-connected mode of operation. Similar power conversion systems are also required for the energy storage systems often associated with SE sources. To realize the economical and environmental benefits of these SE sources, a significant amount of effort is required to develop novel power electronic circuit topologies as the interfaces between distributed generation units and local loads and/or the grid. In addition, the associated control schemes, as well as prognostic and self-healing control strategies, which will lead to a broad-spectrum of control techniques to accelerate the move towards the so-called smart micro-grid concept [1], are in need of development. In these SE conversion systems, the technical challenges can be categorized into two groups. The first group of concerns is related to the interconnection issues between solid-state power converters and local networks (the grid and local loads). The second group of concerns is related to the power management and power flow in distributed generation systems. These concerns are due to the variable nature of power flow from SE sources, e.g., wind and solar, and the fact that the power generation units are not centralized in these modern power systems.

Power electronic interface circuits are required to perform several important tasks. The first task is to boost the DC input voltage into a desired (rated) voltage level and invert the DC voltage to an AC voltage with a fixed frequency and amplitude. In the case of photovoltaic systems, it is desirable to keep the number of PV panels as low as possible. Thus, the amplitude of the generated DC voltage (e.g., from PV arrays and batteries) will be lower than the grid voltage (in grid-connected cases) or the desirable load voltage (in stand-alone cases). Meanwhile, the power capability of SE sources typically varies due to their natures, e.g., the output voltage of PV arrays vary in a wide range according to various operation conditions such as when there is a lack of incident solar radiation, or even when the face of the panels are dirty or obstructed. The second task is to utilize the maximum available power of the SE sources, i.e., maximum power point tracking (MPPT). Finally, the harmonic contents of the AC voltage and current have to be minimized by installing line filters.

All of the above mentioned tasks should be done by the power electronics interface systems, considering the cost, volume, efficiency, and reliability. There are currently available technologies to address these problems and perform the required tasks. In this dissertation, the use of current-source boost-inverter (CSBI) will be investigated, and its advantages over the other systems will be pointed out. Furthermore, a new switching pattern will be derived and implemented for the CSBI that is capable of doing all of the mentioned tasks in one single stage.

1.2 Literature Search

Voltage-source inverters have been widely used in industrial applications such as variable speed drives, uninterruptible power supplies, and also renewable energy systems. Since they are capable of continuous and linear control of the frequency and fundamental component of the output voltage, they have been extensively used in various industries.

The conventional voltage source inverter (VSI), sometimes referred to as buck inverter, is definitely the most popular and important power converter topology. There is a drawback in the operation of this inverter, and that is the amplitude of the inverter output voltage is always lower than the input dc voltage. This drawback does not allow using VSI alone as the inverter system for many SE sources. However, a couple of solutions have been proposed to tackle this issue [1-26].

A simple way to increase the output voltage of SE sources is to connect a number of them in series and use a conventional voltage source inverter. However, this series configuration has some drawbacks, such as low reliability and low efficiency [1]. In order to find solutions to these technical challenges, several power electronic circuit topologies have been presented in literature [1-12]. In Fig. 1-(a), a step-up transformer is utilized at line-frequency to boost the voltage after the inverter. However, this solution has several disadvantages, such as large size, loud acoustic noise, and relatively high cost. Furthermore, the transformer should be designed for a relatively wide range of power, which leads to a low system efficiency. In Fig. 1-(b), a two-stage circuit topology is used in which a DC-DC converter and an inverter are cascaded. In the first stage, the DC-DC converter boosts and regulates the DC-bus voltage, and in the second stage, the inverter converts the DC voltage into an AC voltage. This topology, in comparison with the topology displayed in Fig. 1-(a), requires two individual control systems and uses one more solid-state switch, as well as an electrolytic capacitor bank at the DC-bus. This will result in a lower reliability and efficiency, as well as a more complicated control scheme. [2].

Three-phase multi-level inverters can also be employed to interface the output of several SE sources to the grid [3]. Although the multi-level inverters are effective for this application, the added complexity of the circuit and the additional components reduce both the overall efficiency and reliability of the system, and may raise the overall cost of the power electronic interface.

Another option is the z-source inverter that can be applied for SE systems. The z-source inverter has the capability of boosting and inverting the DC voltage in a single-stage, with fewer solid-state switches in comparison with multi-level inverters and the above-mentioned two-stage topologies depicted in Fig. 1-(a) and Fig. 1-(b), respectively. As can be seen in Fig. 1-(c) [4], the z-source inverter is a combination of a voltage source inverter and a current source inverter. The z-source inverter contains relatively high input current ripples, which may result in high stresses on the DC-link inductors and capacitors [5]. The application of this topology was reported in [6-8] as a grid-connected single-stage inverter for distributed generation systems, specifically for residential PV systems.

The current source inverter (CSI) topology in conjunction with an appropriate control scheme can form a single-stage boost-inverter that can be used for SE conversion systems. The current source inverter has a DC-link inductor and AC capacitors, as one can observe in Fig. 1-(d). In this dissertation, a switching pattern is introduced for current source inverters in order to boost and invert the DC voltage to a fixed voltage magnitude and fixed frequency for both stand-alone and grid-connected conditions.

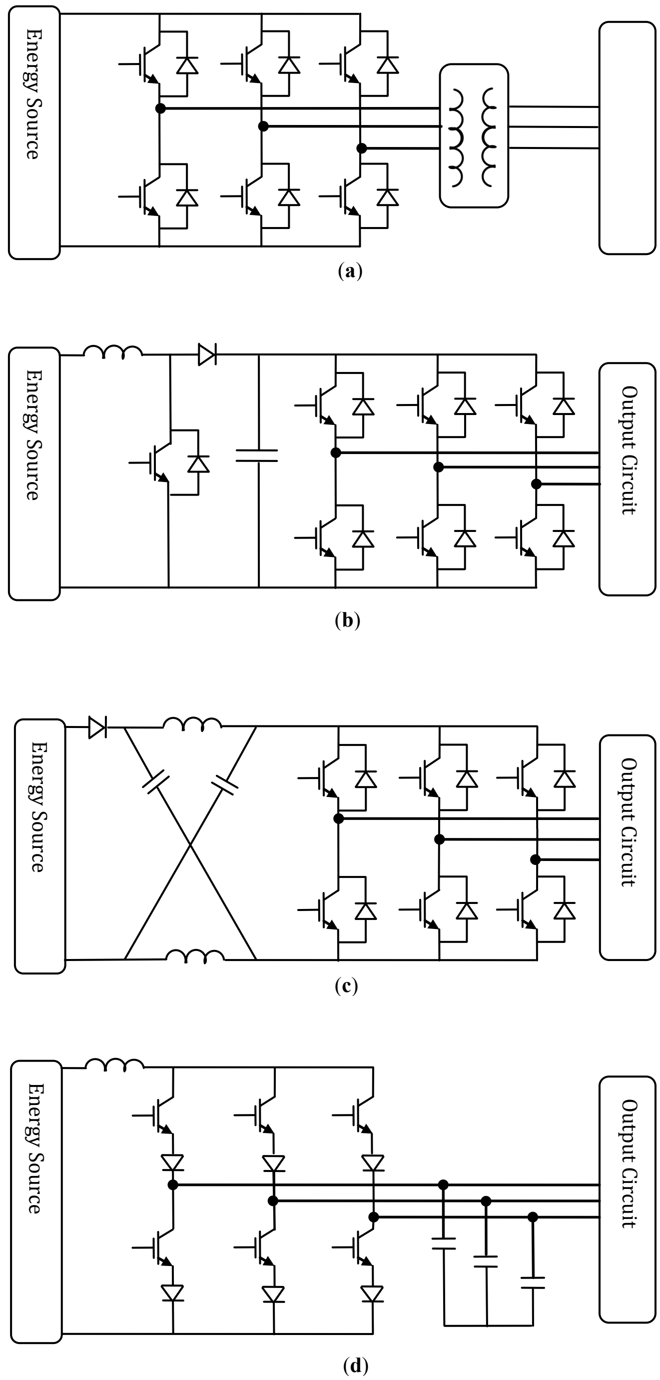

Figure 1.1: Four options for connecting SE sources (fuel cells and PVs) to the grid or loads: (a) VSI cascaded by transformer, (b) Boost DC-DC converter cascaded by VSI, (c) Single-stage z-source inverter, and (d) Single-stage CSI.

1.3 Objectives and Contributions of the Dissertation

In order to utilize photovoltaic energy, power electronic interface systems are needed to connect them to either a local load, or a utility grid. Thus, efficiency and reliability of the power electronic interface systems are two important factors to make the energy economic and reliable. In a conventional system, a PV array in which many PV modules are connected in series is used to obtain sufficient dc-bus voltage for generating ac utility line voltage from an inverter circuit. However, due to the shadows over some of the PV modules, the maximum power generated by each module is not the same. Thus, all the modules cannot work at their maximum current, since the current must be the same for a series connected array. Consequently, the overall efficiency is decreased in such a system. To overcome this defect, a micro-inverter PV module system has been proposed [1]. Each micro-inverter PV module system is composed of a PV panel associated with a small dc/ac converter. Thus, each module can operate in its maximum power conditions and inject its own generated power to the grid, independently from the others [2].

The benefits of such a configuration are higher efficiency (due to the single-stage power topology, and also separate maximum power point tracking (MPPT) for each PV panel), as well as higher reliability (since every PV has its own inverter). The manufacturing and installation cost of the system will be also decreased. The concept of plug-and-play single-stage boost inverters provides many advantages: (1) simple control strategy unlike many other proposed control methods; (2) capable of being applied to both stand-alone and grid-tie systems; (3) easy implementation of MPPT by controlling two control parameters; (4) better stability compared to other control methods; and (5) easy dealing with unbalanced conditions [3].

Among many conversion systems for PV sources, the single-stage boost-inverter seems to have the best efficiency and reliability, and longest life time [3]. It is composed of a current-source inverter, associated with a recently proposed switching pattern that allows it to have an ac voltage at its output, larger than the input dc voltage. One of the most important features of the proposed switching pattern lies in its simplicity and ease of implementation. Since it is based on the well established concept of Space Vector PWM (SVPWM), and due to the popularity of this switching pattern in industry, the proposed switching pattern can have advantages over the existing technologies.

The efficiency of a CSBI is high because it processes the energy in a single stage, while the others use multiple stages (at least two) to do the same job. Since there are losses of energy in any processing stage, the total loss will be decreased if the system uses only one stage. On the other hand, CSBI eliminates the need for using electrolytic capacitors. Since electrolytic capacitors have the least life time, and reliability among all used devices in any inverter systems [4], the life time and reliability of the conversion system will significantly improve by eliminating these capacitors.

Having all the advantages of CSBI and the concept of a micro-inverter PV module system, it makes sense to combine these two technologies to make an efficient and reliable option for PV applications. However, according to the tasks of a conversion system for PV, the SCBI should be able to perform MPPT, boost, and dc-ac conversion at the same time. Hence, it is critical for a CSBI to have an advanced control strategy, capable of doing all of the tasks within the system by controlling only six switches. One of the objectives of this dissertation is to propose a new switching pattern for a CSBI, capable of doing the mentioned tasks.

The next step is to add more capabilities to the micro-inverter module by extracting the relationship between the control parameters, and the system components. In the stand-alone mode of operation, the relationship between the load voltage and the control parameters should be derived, in order to have a voltage-regulated current-source inverter. However, in the grid-connected case, the major task is to have the capability of controlling the injected active and reactive power to the grid. This is performed by deriving the equations of the dc link inductor current and the output injected current. The two dominant control parameters in the proposed switching pattern are the modulation index, and the switching angle. It will be shown that the injected active and reactive power can be controlled by regulating these two parameters.

Accordingly, the objectives of this PhD dissertation can be summarized as follows:

i. Presenting and discussing the concept and topology of the CSBI, its advantages over other PV conversion systems, and rooms for improvements with the concept of micro-inverter
ii. Developing an appropriate switching pattern and control strategy for CSBI in both grid-connected and stand-alone cases, based on the SVPWM concept
iii. Investigating the effects of the circuit parameters (such as the dc inductor and ac filter) on the system performance

iv. Deriving appropriate formulations and relationships between the CSBI output and the control parameters, i.e., regulated voltage in the stand-alone case, and the active and reactive power values in the grid-connected case

v. Verifying the validity of the derived formulas and the control capability of the system by simulations and experiments

1.4 Organization of the Dissertation

Besides this chapter, this dissertation contains six additional chapters. Chapter 2 presents the literature search for the boost inverter. The goal is to have a thorough understanding of the state-of-the-art conversion systems which do both boosting and dc-ac conversion in one single stage. In other words, any power conversion circuit aims to convert a lower dc voltage to a higher ac voltage will be covered. Both single-phase and three-phase topologies are considered in this section, and various technologies with their advantages and drawbacks will be analyzed.

Chapters 3 presents a comprehensive review of the existing dc-ac power conversion systems with the associated PWM methods, used for sustainable and renewable-based distributed generation applications.

Chapter 4 presents the proposed switching pattern for the three-phase CSBI. All the steps towards developing the switching pattern are covered with complete mathematics, for both stand-alone and grid-connected modes of operation. It is shown how the concept of the classic SVPWM is taken, and a novel switching is derived based on the same concept, but with big differences. A comparison between the classic SVPWM method for VSI, and the proposed SVPWM-based method for CSI is also performed and various aspects of the switching pattern for the voltage and current values of the inverter system are explained.

In Chapter 5, the relationship between the control parameters with the output injected active and reactive power of the inverter in the grid-connected mode of operation will be derived. It will be shown how the desired dc current is constructed inside the dc inductor, and how the desired values of active and reactive power are injected into the grid through controlling and regulating two major control parameters: the modulation index, and the switching angle.

Chapter 6 presents the experimental results for all of the previously derived equations. In order to verify the claimed capabilities of the proposed system, a setup was built in the lab, and the real waveforms of different parts of the CSBI are illustrated in this section. Both grid-connected and stand-alone modes of operation are taken into account. Furthermore, the capability of the control system on regulating the amount of the active and reactive power is shown.

Chapter 7 provides a summary of this research work along with some conclusion regarding the significant contributions of this work. Suggestions are given for future work on how the presented control pattern in conjunction with the micro-inverter configuration can be used to form a CSBI PV micro-inverter module in order to improve the reliability and efficiency of the PV energy systems.

CHAPTER 2

LITERATURE REVIEW

In the previous chapter, the concept of the current-source boost-inverter (CSBI) was introduced, and its advantages over the current technologies in the renewable energy systems were outlined. In this chapter, a deeper review will be given on the boost inverter systems, with a closer look at the features (advantages and drawbacks) of each of the topologies. Both single-phase and three-phase topologies are considered in order to cover all the current technology possibilities. In the first section, the single-phase PV systems are considered, while the three-phase PV systems are covered in the second section.

2.1 Single-phase PV systems

There are some related works in the literature regarding CSBI converters [6-19]. They use various topologies with different principles of operation. Topologies composed of two dc/dc boost converters [6], based on buck-boost configuration [7,8,11,15], based on the flyback configuration [9], full-bridge and half-bridge series-resonant buck-boost inverter [10,12], z-source inverter [14], current-source inverter based on the boost converter topology [18], and a coupled-inductor double-boost inverter [19] have been reported in the literature. They are different in various aspects that are important to notice. For instance, most of them use 2 switches as the high-frequency (HF) switches. It is evident that more HF switches leads to higher EMI and losses, which are two important factors in any power electronics circuit. Another issue is the rated power level of the topologies. Most of them [7-12, 19] are for medium and low power levels (P < 2 kW), while there are some topologies proper for high power applications [6, 13, 14, 18]. There are also other issues with some topologies that should be noticed. For example, for the z-source inverter [14], the inverter imposes high ripple on the input current drawn from the source. This might be undesirable in case of PV, and harmful in case of fuel-cell.

In [6], a configuration composed of two boost converters has been proposed. This topology uses 4 switches, all of them work at high frequency (HF) at any time. This is the main drawback for this configuration, as the rest of the topologies try to have less switches, particularly for HF usage. It should be noted that more HF switches leads to more EMI which is an important concern in every power electronic system. Another drawback is the utilization of two electrolytic capacitors, along with two large inductors in the topology. The values for these parts have been reported as 40 uF and 800 uH, respectively.

In [7], a single-stage topology based on the buck-boost configuration has been proposed. It utilizes four switches, two of which work at HF (one at any half cycle), and the other two work at low-frequency (either 50 or 60 Hz). The main drawback of this topology lies in its asymmetrical operation during the positive and negative half-cycle of the grid voltage. This may lead to a complex control system for this circuit [13]. The advantages of this topology are avoiding of electrolytic capacitor, and also low switching losses. Since it is a German patent, there is no information available about its implementation.

Kasa et al. have introduced another topology based on the half-bridge buck-boost configuration [8]. The number of switches used in this topology is the same as the previous one; however, this topology does not have the drawback of asymmetrical operation. The main disadvantage of this configuration is that it uses a pair of PV sources and only one of which is utilized in a given half cycle of the grid voltage [13]. In addition to this, high-value dc capacitors are needed to be placed in parallel with the two PV panels.

In [9], a topology is introduced which contains a HF transformer based on the fly-back converter topology. The advantage of utilizing such a transformer is the isolation that can be achieved between the input and output of the converter, while it has the disadvantage of adding to the losses, and consequently lowering the efficiency of the system. However, this configuration uses only three switches, which lowers the cost of this circuit. Another drawback is using a very large electrolytic capacitor at the input stage of the converter, e.g., 4700 uF for the 300 W experimental setup of this work [9].

A single-stage full-bridge series-resonant buck-boost inverter (FB-SRBBI) has been proposed in [10], which again utilizes 4 switches, 2 for HF and 2 for low-frequency (LF). The proposed inverter only includes a full-bridge topology and an LC resonant tank without auxiliary switches, and provides the main switch for turn-on at ZCS by the resonant tank. This configuration has a large number of devices conducting at a given instant resulting in higher conduction losses. On the other hand, the circuit does not need an electrolytic capacitor at the input stage, and it is a symmetrical topology, which is a benefit for it [13]. On top of that, the total number of components and their size (e.g., input inductors) are less comparing with other topologies.

Another asymmetrical operation converter has been proposed by [11], which is again based on the buck-boost principle. This topology utilizes 4 switches, two of which for HF usage, and the rest for LF. The main feature of this topology is utilizing mutually coupled coils that will cause a limitation on its application for high-power cases. Also, it does not need high value electrolytic capacitors at the input stage.

Ming [12] has introduced a topology based on the half-bridge series-resonant buck-boost inverter which utilizes 5 switches, 3 of which for HF and 2 for LF. The proposed inverter circuit topology provides the main switch for turn-on at zero-current-switching (ZCS) by an auxiliary resonant cell built before the output choke. The main drawback of this topology is the high number of utilized switches, 3 of which are for high-frequency use.

Other than the first topology, all of the mentioned topologies are applicable for low or medium power cases (i.e., P<3 kW). In [13], a high-power topology has been proposed that utilizes 4 switches, 2 of which for HF. A drawback of this converter is that it requires large electrolytic capacitors, as they have used a 2000 uF capacitor in their 500 W experimental setup.

In [14], the application of single-phase z-source converter has been proposed for grid-connected PV systems. This topology uses 2 switches for HF (one at each half cycle) and two for LF. It can have symmetrical operation with simple control scheme. The drawback of this topology is that it needs two large electrolytic capacitors (e.g., 1000 uF for this reference) as well as two large inductors (e.g., 1 mH for the same reference). This increases the size and cost of the system. On top of that, this circuit imposes high ripple on the input current drawn from the source.

Karschny [15] has proposed another configuration based on the buck-boost inverter which utilizes 5 switches. This topology suffers from low efficiency (because of large number of switches) and also high cost and size [16].

In [17], a single-phase, single-stage, doubly grounded, transformer-less PV interface, based on the buck–boost principle, is presented. The configuration is compact and uses fewer components. Only one (undivided) PV source and one buck–boost inductor are used and shared between the two half cycles, which prevents asymmetrical operation and parameter mismatch problems. However, it utilized an electrolytic capacitor at the input stage.

A current-source single-stage inverter has been proposed by [18] based on the dc/dc boost converter topology. In this topology, only 2 switches are utilized for HF, and 2 more for LF.

A coupled-inductor double-boost inverter (CIDBI) has been proposed in [19]. The main attribute of the CIDBI topology is the fact that it generates an ac output voltage larger than the dc input one, depending on the instantaneous duty cycle and turns ratio of the coupled inductor as well. This topology uses 4 switches, all for HF.

2.2 Categorization of the inverter systems

The mentioned topologies can be categorized from different points of view. These factors include: value of the input dc capacitance, number of required PV panels at the input stage of the inverter, number of HF switches, number of all switches used in the topology including transistors and diodes, symmetrical or asymmetrical operation of the inverter, whether or not utilizing a (HF or line frequency) transformer, simplicity of the control system, and capability of both buck and boost operation. In the following, these classifications are performed.

2.2.1 dc input capacitor

In many inverter topologies, the PV panel is repeatedly connected and disconnected to the rest of the circuit (mostly inductors) by means of switching. This disconnection causes the current and voltage of the PV panel to vary in a wide range, and consequently decreases its efficiency dramatically. In order to suppress this problem, a large capacitor is usually placed at the input stage of these inverters. For instance, in [7], the PV panel is connected to an inductor through a switch. Neglecting the capacitor for a moment, once the switch turns off, the PV panel gets disconnected from the inductor, and consequently its current goes to zero. However, by adding a large dc capacitor, this process may change, and the PV panel current and voltage may remain at almost a fixed level in order to have the best efficiency.

Most of the mentioned topologies suffer from this drawback. Even in the z-source inverter [14], where the inductor is connected directly to the panel, the two input capacitors need to have large values, as they should suppress the voltage and current fluctuations caused by the nature of the topology. However, the topologies [6, 11, 13, 18, 19] do not need large dc capacitors at their input stage.

In the proposed topology, the dc inductor is directly connected to the PV panel. Therefore, it never gets disconnected from the panel, resulting in a very smaller range of change in the panel current. Thus, it does not need a large electrolytic capacitor in parallel with the panel. However, in order for the current to have the smallest possible fluctuations, the dc inductor value needs to be as high as possible, and this is one of the drawbacks of the proposed topology.

2.2.2 Number of required PV panels at the input stage

In some topologies, a pair of PV panels is used instead of a single panel [8]. The reason is to utilize different panels during the positive and negative half cycles of the grid voltage in order to have a symmetrical operation. In other words, one of the panels operates only in the positive half cycle, and vice versa for the other one. This will lead to lower efficiency (utilization), since the panels are not working all the time.

In the proposed topology, only one panel is required for the proper operation of the inverter. Since it has the capability of boosting the input voltage, even low-voltage panels (say 15V) could be used with this system.

2.2.3 Number of HF switches

One of the most important factors that dramatically affects the performance of the inverter (efficiency, reliability, EMI, control complexity, …) is the number of switches that operate at HF. In many topologies, there are only two HF switches that only one of them operates at any given half cycle of the grid voltage (The topologies [7, 8, 10-18]). Also, the topology [9] uses only one HF switch, and the topologies [6, 19] use 4 HF switches all the time.

One of the merits of the proposed topology is that it uses only one HF switch at any given half-cycle of the grid voltage. It improves the efficiency and reliability of the inverter, while decreases the EMI and simplifies the control system.

2.2.4 Number of all switches (transistors and diodes)

In addition to the HF switches, there are other semiconductor devices in the paths of current in each topology that increase the conduction losses, and decrease the efficiency of the system. For example, the topologies [15, 17] utilize 2 more diodes in the current path, in addition to the two transistors. This will add to the conduction loss in these inverters.

2.2.5 Symmetrical or asymmetrical operation

Every inverter has two separate states in the two (positive and negative) half-cycles of the grid voltage. For some of the topologies, these two states have the same equivalent circuit and principle of operation, while for others, they might be different than each other. For instance, the principle of operation for the two half-cycles is different in topology [7]. This inverter operates like a buck-boost converter in the positive half-cycle, while it operates like a boost converter in the negative half-cycle [13]. This leads to asymmetrical operation, and the control system needs to take it into account and compensate for it. Other examples are the topologies in [9, 11] which use the coupled inductors only in the negative half-cycle. Thus, the inverter equivalent circuit is quite different for these two states. Also, in topology [8], two different panels are used for the two states, and it will evidently lead to different performances. In the topologies [15, 17], the number of semiconductors in the current path for the two states are different (two diodes for the positive, and one for the negative half-cycle). This is another example of asymmetrical operation. The rest of the inverters do not suffer from this drawback.

The proposed topology acts quite the same for the two states, regarding the principles of operation, the equivalent circuits of the inverter, and number of devices in the current path during the two states. So it does not suffer from asymmetrical operation.

2.2.6 Need for utilizing coupling inductors (transformers)

One of the potential elements that can be used in order to boost the output voltage is coupling inductors, or transformer. This transformer can be either a line frequency or a high frequency one. In the topologies [9, 11, 19] a means of coupling inductors has been used. Utilizing this component leads to larger size and higher cost for the system, as well as higher losses due to their stray resistors and inductors.

The proposed topology utilizes the boost converter principle of operation in order to generate a larger output voltage than the PV panel voltage, and it does not need to have any kind of coupling inductors. This will make the system smaller, cheaper, and more efficient.

2.2.7 Simplicity of the power circuit and the control system

The power circuit of a single-phase grid-connected inverter plays a key role in the simplicity of the overall system. The control system is responsible for several tasks such as: the output power quality assurance, the maximum power extraction from the source, injecting proper amount of reactive power into the grid in case of necessity, performing various protection mechanisms, and so on.

The proposed topology does not use a complicated power circuit; instead a simple H-bridge topology is used as the power circuit, which makes the control system simpler. Also, the continuous nature of the dc inductor current makes it easier to track the maximum power point of the PV source by means of control on this current. However, for other topologies that may have discontinuous dc inductor current, this control is not that easy. Topologies [8, 9, 10, 12, 13, 17] are examples of such a system.

2.2.8 Capability of both step-down and step-up operation

The acceptable range of the input voltage is another important factor for a grid-connected inverter system. Though the output dc voltage of a PV panel is within a short range, the output dc voltage of a rectifier connected to a wind generator may vary over a wide range. Therefore, if the system is intended for both PV and wind farms, it would be better to have a wide acceptable range of input voltage. In other words, it should be capable of both step-up and step-down operations. Most of the topologies mentioned in this review can perform both operations, (topologies [7-15, 17]). However, the rest of the topologies can only boost the input voltage. The proposed topology also operates based on the boost converter principle, and cannot accept input voltages larger than the grid voltage. Although this issue might seem to be a drawback for the circuit, it can be quite trivial if the inverter is intended only for PV, and not for wind systems.

2.3 Three-phase PV systems

Several investigations have been recently reported on the application of CSIs as single-stage boost-inverters for sustainable energy (SE) conversion systems [20-23]. In [20], a single-stage CSI-based topology has been proposed for high voltage PV systems. It was reported that this topology is capable of providing an output voltage of several hundred volts and it can directly feed the grid. The switching pattern in this work is based on a space-vector approach for the output line currents. A space-vector reference frame for the three-phase line currents was used to calculate the proper duty-cycles or time-intervals for the inverter switches. These time-intervals were calculated such that the average value of the inductor current stays constant, while power flows into the grid. Meanwhile, a modified modulation strategy was used to attenuate common-mode currents, and an overall system efficiency of 97% has been achieved. The DC inductance value was relatively high (i.e., 24 mH) with a switching frequency of 25 kHz.

In [21], a CSI-based single-stage grid-connected inverter has been introduced using the so-called OCC (One Cycle Control) strategy. Meanwhile, a conventional SPWM method was applied as the second control scheme for the CSI topology. The presented control schemes are used to convert DC power to an AC power in a single-stage by injecting synchronized, three-phase, sinusoidal currents into the grid. The DC inductance value can be kept low (i.e., 0.55 mH) with a switching frequency of 40 kHz, which is relatively high for SE conversion applications. It has been stated that with the OCC method, the inverter preserves the advantages of simple circuitry, good stability and fast dynamic response.

In [22], a stand-alone SPWM based CSI has been introduced where a "shoot-through" state, for so-called Tri-level PWM logic, was emphasized as the boost mechanism of the DC input voltage. In their experimental setup, the maximum boost ratio of 3.3 was achieved where the DC-link inductance value was 100 mH and the PWM switching frequency was about 1.2 kHz.

In [23], a single-stage inverter has been used for a grid-connected PV-based energy conversion system, however, their proposed circuit topology is different than that of a CSI, and is closer to the circuit topology of the voltage source inverter (VSI).

2.4 Summary

In this chapter, a thorough review of all the related single-stage inverters intended for solar systems was given. Both single-phase and three-phase inverters were considered, and the advantages and drawbacks of every category of the inverters were pointed out. The applicability of the inverters for PV systems, particularly in low-power cases was one of the main issues taken into account. Furthermore, the reliability, efficiency, cost, and complexity of the control system were considered.

CHAPTER 3

DC-AC CONVERSION IN DISTRIBUTED GENERATION SYSTEMS

This chapter provides a review of the history and contribution of existing literature that relates to dc-ac power conversion systems. The focus of the work is on sustainable- and renewable-based distributed generation systems, in which the converters have to produce high voltages from low voltage dc inputs.

This chapter contains five sections. The six-step inverter is introduced in Section 1. Four major types of pulse-width-modulated inverters are presented in Section 2. Section 3 reviews three common configurations of multilevel inverters. The background work, related to existing boost-inverting power conversion systems for distributed generation applications are reviewed in Section 4, and Section 5 is the summary of the chapter.

3.1 Six-Step Inverter

The six-step inverter, with an H-bridge topology, is the simplest type of dc-ac conversion system. The three-phase H-bridge converter topology, which serves as the basis for nearly all three-phase inverters, is presented in Figure 3.1. Metal-oxide field-effect transistors (MOSFETs) have been used as switches in this figure. However, different types of semiconductor controllable switches, like bipolar junction transistors (BJTs), insulated-gate bipolar junction transistors (IGBTs), and metal-on-silicon controlled thyristors (MCTs), can be used in this inverter [28].

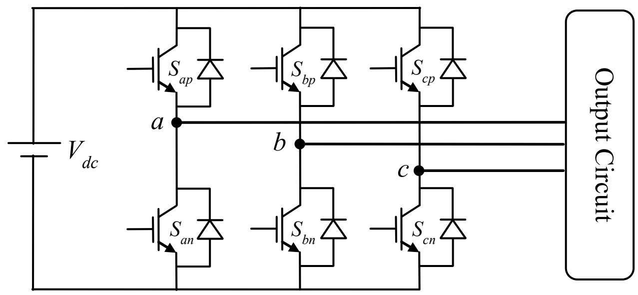

Figure 3.1: Six-step inverter

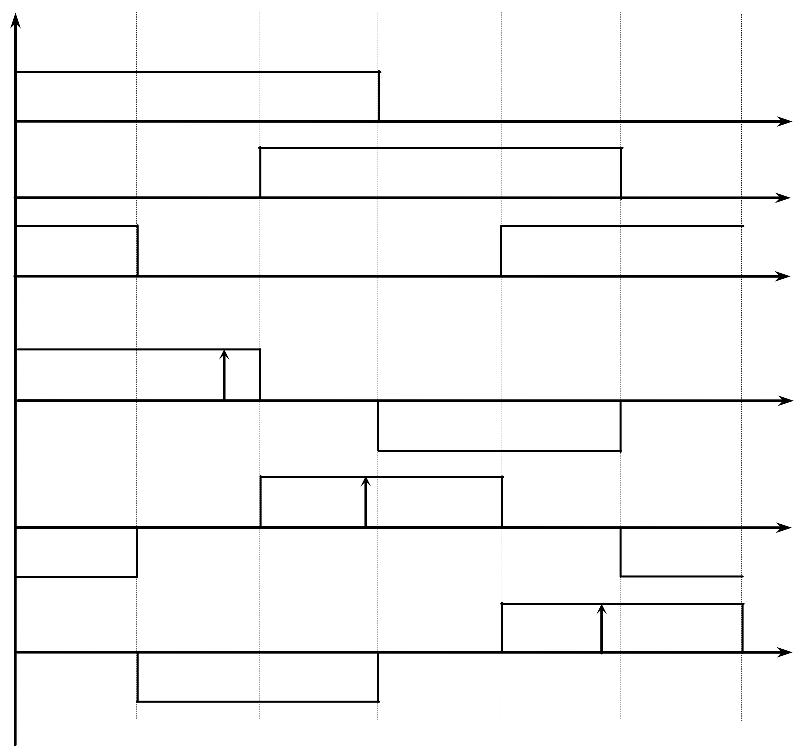

Figure 3.2: Gate signals and line-to-line voltages of six-step inverter

The gate signals that are driving the switches of a six-step inverter, and its line-to-line output voltages are shown in Figure 3.2, where the hat sign ( ) denotes the logical complement. As can be seen in this figure, each switch conducts for 180 electrical degrees per each switching cycle. Also, using this figure, one can calculate the line-to-line rms voltage of the six-step inverter:

(3.1)

This equation indicates that the output voltage of the six-step inverter is only a function of the applied dc voltage; therefore, the output voltage cannot be regulated unless the applied dc voltage is adjusted. High total harmonic distortion (THD), especially at low-order harmonics of {5, 7, 11, 13, 17, 19, …}, is another major disadvantage of the six-step inverter. This is due to the square waveform of the generated voltage.

3.2 Pulse-Width-Modulated Inverter

Similar to the six-step inverter, the output line-to-line voltage of this type of inverter can be at three voltage levels, i.e. , 0, and . However, a pulse-width-modulation (PWM) strategy allows the rms voltage (and amplitude of the fundamental component) to be readily controlled. There are various schemes to pulse-width modulate the inverter switches. Four major types of these schemes, i.e. sinusoidal PWM, third-harmonic injection, selective harmonic elimination, and space-vector modulation, will be discussed in the following subsections.

3.2.1 Sinusoidal Pulse-Width-Modulation (SPWM)

Sinusoidal pulse-with-modulation is based on generating a sequence of voltage pulses at a certain frequency and sinusoidal modulated pulse-widths. This can be achieved through comparing three sine-wave control voltages, , , and , with a triangular waveform, , which is called the carrier. The ratio between the amplitude of the control voltages, , and peak of the triangular voltage, , is defined as the modulation index, . The frequency of the triangular waveform, which is usually kept constant, establishes the inverter switching frequency, and the frequency of the control voltages determines the output voltage frequency. Because of its simplicity and ease of implementation, the SPWM is widely used in industrial applications [84]. The concept of PWM, applied to a three-phase H-bridge converter topology is shown in Figure 3.3.

By changing the modulation index, , the widths of pulses vary, which results in variations in the amplitude of the output voltage. Another advantage of the SPWM over six-step switching pattern is its higher quality voltage waveform. The harmonics in the output voltage appears as sidebands, centered around the switching frequency, , and its multiples. If the ratio between the switching frequency and the desired output frequency, , is defined as the modulation frequency ratio, i.e. , the frequency spectrum of the output voltage of a SWPM inverter contains harmonics orders around , , , and so forth [25]. It is also worth mentioning that for a frequency modulation ratio (which is always true except for very high-power applications), the harmonic amplitudes are almost independent of . Moreover, odd integer modulation frequency ratios are recommended for avoiding even-order harmonics, and in particular a small dc component, at the output voltage [85].

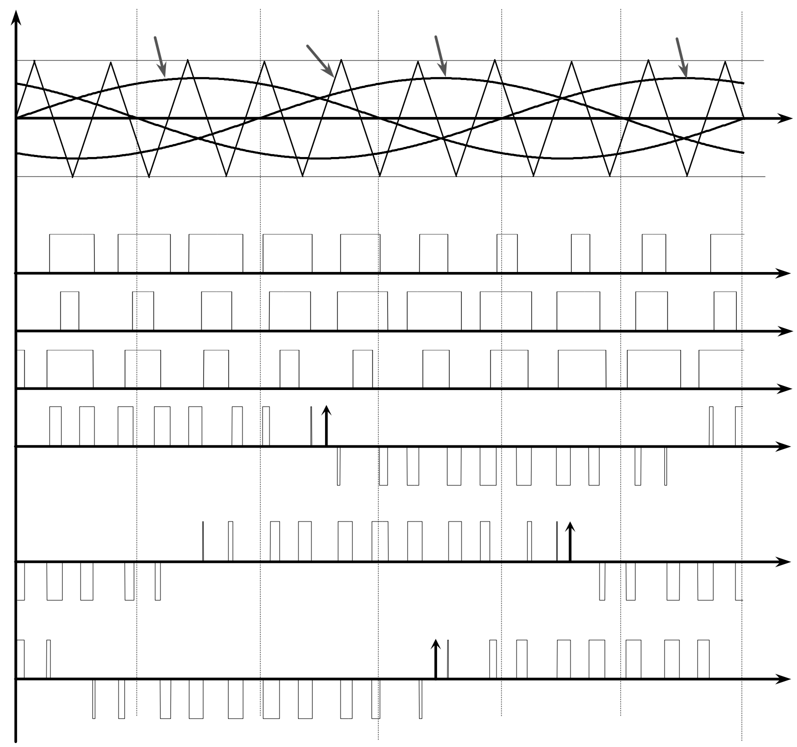

Figure 3.3: Sinusoidal PWM: control and carrier wavefroms, gate signals, and line-to-line voltages

Besides the harmonic components, an inappropriate choice of may cause sub-harmonics in the output voltage of the SWPM inverters. The sub-harmonics may occur when and it is not an integer number. Thus, in order to avoid sub-harmonics the modulation frequency ratio should be an integer number, this is so-called *synchronous PWM*. On the other hand, *asynchronous PWM*, in which the frequency modulation ratio is not an integer number, can be applied when the modulation frequency ratio is sufficiently large, i.e.   [25]. However, it should be kept in mind that, increasing   results in higher switching frequencies, which increase the switching losses and decrease the efficiency.

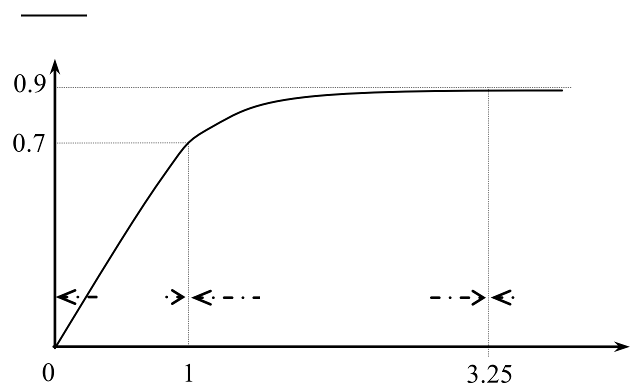

Figure 3.4: Variations of the fundamental component of the output voltage versus the modulation index

The waveforms of Figure 3.3 are a case with a modulation index   (linear range of   ), in which the amplitude of the control signal is smaller than the peak of the carrier signal. However, it may happen that the modulation index exceeds 1. In this situation, which is called *over-modulation*, the control voltages may not intersect the triangular waveform for a period of time. In general, over-modulation causes the output voltage to contain many more harmonics in the sidebands as compared with the linear range. Furthermore, during over-modulation conditions, the amplitude of the fundamental component of the output voltage does not vary linearly with   , which is the case within the linear range of operation, i.e.   . Moreover, it is observed that, as the modulation index increases beyond one, the output waveform turns more and more to square-wave, like that for a six-step inverter. The over-modulation effect on the fundamental component of line-to-line output voltage of the SPWM inverter, , is shown in Figure 3.4.

3.2.2 Third-Harmonic Injection

As was mentioned in the previous section, the maximum value of high-quality output voltage can be achieved at the upper bound of the linear range of operation, . This is one of the main limitations of SPWM. However, this limit can be increased by introducing a third harmonic to the control voltage. It has been shown in [28] that, with a proper choice of the fundamental and third-harmonic components for the control voltage, the inverter can output 15% more voltage without suffering from the consequences of over-modulation.

3.2.3 Selective Harmonic Elimination

Selective harmonic elimination is another PWM method that has low baseband distortion [87]. This method is particularly suitable for low switching frequency inverters, which are either high-power or have slow switching devices. This method is based on the idea of chopping the square-waveform of the six-step inverter at some certain angle-intervals in order to eliminate some specific low-order harmonics from the output voltage waveform [86]. An example of selective harmonic elimination with two degrees of freedom, corresponding to one notch between 0 to , is demonstrated in Figure 3.5. In order to avoid even harmonics, it is assumed that the output waveform has quarter-wave and half-wave symmetry. The periodic waveform of line-to-line voltage, , can be written as follows:

(3.2)

where, the Fourier coefficient is defined as:

(3.3)

Because of the quarter-wave symmetry in Figure 3.5, can be rewritten as:

(3.4)

As a result:

(3.5)

which can be simplified to:

(3.6)

This equation can be solved for and , to eliminate two selected harmonics. For instance, the following set of equation provides and for elimination of the 3th and 5th order harmonics from the line voltage waveform.

(3.7)

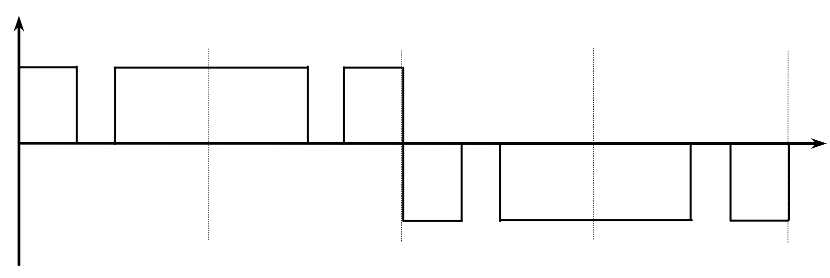

Figure 3.5: Waveform of a selective harmonic elimination with two degrees of freedom

Accordingly, the methodology can be extended to eliminate more harmonic orders by introducing more notches between 0 to (to increase the degrees of freedom of the equations).

3.2.4 Space-Vector Modulation

Space-vector pulse-with-modulation (SVPWM) is another technique of driving a voltage source three-phase H-bridge inverter, for generating voltage waveforms that are devoid of low-frequency harmonic content [90]. The approach is based on the space-vector representation of the output voltages, in which the three inverter voltages are represented by a voltage space-vector, , defined as:

(3.8)

In total, the voltage source inverter (VSI) can operate in eight different states that are associated with eight switching positions. The switching table and the corresponding voltage space-vectors are presented in Table 3.1 and Figure 3.6, respectively. As can be seen in the figure, a reference voltage space-vector, , can be developed by adding its two adjacent space-vectors. For instance, when the reference voltage space-vector is placed in Sector (I), it can be produced by operating the inverter is States 1 and 2, for duty ratios of and , respectively. These duty ratios can be calculated by the well-known law of sines, which is:

(3.9)

Substituting the voltage space-vectors of Table 3.1 provides and as the following:

$$(3.10)$$

It should be noted that, these duty ratios are only valid if , i.e. when lies within the largest circle that can be circumscribed within the boundaries of the hexagon connecting the voltage space-vectors in Figure 3.6. The conditions that the reference voltage space-vector exceed the boundaries of the incircle, which is , is called *over-modulation*, which results in an increase in the harmonic content of the output voltage. On the other hand, once , the inverter has to operate in the zero state (either State 0 or State 8, or a combination of the both) for the rest of the switching cycle. This interval corresponds to a duty ratio of .

It is also worth mentioning that to obtain the minimum switching frequency of each inverter leg, it is necessary to arrange the switching sequence in such a way that the transition from one state to the next is performed by switching only one inverter leg.

Table 3.1: Switching table and output voltages of a three-phase inverter

State	Sectors							Space-Vector,
0	All	0	0	0	0	0	0	
1	VI, I	1	0	0		0		–
2	I, II	1	1	0	0			–
3	II, III	0	1	0			0	–
4	III, IV	0	1	1		0		–
5	IV, V	0	0	1	0			–
6	V, VI	0	0	1			0	–
7	All	1	1	1	0	0	0	

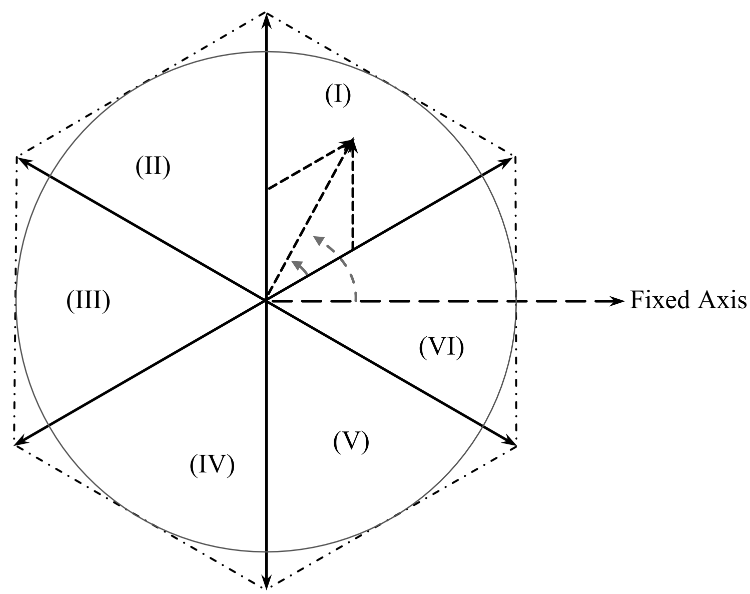

Figure 3.6: Inverter output voltage space-vectors

3.3 Multilevel Inverter

The multilevel inverter is another type of dc-ac converter which is more suitable for high-voltage and high-power applications. A major advantage of this inverter is a reduction in the harmonic content without increasing the switching frequency, or decreasing the inverter output power [91-93]. Besides the ability to provide a proper harmonic spectrum (making possible the use of smaller and less expensive filters), the multilevel inverter has a good dynamic response and relatively low voltage ratings for the switches. Moreover, multilevel inverters are a good tradeoff solution between performance and cost in high-voltage and high-power systems [11].

The output voltage waveform of the multilevel inverter is composed of a number of levels of voltage, typically obtained from capacitors or dc voltage sources. The so-called multilevel inverter starts at three levels, and as the number of levels increases the output THD decreases, and once the number of levels reaches infinity, the THD reaches zero. Multilevel inverters are categorized into three general topologies; diode-clamped multilevel inverter (DCMI), flying-capacitor multilevel inverter (FCMI), and cascaded multilevel inverter with separate dc sources.

3.3.1 Diode-Clamped Multilevel Inverter (DCMI)

This multilevel inverter has series capacitors at the dc-bus in order to divide the voltage into a set of voltage levels. In general, *M*-1 capacitors are used in an *M*-level diode-clamped inverter. It should be noted that the level of multilevel inverters are defined as the number of phase voltage levels, while the number of line-to-line voltage levels of a *M*-level inverter is 2*M*-1. A three-phase three-level diode-clamped inverter is shown in Figure 3.7. Each of the three phases share a common dc-bus, which has been subdivided by two capacitors into three levels. The voltage across each capacitor is , and the voltage stress across each semiconductor switch is limited to through the clamping diodes. Table 3.2 lists the output phase voltage levels, with the negative dc rail voltage as a reference (point *n*), and the corresponding output line-to-line voltages are presented in Figure 3.8.

Table 3.2: Switching table of a three-level diode-clamped inverter

	1	1	0	0
	0	1	1	0
0	0	0	1	1

As can be seen in Figure 3.8, the output voltage waveform of a multilevel inverter has half-wave and quarter-wave symmetry. Thus, its Fourier series can be written as (3.2) and the Fourier coefficients can be obtained according to (3.4). In general, the Fourier coefficients of the line-to-line output voltage of an *M*-level inverter are obtained as the following:

(3.11)

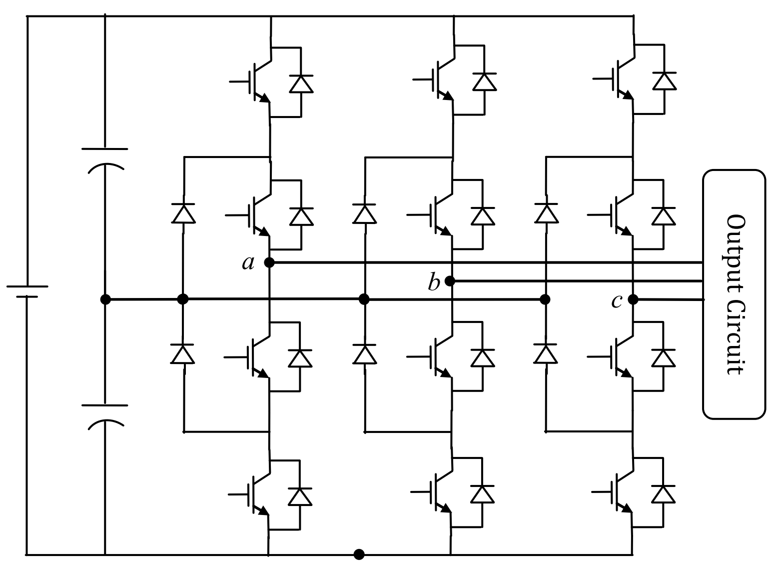

Figure 3.7: Three-phase three-level diode-clamped inverter

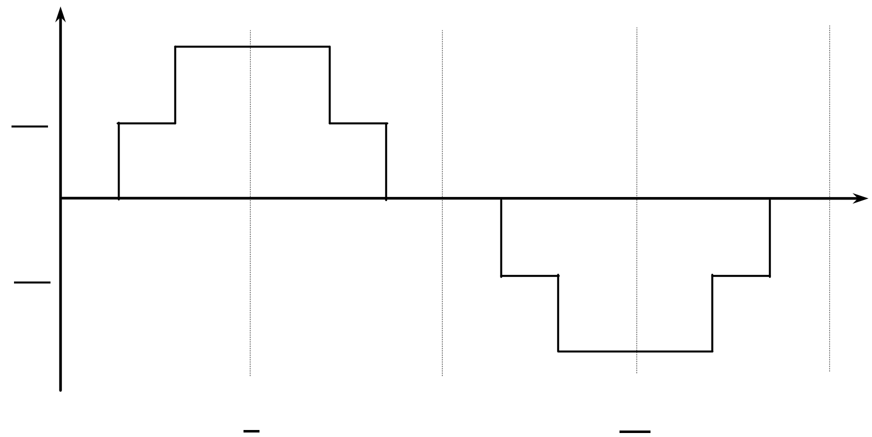

Figure 3.8: Line-to-line voltage waveform for a three-level diode-clamped inverter

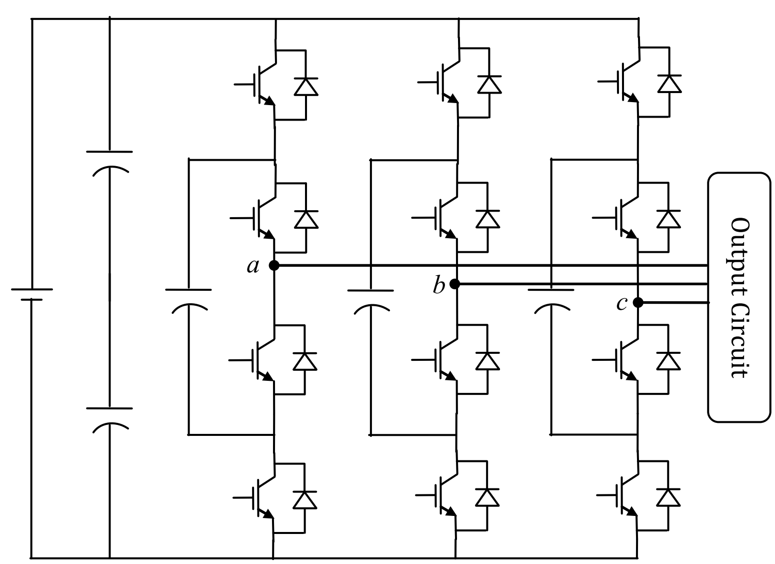

Figure 3.9: Three-phase three-level flying-capacitor inverter

3.3.2 Flying-Capacitor Multilevel Inverter (FCMI)

The flying-capacitor multilevel inverter has a similar structure to the diode-clamped inverter except that is uses capacitors instead of clamping diodes. This inverter uses a ladder structure of dc-side capacitors, where each capacitor has a different voltage from the other capacitors [94-96]. The size of the voltage increment between two capacitors determines the size of the voltage levels in the output waveform. The circuit topology of three-level flying-capacitor inverter is shown in Figure 3.9.

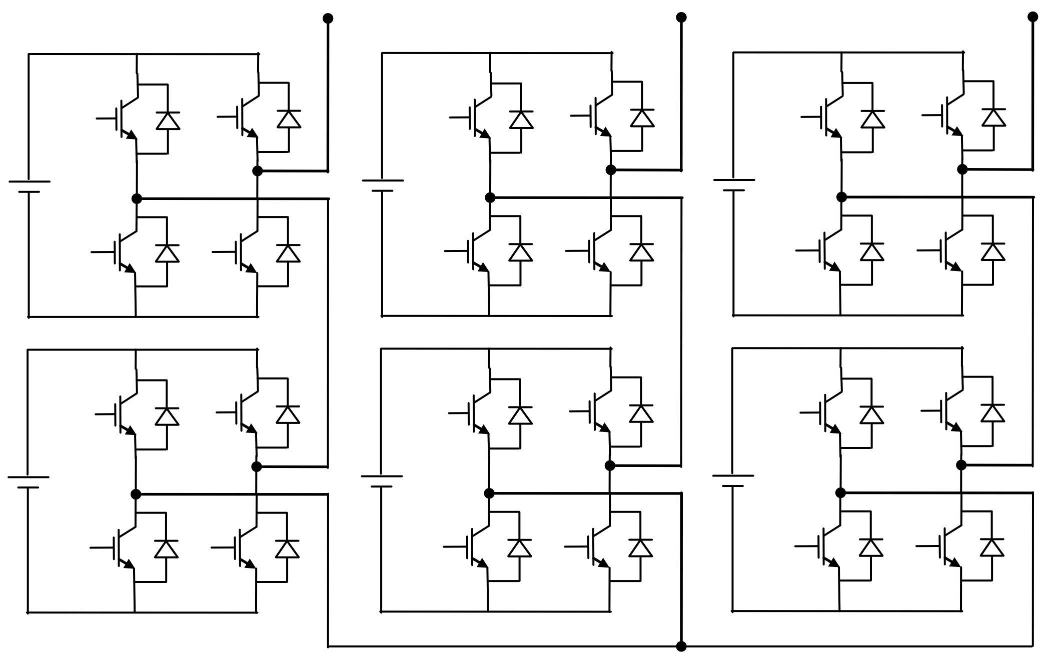

Figure 3.10: Three-phase three-level flying-capacitor inverter

In addition to the (M-1) dc-bus capacitor, an M-level flying-capacitor inverter requires (M-1)×(M-2)/2 inner-loop (auxiliary) capacitors. It can be seen in Figure 3.9 that all phase legs share the same dc-link capacitors, and . Also, the inner-loop balancing capacitors for each phase leg (, and) are independent from those for the other legs. An advantage of the flying-capacitor multilevel inverter is that several switching combinations may be used to synthesize an output voltage. For instance, the switching table of Table 3.2 is one of the possible switching combinations for the three-level flying capacitor inverter of Figure 3.9.

3.3.3 Cascaded-Inverters with Separate dc-Sources

Cascaded-inverters with separate dc-sources are another prevalent structure for the multi-level inverter. Its functionality is similar to the other two types of multilevel inverters of the previous subsections, but it synthesizes a desired output voltage waveform from several independent dc-sources. Photovoltaic panels, fuel cells, and batteries, can be some of the possible choices. A three-phase, three-level configuration of the cascaded-inverter is illustrated in Figure 3.10. As can be seen, it is a combination of three Y-connected single-phase cascaded-inverters. Each inverter level can generate three different voltage outputs, e.g. , 0, and , by connecting the dc-source to the ac output by different combinations of the switches.

3.3.4 A Comparison among the Multilevel Inverters

A comparison between the three introduced types of multilevel inverters is presented in Table 3.3. It shows that all inverters need the same number of switches and main diodes in order to generate the same number of levels. The flying-capacitor and cascaded-inverters do not require clamping diodes, while the flying-capacitor inverter needs inner-loop balancing capacitors. Technically, the cascaded-inverter requires the least number of components, apart from the voltage sources. It has a modular circuit layout and its packaging is simple. The reason is that all levels have the same structure and no clamping diodes or balancing capacitors are needed. Moreover, by adding or removing the H-bridge cells, the number of output voltage levels can be easily adjusted.

Table 3.3: Comparison of power components, required per phase leg, among the multilevel inverters

Inverter Configuration	Diode-Clamped	Flying-Capacitors	Cascaded-Inverters
Switches	$2(M\text{-}1)$	$2(M\text{-}1)$	$2(M\text{-}1)$
Main Diodes	$2(M\text{-}1)$	$2(M\text{-}1)$	$2(M\text{-}1)$
Clamping Diodes	$(M\text{-}1)\times(M\text{-}2)$	0	0
dc-Bus Capacitors	$(M\text{-}1)$	$(M\text{-}1)$	$(M\text{-}1)/2$
Balancing Capacitors	0	$(M\text{-}1)\times(M\text{-}2)/2$	0

3.4 DC-DC Converters for DG Applications

Dc-ac power converters (inverters) play key roles in connecting sustainable energy (SE) sources, and energy storage (ES) devices, to local loads and the utility grid. The power electronic interface circuits of the DG units perform several important tasks in order to make the output power of the SE sources and ES devices adequate for electric appliances. Typically, the first task is to boost the dc input voltage to a desired (rated) voltage level and invert the dc voltage to an ac voltage with a fixed frequency and amplitude. In the case of photovoltaic (PV) systems, it is desirable to keep the number of PV panels as low as possible. This means that the amplitude of the generated dc voltage will be lower than the grid voltage (in grid-connected mode) or the desirable load voltage (in stand-alone mode). Meanwhile, due to the nature of the ES sources, their generated power is usually varying by time. For instance, the output voltage and power of a PV panel vary in a wide range based on the operating conditions. Some of the affecting variables are incident solar radiation, ambient temperature, deposited dust and dirt on the panel surface, and the load current. The second task of the power electronic conversion system is to utilize the maximum available power of the SE sources. Besides the aforementioned functionalities, DG inverters have to meet some requirements like stability, efficiency, reliability, and power quality, which are common to all conversion systems. Several power electronic circuit topologies, along with the associated switching patterns and control algorithms, have been presented in literature, which perform the discussed tasks and address the aforementioned issues [1-22].

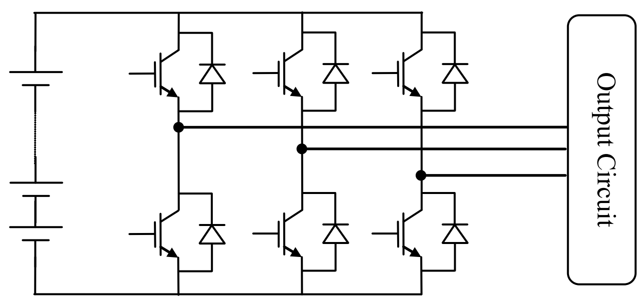

Figure 3.11: Basic single-stage power conversion system, consisting of series connected dc-sources

3.4.1 Basic Single-Stage Conversion System

A simple way to increase the output voltage of SE sources is to connect a number of them in series (to develop a high dc voltage without utilizing a boost circuit), and use a central pulsed width modulated (PWM) buck voltage source inverter (VSI) to produce an ac voltage [7] (see Figure 3.11). However, because of the high cost of PV panels, this series configuration seems as an expensive solution. In addition, putting a number of components in series usually lowers the reliability of the system. This is because the failure of one of the panels, or outage of the inverter, results in a complete loss of generation [7]. Moreover, mismatch of the series PV panels results in a reduction in the utilized energy, which can be interpreted as low efficiency [1].

3.4.2 Conventional Two-Stage Conversion System

In Figure 3.12, a step-up transformer is utilized at line-frequency to boost the output voltage of the PWM buck inverter. This well-known topology is robust and relatively efficient and reliable. Additionally, it can be used in module-integrated (or module-oriented) applications, which provides a higher flexibility than the topology of Figure 3.11. Besides that, each module has its own maximum power point tracking (MPP) system that increases the overall energy utilization. Its plug-and-play feature is also attractive, in which a complete PV system is achieved at a low investment cost [7]. On the other hand, this solution has some disadvantages, such as huge size, loud acoustic noise, and relatively high cost. Furthermore, the transformer should be designed for a relatively wide range of power, which leads to a low system efficiency. Overall, this topology is regarded as a poor solution [1].

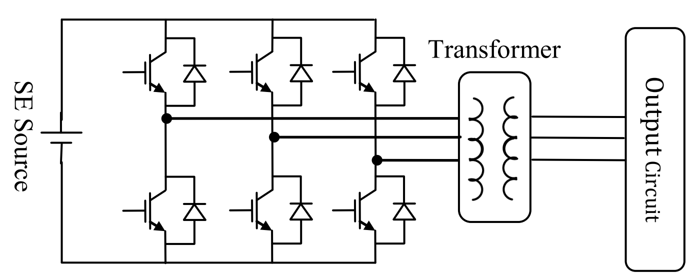

Figure 3.12: Transformer-based two-stage conversion system

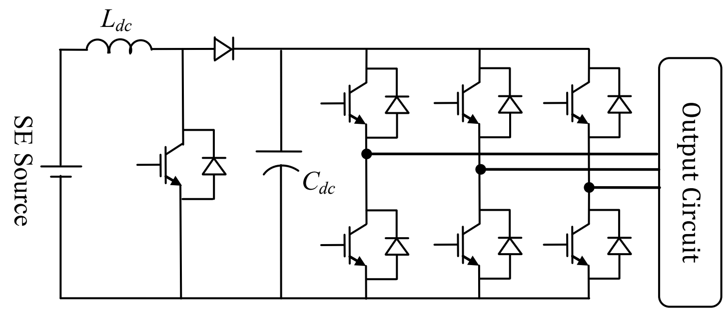

Figure 3.13: Transformer-less two-stage conversion system, consisting of a dc-dc boost converter cascaded with a PWM buck VSI

Transformer-less two-stage power conversion systems are one of the most commonly used interface circuits in SE-based DG applications. As can be seen in Figure 3.13, in this two-stage conversion topology, a dc-dc converter and an inverter are cascaded. In the first stage, the dc-dc converter boosts and regulates the dc-bus voltage at a fixed level, and in the second stage, the PWM buck VSI converts the regulated dc voltage into an ac voltage. Since this topology does not contain a transformer, it has less magnetic components and higher efficiency. In comparison with the topology displayed in Figure 3.12, this topology requires two individual control systems and uses one more solid-state switch, as well as an electrolytic capacitor bank at the dc-bus. This will result in a lower reliability (and perhaps efficiency), and a more complicated control scheme [7].

3.4.3 Multilevel Inverter

Three-phase multilevel inverters can also be employed to interface the output of several SE sources with the grid [2, 8]. Figure 3.7 presents the circuit diagram for the connection of a generic SE source to the output circuit by means of a diode-clamped three-level inverter. The SE source and additional components are represented as a voltage source, connected to the dc-side of the inverter. Like most inverters, multilevel inverters are connected to a grid through an inductive filter. A general model for the three-level inverter is presented in [9-10]. This model describes the dynamics of the dc- and ac-sides, including the dynamics of dc and ac neutral points. Although the multilevel inverters are effective for this application, the added complexity of the circuit and the additional components reduce both the overall efficiency, and reliability of the system, and may raise the overall cost of the power electronic interface [2].

3.4.4 Z-Source Inverter

The z-source inverter has the capability of boosting and inverting the dc voltage in a single stage, with fewer solid-state switches in comparison with the multilevel inverters and the above-mentioned two-stage topologies depicted in Figures 3.13 and 3.14 [3].

The z-source inverter is a combination of a voltage source inverter, and a current source inverter. The circuit diagram of this inverter topology is shown in Figure 3.14. This inverter topology transforms the dc input voltage into the grid voltage, while the dc voltage can be above or below the grid voltage. The z-source inverter contains relatively high input current ripples, which may cause high stresses on the dc-link inductors and capacitors [12]. The application of this topology was reported by [13-15] as a grid-connected single-stage inverter for distributed generation systems, specialized for residential PV applications.

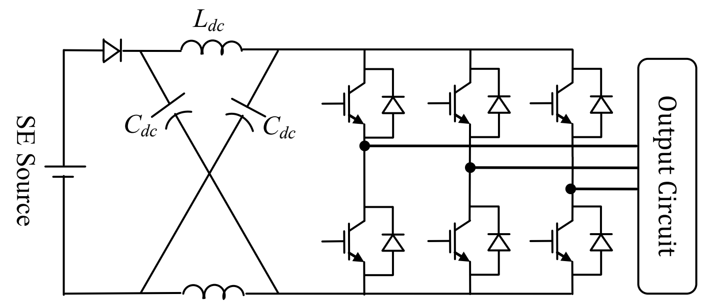

Figure 3.14: Single-stage Z-source inverter

3.4.5 Single-Stage Boost Inverter

In the last several decades, current source inverters have been replaced with voltage source inverters in many industrial applications. However, the CSI topology in conjunction with an appropriate control scheme can form a single-stage boost inverter that can be used for SE conversion systems. Several investigations have been recently reported on the application of CSIs as single-stage boost inverters for SE conversion systems [16-19]. As can be seen in Figure 3.15, the current source inverter utilizes a series inductor at the dc-link and a capacitor bank at the ac-side. In [4], a new switching pattern has been proposed for the CSIs in order to boost and invert the dc voltage to a fixed voltage magnitude and fixed frequency for both stand-alone and grid-connected conditions. Besides the simplicity of the control scheme, elimination of dc-bus electrolytic capacitors is one of the greatest advantages of the single-stage boost inverter over the conventional two-stage converter, the multilevel inverter, and the Z-source inverter. This will significantly improve the reliability of the overall system, particularly in photovoltaic (PV) energy conversion systems, in which the mean-time-to-the-first-failure of inverters is about 5 years and the average lifetime of PV panels is about 20 years [6]. These attractive features have turned the attention of some of the latest research studies in the field of power electronics, to modeling and control of single-stage boost inverter [20-22]. This topology, along with a modified space-vector pulse-width-modulation (SVPWM) technique, the so-called phasor pulse-width-modulation (PPWM), is the core of this dissertation, which will be elaborated upon in Chapter 4, and its state-space-averaged model will be derived in Chapters 5 and 6.

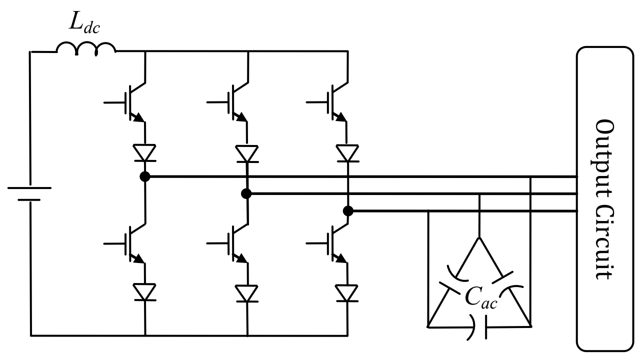

Figure 3.15: Single-stage current source boost inverter

3.5 Summary

Extensive research has been carried out on the related work to dc-ac power conversion systems, used in distributed generation applications. The most common converter topologies for grid-connected and stand-alone operations of sustainable energy-based distributed generation system have been reviewed and compared. It should be mentioned that, besides the converter topologies reviewed in this chapter, the resonant converters are another major type of power electronic converters, which can be used for the same applications. However, since they are not related to the subject of this dissertation, they have not been discussed.

In the next chapter, the new switching pattern for the CSBI is covered using the associated formulations of the converter topology and performance.

CHAPTER 4

THE PROPOSED SWITCHING PATTERN

4.1 System Description

In this dissertation, a single-stage CSI-based boost-inverter with a novel control strategy is proposed for SE (particularly for PV and fuel-cell) applications. A new method is developed based on the concept of SVPWM. However, the developed switching pattern is formulated based upon the phasor quantities, and not the space-vectors. Nevertheless, this strategy preserves all the advantages of an SVPWM technique such as simplicity, robustness, and ease of programming in digital processors. Figure 4.1 shows the power circuit of the three-phase boost-inverter, where is a DC voltage source (representing an SE source), is the DC-link inductor, represents the AC side film capacitors, represents the line inductors, and represents the high-frequency filter capacitors. In the laboratory scaled power circuit, the above-mentioned design parameters were = 2.0 mH, = 5.6 μF line-to-line (in a Δ-connection), = 0.12 mH per phase, and = 0.1 μF per phase (in a Y-connection). In this circuit topology, at any given instant, one of the upper IGBTs and one of the lower IBGTs are kept ON. During the charging times the IGBTs in a same leg are simultaneously ON, so that the magnetic energy in is increased to boost the output voltage and inject power to the output circuit. This will be further elaborated upon in next sections.

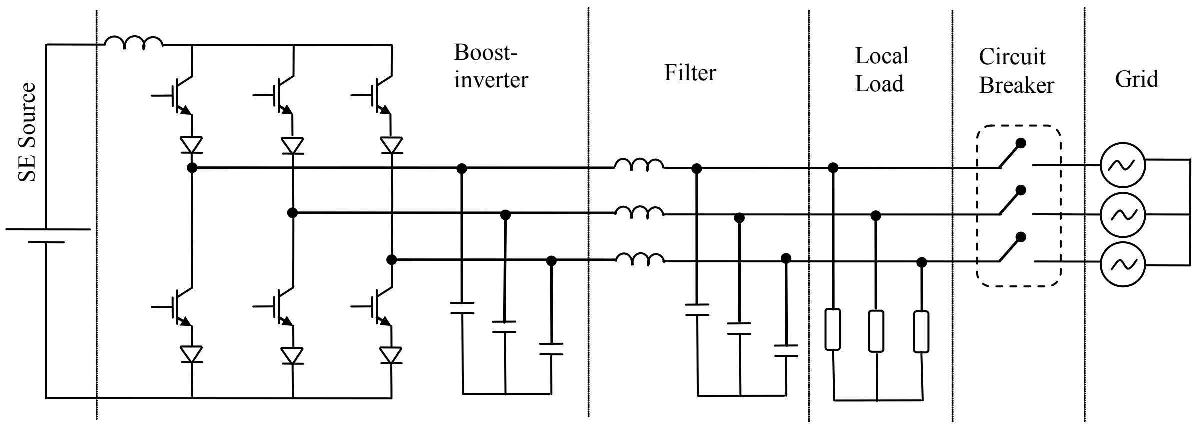

Figure 4.1: The complete power circuit schematic of the case study CSI-based boost-inverter.

4.2 Presented Control Scheme

In this section, the control method, which is utilized for the CSI based boost-inverter topology, will be elaborated upon through mathematical formulations. The PWM switching pattern and formulation developed herein is very close to the conventional SVPWM, however the space-vector of the currents and voltages are not applied in the development of the new formulations. It should be also emphasized that in the conventional space-vector formulation, the inverter switching time-intervals (or duty cycles) are in direct proportion to , where the time-intervals in the presented formulation for CSI-based boost-inverters are in direct proportion to . Meanwhile, the six main switching states, and two zeros, with three switches conducting at any given instant in conventional SVPWM techniques, are adapted to six states with only two switches conducting at any given instant, as well as three charging states in the proposed/developed switching pattern for the CSI based boost-inverter. These charging states are necessary in order to boost the DC input voltage. The control scheme is capable of being applied to both grid-connected and stand-alone cases. The calculations for obtaining the control parameters are presented in the next two subsections. In the first case, the inverter is grid-connected, therefore the output voltage is maintained by the grid, and the inverter has to regulate the output current in such a way as to control the delivery of power to the grid. In this situation, the inverter operates in a current-source, current-regulated mode. In the second case, the inverter is merely connected to a local load (R-L), and therefore has to regulate the output voltage. While the inverter is still a current-source, it operates in current-source voltage-regulated mode. The following calculations further elaborate upon the difference between these two modes.

4.2.1 Control Method for the Grid-Connected Case

In Figure 4.2, there are six sectors separated by six line-to-line voltage phasors, , , , and . The desired volt-second, , is demonstrated in Sector (I) of Figure 4.2 and its corresponding discharging and charging time-intervals can be calculated as shown in Figure 4.3. In each switching cycle, , there are three time-intervals; one time-interval for charging the DC-link inductor and two time-intervals for injecting current into two different phases. For example, while Sector (I) is passing the x-axis in Figure 4.2, is when falls in between and , this is when the voltage of Phase-A is in its positive extreme. Thus, the proposed method uses Phase-A in the entire sector to close the path of the load current, i.e. stays ON over this switching cycle. On the other hand, Phase-B and Phase-C are intermittently used for the negative part of the load current, see Figure 4.4. Thus, there are three states and consequently three time-intervals in Sector (I):

(1) The charging time-interval, , in which two switches from Leg-A are closed and the DC-link inductor is being charged, see I-C1 ( ) of Figure 4.4,

(2) The first discharging time-interval, , where the inductor current is directed into Phase-A. During this period of time, the upper-switch of Leg-A and the lower-switch of Leg-B of the inverter are closed, see I-D2 ( ) of Figure 4.4,

(3) The second discharging time-interval, , where the inductor current is directed into Phase-A. During this period of time, the upper-switch of Leg-A and the lower-switch of Leg-C of the inverter are closed, see I-D3 ( ) of Figure 4.4.

It should be noted that within a given sector one of the switches does not have to be switched at all, as shown in Figure 4.4. The six sectors along with the proper switching time-intervals are summarized in Table 4.1 for all six sectors. In this table, and denote the associated first and second voltage vector in each sector in Figure 4.2, and represent the positive (upper) and negative (lower) switches in each leg of the inverter, see Figure 4.1, and , , and illustrate the time-intervals of the charging states, as well as, the two consecutive discharging states corresponding to each sector.

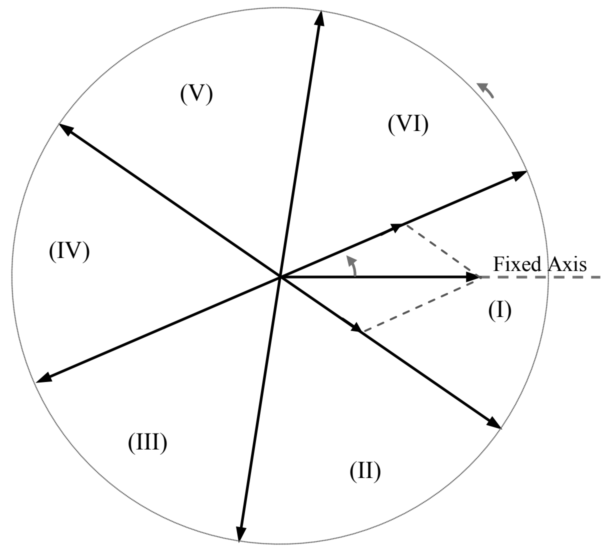

Figure 4.2: The line-to-line voltage phasors indicating the six sectors of the proposed control scheme.

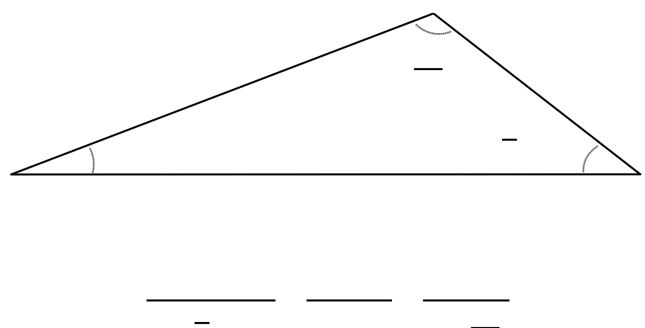

Figure 4.3: Sector (I) and the discharging time-intervals, and , as well as charging time-interval, , calculations.

Table 4.1: Sectors and switching states

I			0		0	
II		0		0		
III	0				0	
IV				0		0
V	0		0			
VI		0				0

Let us assume that the DC-link inductance, and the DC input voltage, , stay constant over a switching cycle, . Figure 4.5 shows the voltage and current waveforms of the DC-link inductor under this assumption. Using Figure 4.5, one can write the following equations based on the applied voltage across the DC-link inductor, over one switching cycle in Sector (I):

$$\text{—} \quad \text{for} \qquad (4.1)$$

$$\text{———} \quad \text{for} \qquad (4.2)$$

$$\text{———} \quad \text{for} \qquad (4.3)$$

where, and are the DC-link inductor currents at the beginning and the end of one switching cycle, respectively. Also, is the DC input voltage, is the value of the inductor, is the time elapsed for charging the DC-link inductor, and are the time-interval of injecting power from Phase-A to Phase-B and Phase-C respectively, and and are the instantaneous line-to-line voltages. Adding up the three above equations yields:

— ——— ——— (4.4)

Thus, one can write as follows:

— — — (4.5)

For a fixed switching frequency, , is constant and also .

Thus, (4.5) can be simplified as:

— — — (4.6)

Substituting, , by , one can write:

(4.7)

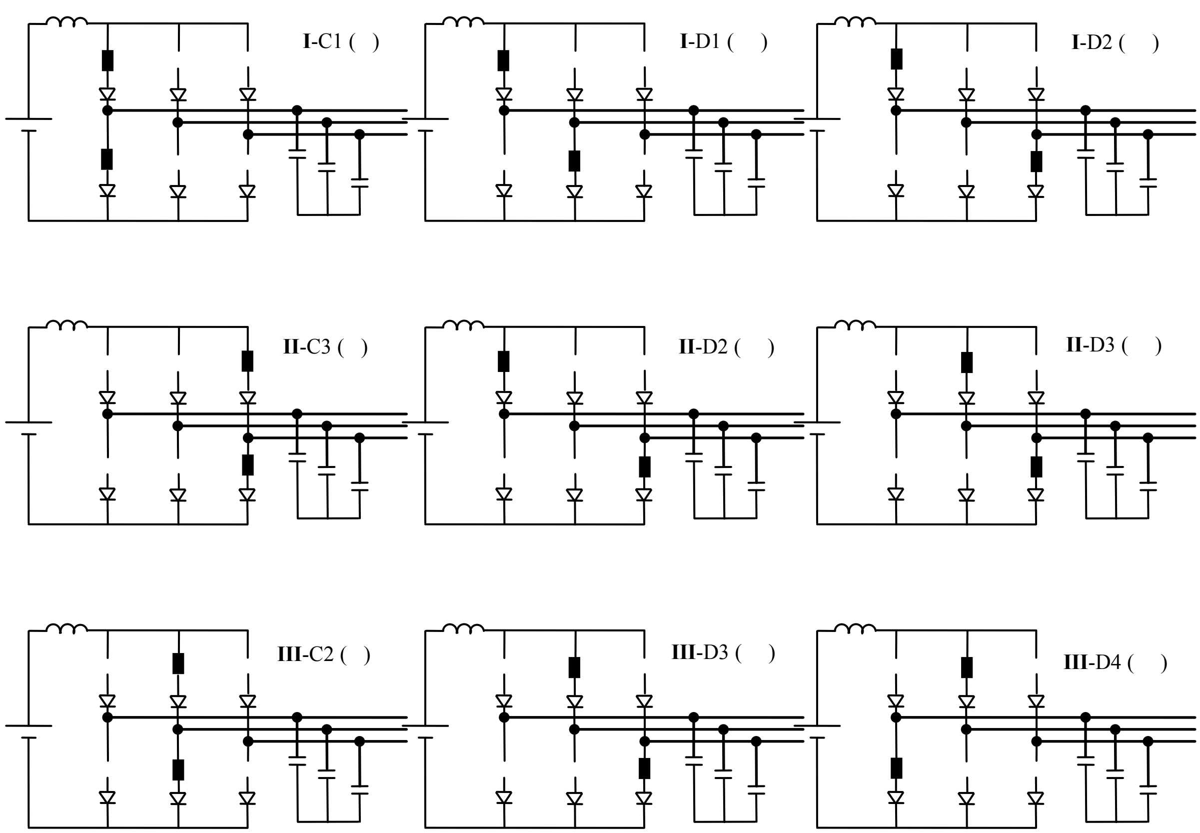

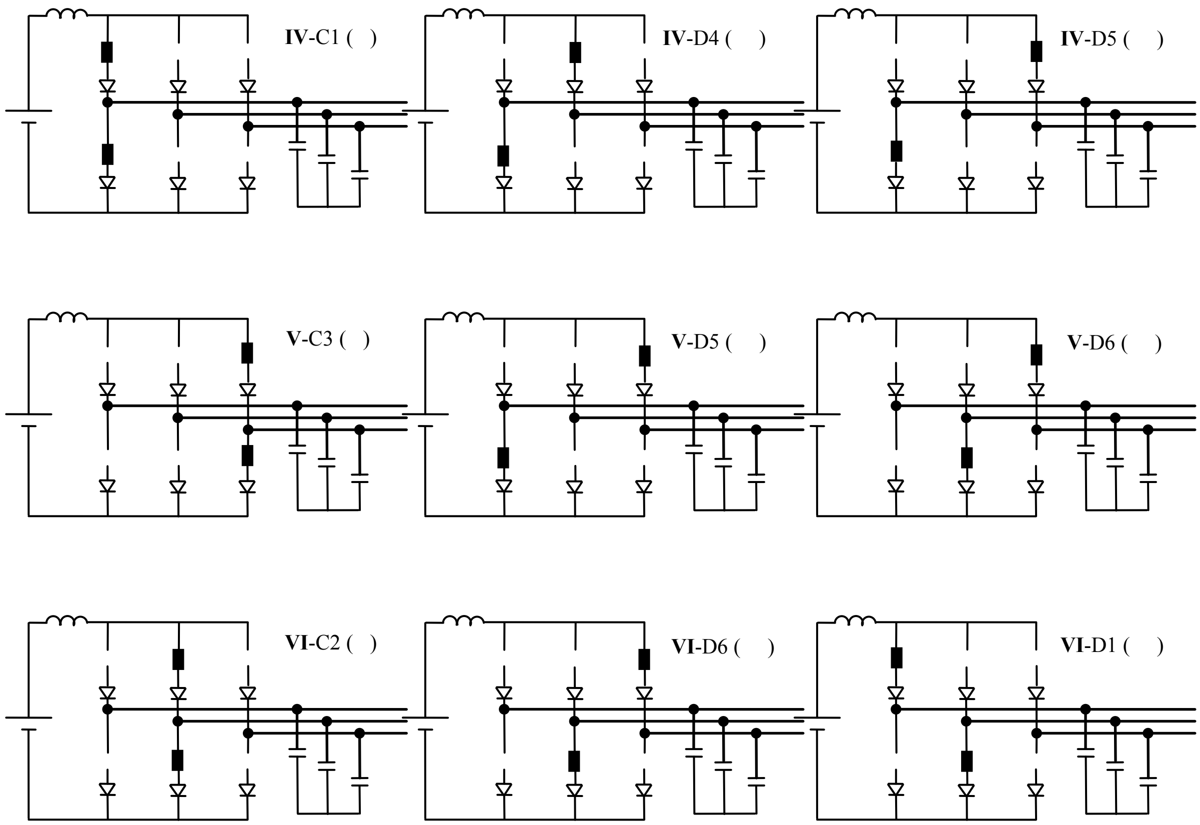

Figure 4.4: The charging (C1 – C3) and discharging (D1 – D6) states of operation for the CSI-based boost-inverter in each sector (three charging states and six discharging states in six sectors); the Roman numeral shows the sector number, and it is followed by the state number along with the time-interval in the state.

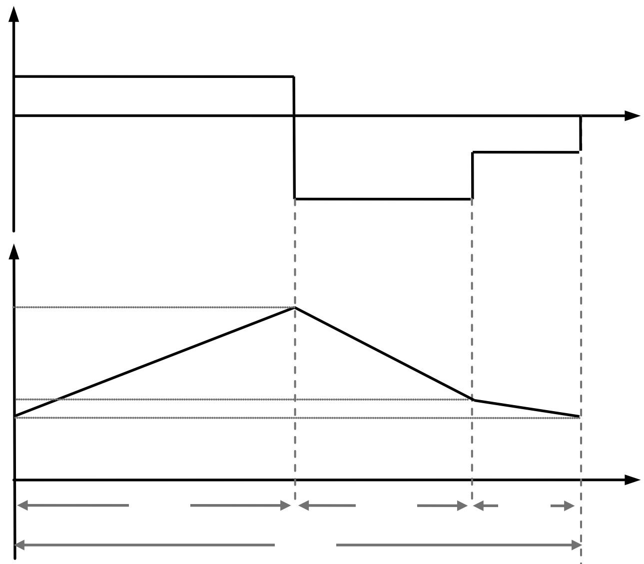

Figure 4.5: The voltage and current waveforms of the DC-link inductor over one switching cycle in Sector (I).

Notice, one can write the line-to-line voltages of the grid (or desired output voltages) as follows:

and

(4.8)

Thus, is given by:

(4.9)

Let us pick the discharging time-intervals, and , as follows:

, and

, for (4.10)

Accordingly, one can write the following expressions:

(4.11)

(4.12)

Substituting by (4.11) and by (4.12) in (4.7) yields:

(4.13)

In order to keep (4.13) always valid, the right side term of this equation should be a time-independent expression. Accordingly, must follow at the same angular speed, i.e., Hence, (4.13) can be rewritten as:

(4.14)

where, – – for Sector (I), see Figure 4.2, From (4.14), can be obtained as:

(4.15)

where, for the valid range of , the coefficient can vary within a range of . Therefore, if in (4.10) is substituted by (4.15), the discharging times, and , can be calculated, in steady-state and balanced conditions (i.e.), from the following equations;

(4.16)

(4.17)

Therefore, the charging time is obtained as; . Meanwhile, for , equations (4.16) and (4.17) can be rewritten as:

(4.18)

(4.19)

It should be noted that these are exactly identical to what one can obtain from the trigonometric identity illustrated in Figure 4.3, if and are replaced by .

4.2.2 Control Method for the Stand-Alone Case

For stand-alone conditions, one can consider the circuit topology shown in Figure 4.1, while the circuit breakers are open. Again, let us consider Sector (I) in Figure 4.2. Accordingly, one can write the following expression for the voltage phasor quantities:

(4.20)

For simplicity, let us assume that the output circuit is a series R-L load, i.e. ,. In this case, the line-to-line phasor voltages are obtained as and in term of , , and , which are the line currents of “A”, “B” and “C” phases, respectively. Notice that the line-to-line voltage, , , and , waveforms become sinusoidal when the line current waveforms are sinusoidal. If the PWM switching pattern is applied in the presence of the output AC capacitors, , as shown in Fig.2, the line current waveforms will be very close to sinusoidal. This means that the final equations in (4.16) and (4.17) will be valid for the stand-alone case, where the line-to-line voltages, , , and in (4.8) can be considered as the reference voltages. In this case, a closed-loop PI controller is required to regulate the output voltage through tuning the coefficient. This will be further discussed in the following subsection.

4.2.3 Controlling DC-link Inductor Current

In the previous subsections, the method of maintaining the DC-link inductor current at a fixed level was discussed and the charging and discharging time-intervals were formulated. It is now necessary to discuss the method of controlling the DC-link inductor current for both stand-alone and grid-connected applications. The question is, "what change must be applied to the previously defined coefficient , if the average current of the DC-link inductor is to be increased or decreased?" To answer this question, let us assume an incremental change, , between the DC-link inductor at the beginning and end of each switching cycle, this can be formulated as:

(4.21)

Using (4.7), one can write:

(4.22)

Hence, in (4.10) has to be adjusted as:

(4.23)

Again, the charging time-interval, , and discharging time-intervals, , and , are obtained as:

(4.24)

(4.25)

(4.26)

Accordingly, the modified coefficient, , must be applied to adjust the level of DC current at the DC-link inductor. Furthermore, a closed-loop PI controller is required to minimize the steady-state error. This can control the amount of injected power in the case of grid-connected applications and regulate the output voltage in the case of stand-alone applications.

4.4 Summary

In this chapter, the importance of single-stage converter systems for SE (PV arrays and fuel-cells) applications has been presented. A novel switching pattern has been proposed based on the CSI topology. The proposed pattern is based on the SVPWM concept. However, the presented switching pattern contains a total of nine switching states, including three charging states and six discharging states with only two switches conducting at any given instant. In this method the charging states are necessary in order to boost the output voltages of PV arrays or fuel-cells. It has been also demonstrated that the CSI topology in conjunction with the developed switching pattern is capable of providing the required residential AC voltage from a low DC voltage of one PV panel at its rated power for both linear and nonlinear loads.

CHAPTER 5

POWER CONTROL

The relationship between the dc inductor current, output ac current, reflected voltage from the ac side to the dc side, and the circuit parameters, along with the control variables is investigated in this section. In order to independently control the reactive and active power, the modulation index, , is introduced in the past chapters. This is in addition to the other control parameter, which is the angle between the desired output current of the inverter, and the grid voltage. This angle can be specified such that the output reactive power of the inverter can be controlled. Therefore, by controlling the coefficient and angle , the output active and reactive power are controlled.

5.1 Input Power Calculation

In this subsection, the input power is calculated in terms of the modulation index and the circuit parameters; (see Figure 5.1). The average value of the grid voltage over a sector, in radians or in seconds, referred to the dc side of the inverter, , can be approximately obtained as follows.

From the previous chapter, the two discharging time intervals were calculated in (3.18) and (3.19). In order to have control on the output injected current, the coefficient of the discharging time intervals is called , and should be specified by the control system. Accordingly, one can rewrite (3.18) and (3.19) as:

$$- \quad , \qquad (5.1)$$

where is the angle of the applied voltage, and must vary from to – during any sector. Now, sector "I" is picked up for the rest of the calculations, as mentioned previously, and the three phase-to-neutral voltages are assumed as:

$$ \tag{5.2} $$

In order to replace the inverter system with its equivalent in steady-state, the reflected average voltage from the output of the inverter to its input needs to be obtained. In sector I, phase "a" voltage is in its extreme positive state. Therefore, with the mentioned phase angles for the three-phases, sector I interval will be from — –. So, the averaging is performed in this time frame for sector I.

Note that the two discharging time intervals are calculated with the assumption – during any sector. Also, the angle of phase "a" voltage varies from — – during the sector, i.e., — –. Thus, the angle will be – during the sector. Accordingly, one can have:

$$ \tag{5.3} $$

Now, based on these coordinated time intervals, the average voltage reflected from the output of the inverter to its input can be obtained. Note that in the first time interval, , the line to line voltage is applied, while in the second one, , the line to line voltage is applied to the input. In addition to this, zero voltage is applied during the charging times. Therefore, the integration of the overall voltage reflected to the input during sector I can be written as:

$$ \tag{5.4} $$

---

where is the duration time of sector “I”, and , is the total voltage drop over the switches and diodes in the current path. Note that this voltage drop is present in the current path in both charging and discharging states. Replacing the voltages by (5.2), and the time intervals by (5.3), one can obtain:

(5.5)

Since the switching cycle, , is very small, one can consider it as a differential time interval, , and convert the summation in (5.5) to an integration:

(5.6)

After doing some mathematics and trigonometry, one can obtain the average voltage as:

(5.7)

Equation (5.7) is valid only for the situation in which the injected output current is completely in-phase with the grid. Now, suppose that this current is shifted by an angle of , with respect to the grid voltage. This will cause a different value for the calculated reflected voltage . If this phase shift angle is considered in the previous calculation, i.e., from (5.3) to (5.7), and by doing some trigonometric calculations, the resultant value is:

(5.8)

Using the proposed switching pattern, along with (5.8), one can calculate the average value of the dc-link inductor current as follows:

(5.9)

where, and are obtained from and , respectively. Thus, the input power is a function of the modulation index and can be written as follows:

(5.10)

As can be seen, the input power and the power loss increase as the modulation index decreases.

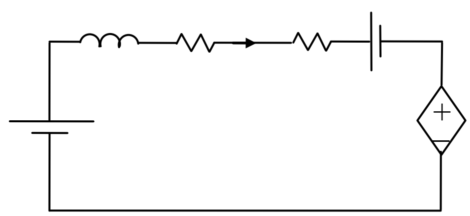

Figure 5.1: The grid-tie boost-inverter equivalent circuit referred to the dc side of the inverter

5.2 Amplitude of the ac current

In this section, the amplitude of the output ac current is calculated, assuming that there is a dc current passing through the dc inductor. The ac current is composed of two parts: one injected from the inverter, and the other from the ac capacitors. These two currents are perpendicular with respect to each other, assuming that the inverter is generating only active power, without any reactive power. The first part is calculated herein, and the total current can be calculated knowing the value of the ac capacitors, and consequently their reactive current. In other words, the total current is the geometric summation of the two mentioned currents. Again, the three voltages are assumed as in (5.2), sector I is picked up for the calculation, and phase "a" current is calculated.

Since phase "a" is in its maximum positive state during the sector, the dc current is injected into this phase in both discharging time intervals. Assuming these time intervals as in (5.3), the average current for a switching cycle can be written as:

$$- \qquad\qquad -$$

(5.11)

In the next sector, phase "c" voltage is in its extreme negative state, and the voltages and are applied during the first and second discharging times. Therefore, the dc current is injected into phase "a" only during the first discharging ( ). Note that the right value for the angle should be replaced, in order for the time durations to be true. Since varies between − and − during the sector, i.e. − −, the angle is then:

$$- \qquad (5.12)$$

Accordingly, the two discharging time intervals are:

$$- \quad , \qquad - \qquad (5.13)$$

Thus, the average current of phase "a" in this sector will be:

$$- \qquad (5.14)$$

If the same process is followed for the next four sectors, the same results will be obtained. Therefore, the output ac current of phase "a" only from the inverter side is calculated to be:

(5.15)

This equation means that the inverter current for any of the three phases is an in-phase sinusoidal current with the amplitude of . Now, the question is what happens to this current when a phase shift of is applied in the switching. Following the same procedure to calculate the current, results in the same amplitude, with a change of in the phase angle. In other words, by shifting the switching time by , (5.15) will be modified to:

(5.16)

In order to obtain the total ac current, the capacitors current should be calculated first, knowing the grid voltage, and the capacitors values. When this current is known, obtaining the total current will be a straightforward geometric summation of the two current parts, considering their amplitudes and phase angles.

Therefore, it can be demonstrated using the aforementioned switching pattern that the fundamental component of the inverter output current in phase-A (before ac capacitors in Figure 3.1) can be written as follows:

(5.17)

Accordingly, the three-phase active and reactive power can be written as:

(5.18)

(5.19)

where, is the generated reactive power of the ac capacitors, , in Figure 3.1 For this purpose, two PI controllers are implemented in order to control these parameters. This means that the desired values of *P* and *Q* are compared with the measured ones to adjust the above-mentioned parameters (see Figure 3.1). It should be noted that the desired value of *P* is normally dictated by the MPPT algorithm. However, the desired value of *Q* can be arbitrarily selected. Notice that as the injected reactive power increases, the total harmonic distortion (THD) of the output current is amplified. Hence, the injected reactive power has an upper level limitation. In many cases, the unity power factor (right before the ac capacitors in Figure 3.1) is a desirable condition. This means that a zero value for injected reactive power. However, the ac capacitors, , always inject a fixed amount of reactive power, as shown in (5.19). This reactive power can be approximately calculated as:

$$= \qquad (5.20)$$

5.3 Maximum Power Point Tracking

One of the most important objectives of any single-stage or multi-stage grid-connected PV converter is to extract as much power as possible from the PV panels. There are various methods to perform MPPT [6]. In the proposed topology, MPPT can be achieved by controlling the dc inductor current. To integrate this capability into the switching method, the modulation index, , was introduced in (5.1). It should be noted that, a larger value of will result in a smaller charging time interval,

, and accordingly, a smaller dc-link inductor current, as can be seen in (5.9).

Therefore, the modulation index can be adjusted to track the PV's maximum power point. Among the various MPPT methods, the method of Hill Climbing seems to be a suitable candidate for the proposed single-stage boost inverter.

5.4 Simulation Results

5.4.1 DC Current and Reflected DC Voltage to the Input

In this section, the derived formulas for the dc current, and the reflected dc voltage to the input are verified through simulations. The simulated circuit is shown in Figure 3.1, and the circuit parameters are chosen as: ,

(i.e., in a Δ-connection) , . The PWM switching frequency is

, and the line-to-line voltage of the grid is set to be equal to 208 Vrms. The simulation results are shown in Table 5.2 for three different PV panels. The electrical specifications of the panels are shown in Table 5.1. These specifications include the panel number provided by its producer, its voltage, current, and power while at the maximum power generation point, and the open circuit voltage and short circuit current at the same conditions.

In table 5.2, the simulation results of the injected ac current into the grid for the two mentioned panels are shown. Panel 1 and Panel 2 are BP3110 and BP4175B, respectively. In this table, and are the input dc voltage (panel voltage). The reflected voltage from the output of the inverter to its input, or the applied voltage from the ac side to the dc side has been shown as . The amplitude of the total injected ac current to the grid, , along with the phase difference between the grid voltage and the injected active current, , and the modulation index of are shown in Table 5.2.

Table 5.1: Electrical Specifications of the PV Panels

Panel					
BP3110	16.9	6.50	110	21.6	7.40
BP4175B	35.4	4.94	175	43.6	5.45

Table 5.2: Simulation Results of the ac current test for the PV panels in Table 5.1

Panel						
BP3110	16	5.5	14.3	2.9	0	0.49
BP3110	16	5.5	14.3	3.7	–	0.56
BP3110	16.9	6.5	14.9	3.5	0	0.51
BP3110	16.9	6.5	14.9	4.5	–	0.59
BP4175B	33	4	31.8	1.2	0	0.12
BP4175B	33	4	31.8	1.4	–	0.14
BP4175B	35.4	4.9	33.9	1.3	0	0.13
BP4175B	35.4	4.9	33.9	1.6	–	0.15

As can be seen in Table 5.2, the amplitude of the ac current has been increased with the – applied phase shift between the grid voltage and the injected active current. This is to show that the inverter has the capability to generate and inject reactive power into the grid, with the same amount of active power. Also, the amplitude of the ac current and the associated , , and is in agreement with the formulas obtained in the previous section.

5.4.2 Active and Reactive Power Control

In this section, the simulation results are presented to demonstrate how the injected active and reactive power can be independently controlled. While the desired (or reference) value of the active power, , can be obtained from the Hill Climbing method for maximum power point tracking, the desired (or reference) value of reactive power, , can be selected within a certain range.

In Figure 5.2 (a), the dynamic behaviors of the injected active and reactive power are shown over 3 seconds (between 1 and 4 seconds) when instantly changes from 200 to 300 watts at and is set to be equal to It should be noted that (which is an equivalent value for right before the ac capacitors, , in Figure 3.1) can be initially obtained after the system installation. This calculation is as a part of the inverter auto-tuning algorithm. In the auto-tuning algorithm, the is calculated while the control parameters are set to be and As can be seen in Figure 5.2 (b), both control parameters vary to keep Vars while P was increasing from 200 to 300 watts (i.e., watts). Moreover, the dynamic of dc-link inductor current over this change is also shown in Figure 5.2 (c). In Figure 5.2 (d), the dynamics of the active and reactive power are shown again over 3 seconds when instantly changes from to 340 Vars at . In this case, Watts.

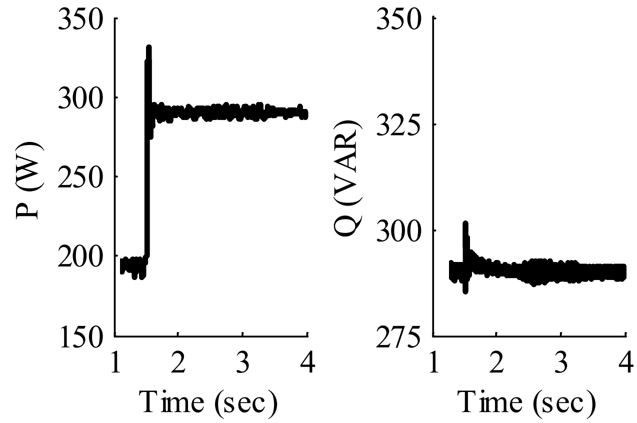

(a) The output P and Q of the inverter

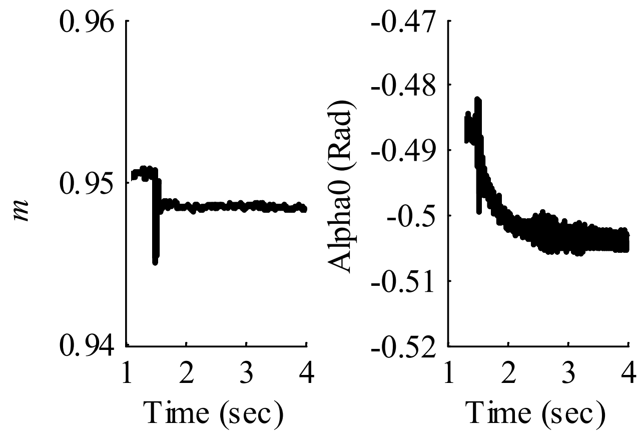

(b) The coefficient and the angle of Figure 5.2 (a)

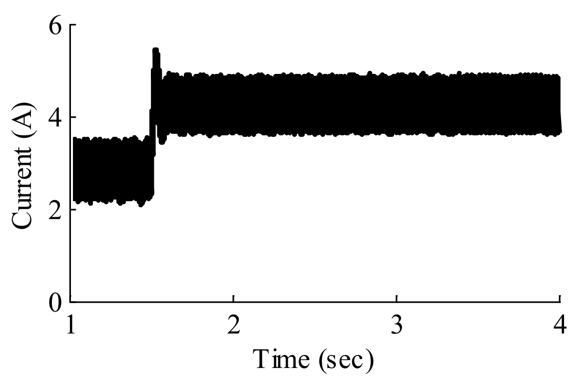

(c) The dc-link inductor current of Figure 5.2 (a)

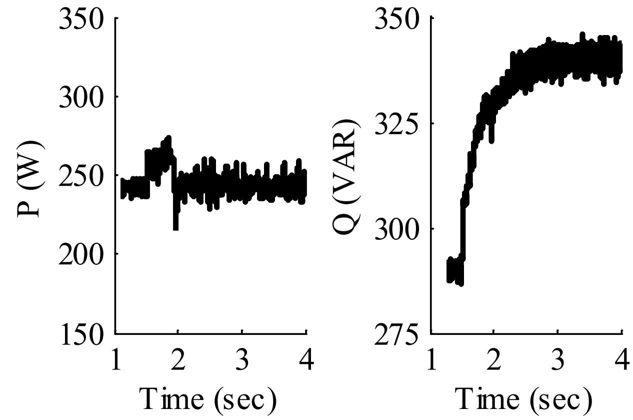

(d) The output P and Q of the inverter

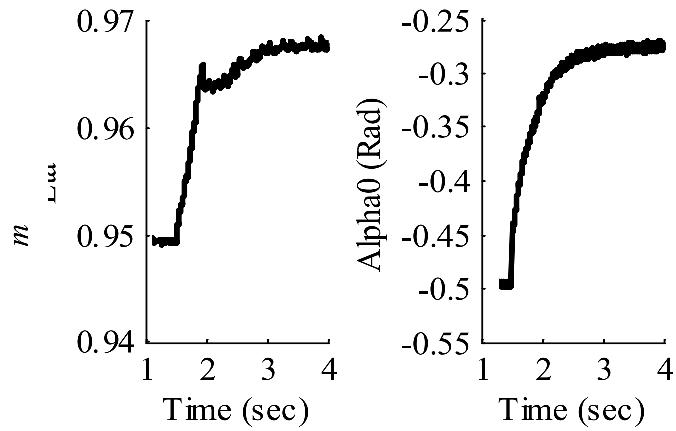

(e) The coefficient *m* and the angle of Figure 5.2 (d)

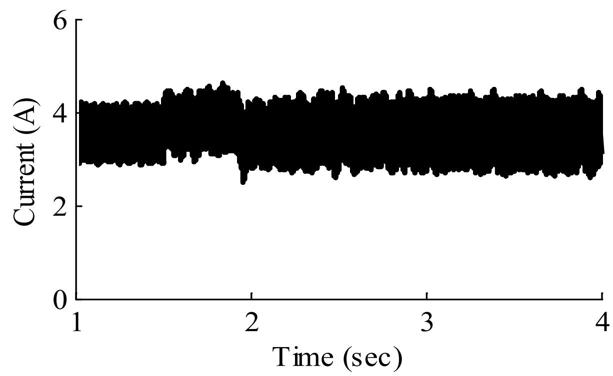

(f) The dc-link inductor current of Figure 5.2 (d)

Figure 5.2: The simulation results, for the independent active and reactive power control cases

5.4.3 Reactive Power Generation and Injection into the Grid

In this section, the capability of CSBI in providing reactive power is examined using simulation results. Thus, the CSBI topology with the associated control scheme and switching pattern are implemented in MATLAB SIMULINK, as shown in Figure 3.1, and main circuit parameters are given in Table 3.3. To simplify the system, a fixed dc voltage source was considered as the input source. It should be noted that this simplification does not affect the concept of generating reactive power in this circuit. The control system consists of two PI controllers, in order to separately regulate the two modulation indices, and m. As mentioned earlier, there is not any need to use the rotational reference frame conversion blocks in the proposed approach. Moreover, the actual values of the active and reactive power will be used as feedback signals of the PI controller for m, and calculations, respectively. In other words, in the controller blocks, one PI (P-PI) regulates the output active power by adjusting the value of m, while the other one (Q-PI) performs the same for the output reactive power by adjusting .

Two scenarios have been studied in Table 5.4 and Table 5.5, and the results are also plotted in Figures 5.3 and 5.4, respectively. In the first scenario, the active power is adjusted at 620 watts, while varies from -30 degrees to 40 degrees. As one can see, as increases m is automatically increased to keep the value of the active power at 620 watts. This is in an agreement with what was explained in the previous section. The results are also demonstrated in Figure 5.3. For better understanding of Table 5.4, it should be mentioned that the column is obtained from the algebraic summation of all generated and consumed reactive powers. In other words, the generated reactive power by the ac capacitors is subtracted from the output injected reactive power, and the result is added to the consumed var by the inductors. The final resultant var is called the net generated reactive power by the inverter, . As can be seen in Table 3.5, the output reactive power increases as the value of decreases. Moreover, the magnitude of the output ac current is also increases, while the output injected active power is kept constant. It means that the angle between the output voltage and current has been increased. Another important point is that the other modulation index, *m*, has an increasing profile, as was expected, to keep the active power at the commanded level.

Table 5.3: The CSBI Important Components in Simulation

70 V	4 mH	11.2 F	2.4 mH	208 Vrms

Table 5.4: CSBI Simulation Results for a Constant Output Active Power, P_g

									)
-30	0.9423	620	600	582	-15	33	214.5	2.4	2.5
-21	0.9505	620	700	586	-18	132	215.1	2.6	3
-9	0.9606	620	840	590	-22	272	215.9	2.9	3
0	0.9715	620	970	594	-27	403	216.6	3.2	4
9	0.9838	620	1130	601	-35	564	217.8	3.6	3
21	1.0061	620	1430	611	-50	869	219.7	4.3	3
30	1.0275	620	1800	627	-76	1249	222.4	5.3	4
39	1.0557	620	2430	653	-133	1910	227.0	7.0	4
40.5	1.0596	620	2590	659	-149	2080	228.1	7.4	6

Table 5.5: CSBI Simulation Results for a Constant Output Complex Power, Sg

									THD
-30	0.9146	1800	660	564	-76	172	210.9	5.3	4
-21	0.9250	1670	920	569	-76	427	212.0	5.3	2.5
-9	0.9404	1470	1220	576	-76	720	213.3	5.3	2.5
0	0.9553	1290	1400	581	-76	895	214.1	5.3	2.5
9	0.9734	1100	1560	584	-76	1052	214.7	5.3	2.5
21	1.000	840	1720	588	-76	1208	215.4	5.3	6

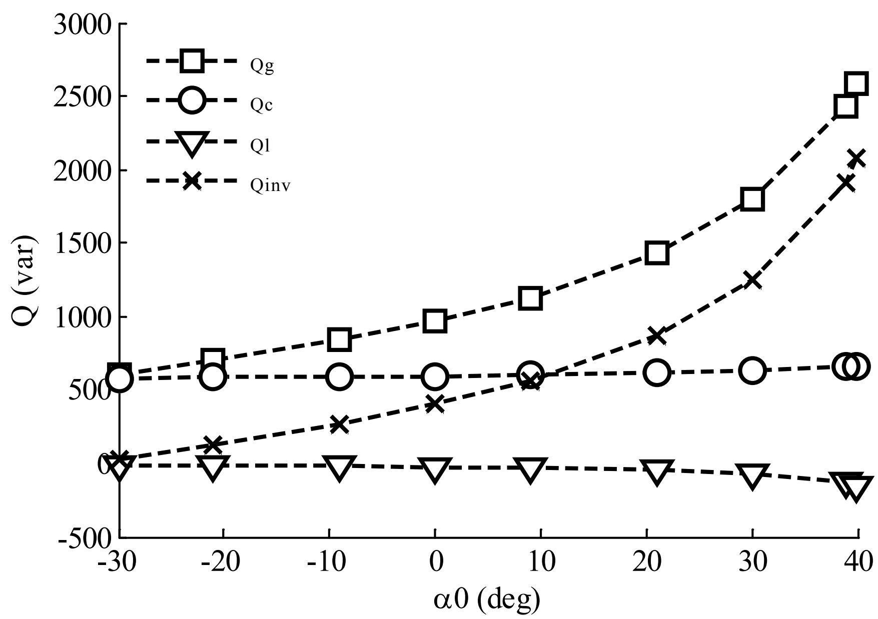

Figure 5.3: Simulation results of reactive power vs. for constant

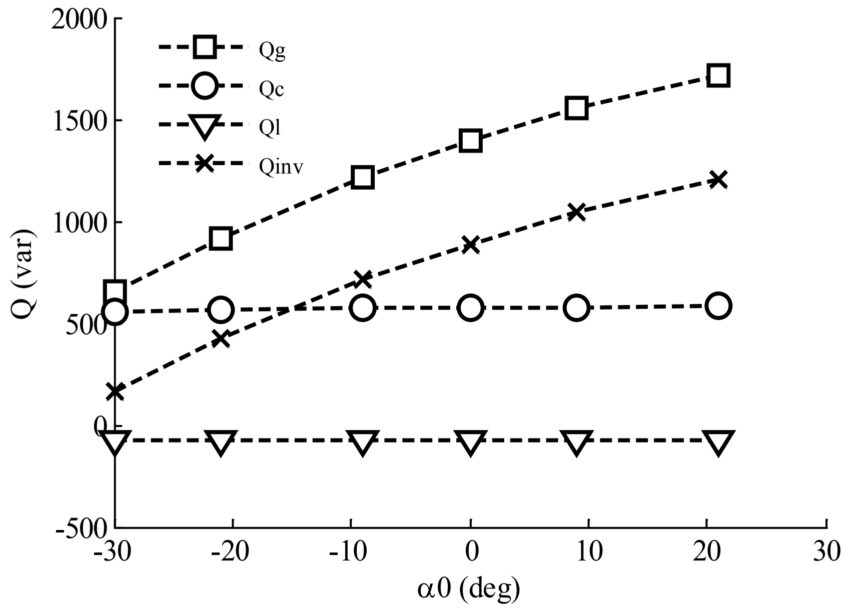

Figure 5.4: Simulation results of reactive power vs. for constant

In the second scenario, the output current is adjusted at 5.3A rms (i.e., S = ~ 1.9 kVA), while varies from -30 degrees to 21 degrees, and the current THD stays below the accepted level of ~ 5%. Again, as can be seen in table V, the output reactive power increases as the value of decreases. It means that the angle between the output voltage and current has been increased, while the magnitudes of current and voltage are constant.

5.5 Summary

In this chapter, the required equations for the active and reactive power control based on the proposed switching pattern were obtained. The relationship between the output injected active and reactive power to the switching parameters were extracted, and the amplitude of the output ac current were calculated. It was shown how the desired dc current is constructed inside the dc inductor, and how the desired values of active and reactive power are injected into the grid through regulating the two major control parameters: the modulation index, and the switching angle. Then, the accuracy of the obtained formulations were examined by the simulation results, doing different scenarios for both active and reactive power control, and the results were in agreement with the claims.

CHAPTER 6

EXPERIMENTAL RESULTS

6.1 Stand-alone case

In order to verify the developed PWM switching pattern, a laboratory scaled CSI was built, (see Figure 6.1), and tested for an R-L load. The switching signals were generated by a CLP1104 dSPACE system which was linked to MATLAB Simulink, and the switching frequency was chosen to be 3.0 kHz because of the limitations of dSPACE. The measurements in this experiment were performed using a LeCroy Waverunner 64XI oscilloscope with one CP031 current probe, one CP030 current probe, and one ADP305 differential voltage probe. The bandwidth of the oscilloscope is 600MHz, while the bandwidths of the CP031, CP030, and the ADP305 are 100MHz, 50MHz, and 100MHz, respectively. Figure 6.1 shows a scene of the experimental setup and Table 6.1 gives some information on the CSI circuit elements.

In Figure 6.2, the output line-to-line voltage and current waveforms are shown when an R-L load with $R=20\Omega$ and $L=2.7mH$ was fed by the CSI. In this test, the input DC voltage was 16V and the desired amplitude of the output line-to-line voltage was 45V (peak). As can be seen in this figure, the output voltage follows the reference well, and the shape of the current and voltage waveforms are very close to a sinusoidal waveform.

Table 6.1: The specifications of the experimental results

				IGBT	Diode
5.6 µF	0.12 mH	0.1 µF	2.0 mH	IRG7PH30K10PBF	SBT350-04L

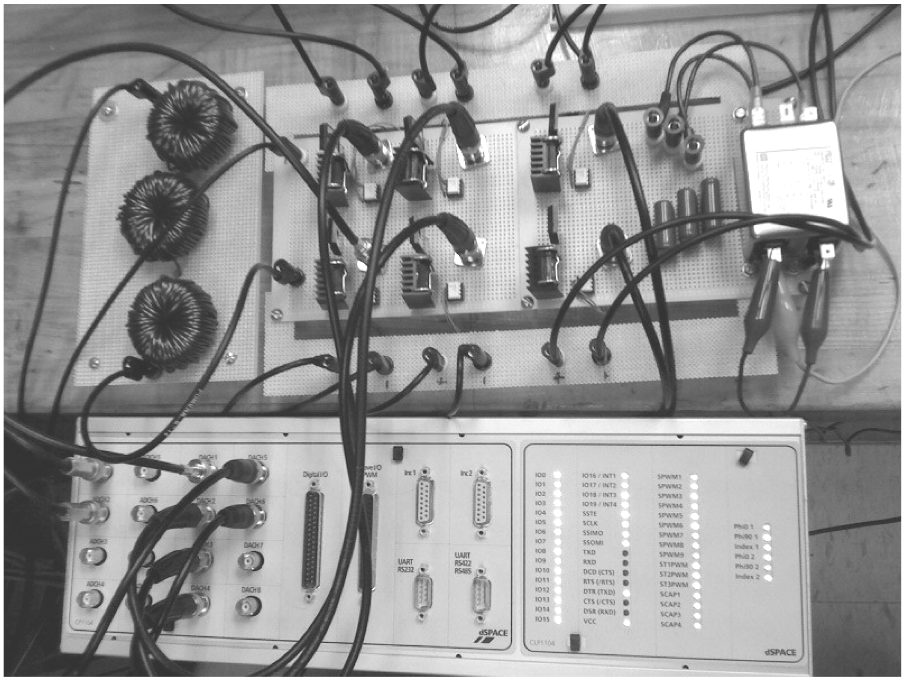

Figure 6.1: The experimental prototype.

Also, the frequency spectrums (FFT) of the voltage and current waveforms are shown in Figure 6.3. As can be seen in this figure, there are some harmonics around 3.0 kHz which are due to the switching frequency. In Figures 6.4 and 6.5, the voltage and current waveforms of the DC-link inductor are shown for the same conditions. The charging and discharging time-intervals (states) are quite visible in Figure 6.5. In Figure 6.6, the output voltage and current waveforms of the inverter are depicted for the same test. Notice that the output current of the inverter is composed of positive and negative pulses, the widths of which are modulated according to a sinusoidal reference, (see Figure 6.7). In order to check the ability of the control system to maintain a fixed output voltage for different load conditions, another test was performed with a DC input voltage equal to 10V and an R-L load of $R=40\Omega$ and $L=5.4mH$. The output line-to-line voltage and current waveforms are shown in Figure 6.8. As can be seen in this figure, the amplitude of the output voltage is constant, although the output current is halved due to the higher impedance of the load. This demonstrates while the inverter is a CSI, it can operate in a voltage-regulated mode.

In particular, for PV based energy conversion applications, the produced DC voltage of a PV panel at its maximum power (150 watts) is typically about 35 V. For instance, if the three-phase boost-inverter should feed a 60Hz, 208V (line-to-line), i.e., 120V (line-to-neutral) AC load (or grid), then the 35 VDC of the PV panel must be boosted and inverted to the required AC voltage, i.e., 208V rms. In order to verify the capability of the presented control scheme, a laboratory test was performed by connecting the prototype boost-inverter to a Y-connected three-phase 340Ω resistive load at 130 watts. The output line-to-line voltage and current waveforms and associated frequency spectrums are shown in Figures 6.10 and 6.11, respectively. Furthermore, the line- to-line voltage and current waveforms at the boost-inverter output terminals as well as their associated frequency spectrums are shown in Figures 6.12 and 6.13, while a resistive load (680 Ω) was fed through a full-bridge three-phase rectifier. As can be seen in this figure, the CSI circuit topology in conjunction with the developed control scheme is also capable of feeding nonlinear loads.

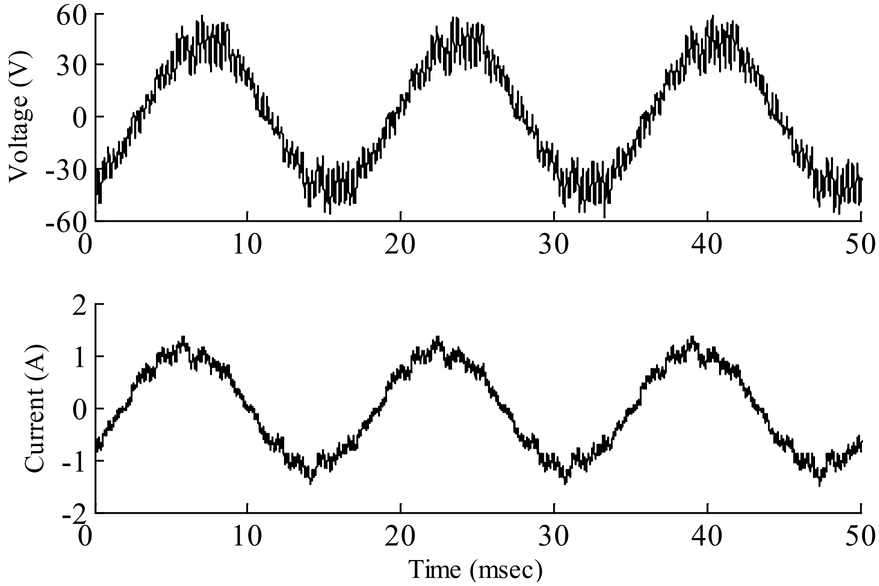

Figure 6.2: The load line-to-line voltage and a phase current waveforms when V_{dc}=16V, R_{load}=20 Ω, L_{load}=2.7mH, and V_{ref} =45V (peak).

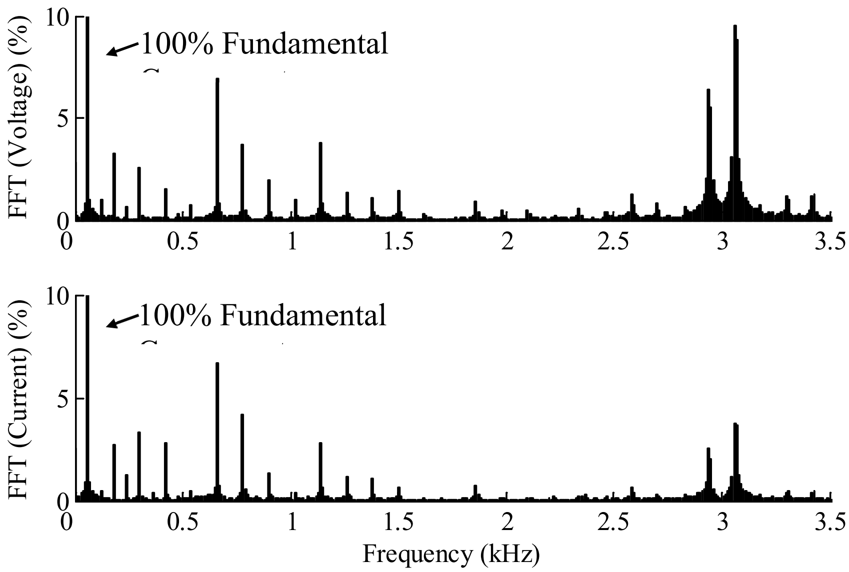

Figure 6.3: FFT spectrum of the load line-to-line voltage and the phase current waveforms of Figure 6.2.

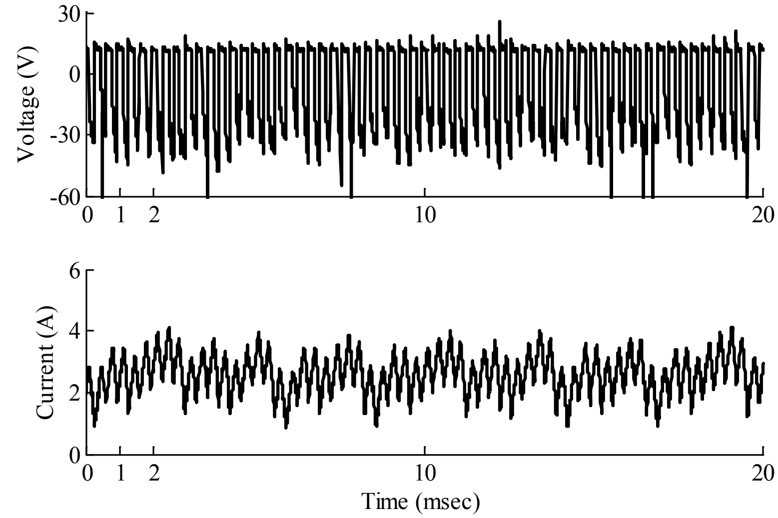

Figure 6.4: The inductor voltage and current waveforms when V_{dc}=16V, R_{load}=20 Ω, L_{load}=2.7mH, and V_{ref} =45V (peak).

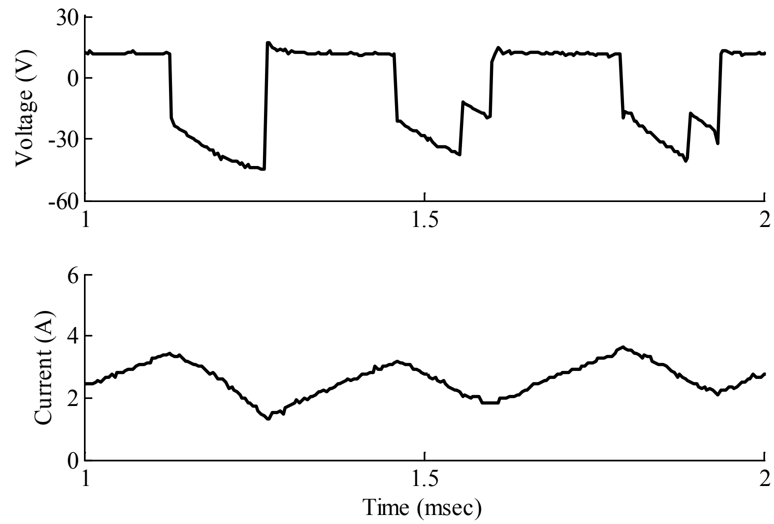

Figure 6.5: The expanded inductor voltage and current waveforms of Figure 6.4 between 1 and 2 msec.

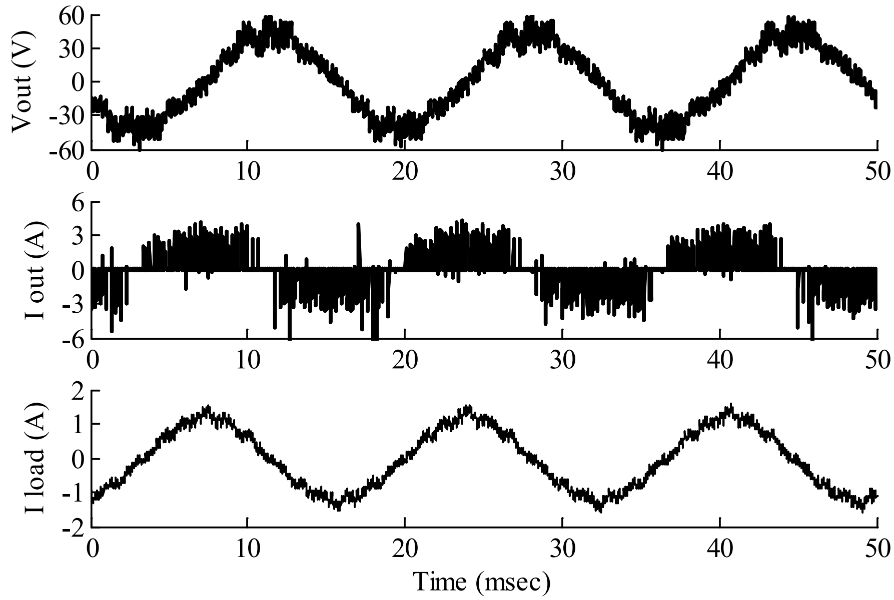

Figure 6.6: The line-to-line output voltage and current waveforms before and after C_{ac}, when V_{dc}=16V, R_{load}=20 Ω, L_{load}=2.7mH, and V_{ref} =45V

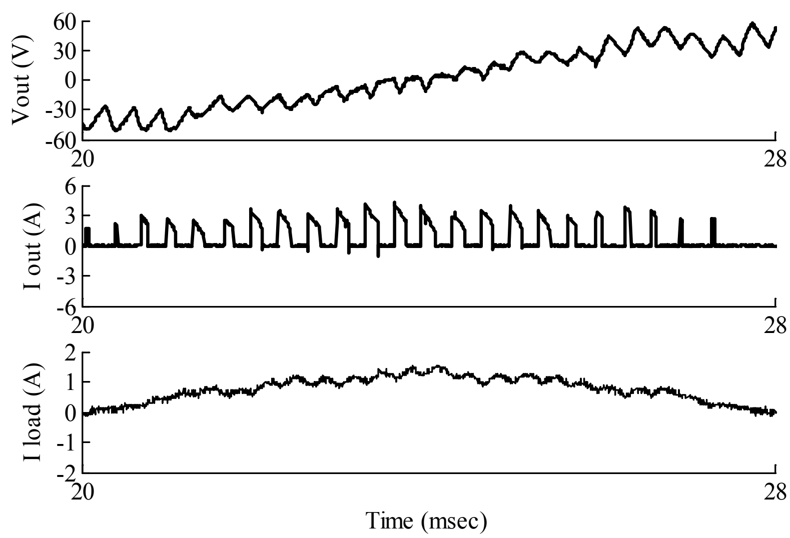

Figure 6.7: The expanded voltage and current waveforms of Figure 6.6 between 20 and 28 msec.

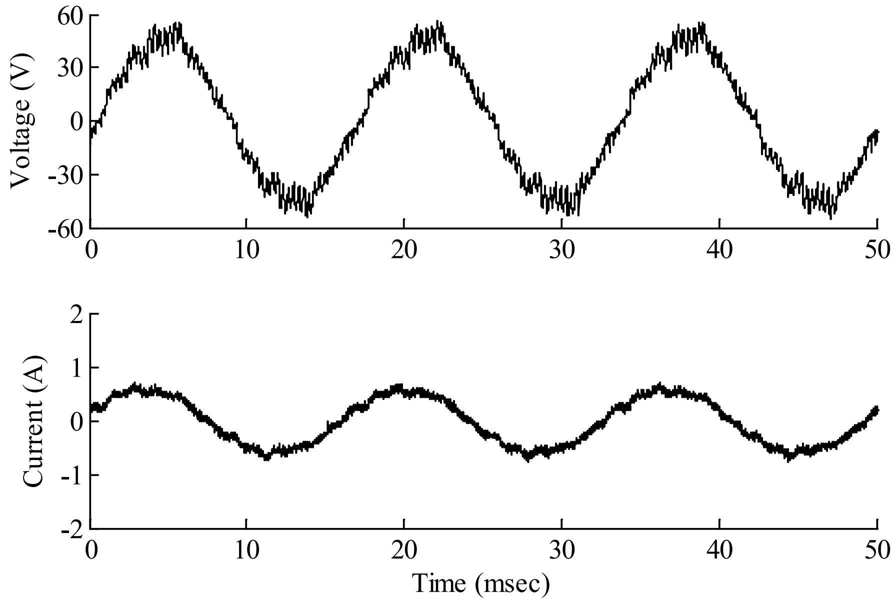

Figure 6.8: The load line-to-line voltage and a phase current waveforms when V_{dc}=10V, R_{load}=40 Ω, L_{load}=5.4mH, and V_{ref} =45V (peak).

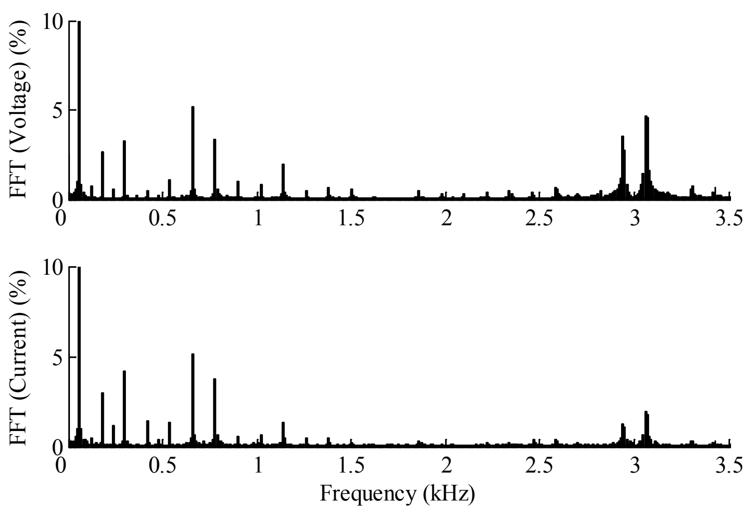

Figure 6.9: FFT spectrum of the load line-to-line voltage and the phase current waveforms of Figure 6.8.

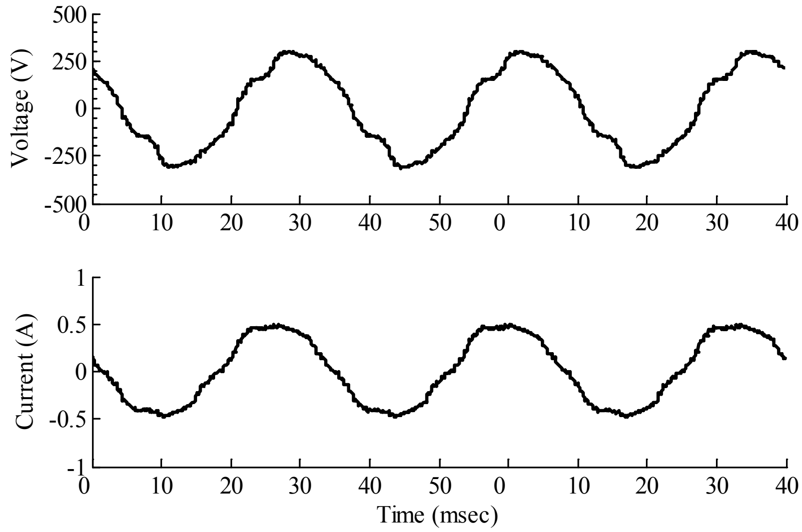

Figure 6.10: The load line-to-line voltage and a phase current waveforms when V_{dc}=35V, R_{load}=340 Ω and V_{ref} =208V (rms).

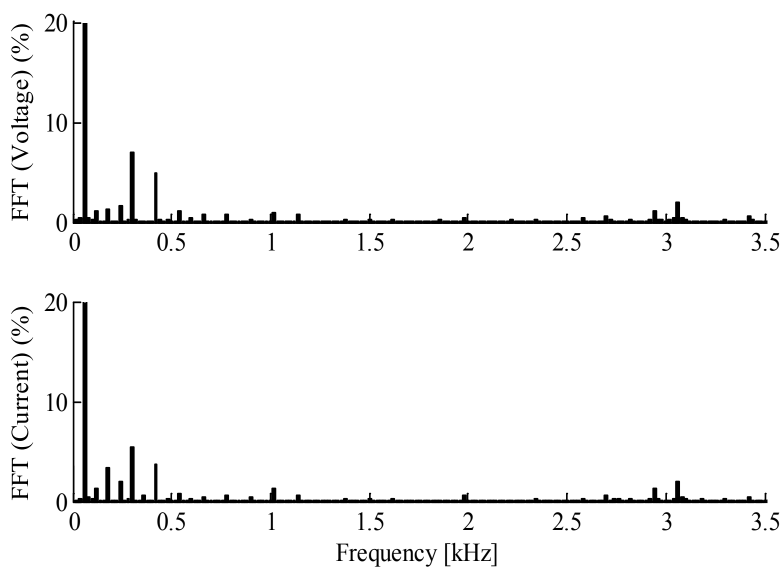

Figure 6.11: FFT spectrum of the load line-to-line voltage and the phase current waveforms of Figure 6.10.

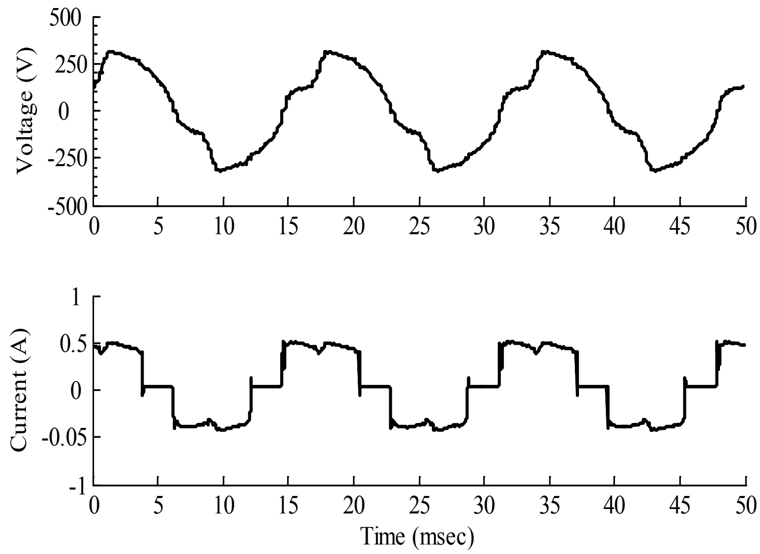

Figure 6.12: The load line-to-line voltage and a phase current waveforms when V_{dc}=35V, R_{load}=680 Ω (fed through a three-phase full-bridge rectifier), and V_{ref} =208V (rms).

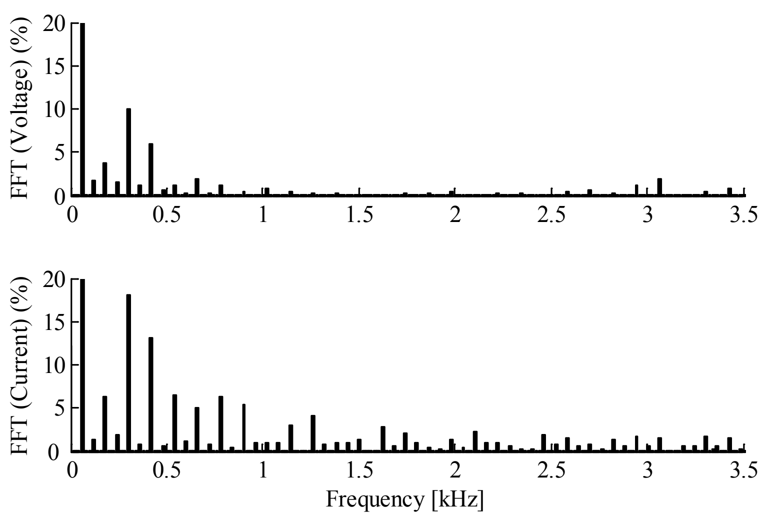

Figure 6.13: FFT spectrum of the load line-to-line voltage and the phase current waveforms of Figure 6.12.

6.2 Grid-connected case

In this section, the experimental results were performed in order to verify the aforementioned claims for the grid-connected case. The control section is implemented using MATLAB Simulink in conjunction with dSPACE 1104 control block, which is interfaced with the hardware. Also, the most important components of the hardware are given in Table 6.2. In this section, the values of voltages, currents, and powers are given in p.u. The output active power, , is calculated using two line-line voltages, along with two phase currents ( ). Then, knowing the amplitude of both the grid voltage, and the phase current, the output apparent (complex) power, , was calculated. Also, the output reactive power was obtained using this equation; , where the harmonics effect on the reactive power calculation were neglected.

As was mentioned in the previous sections, the ac capacitors, , at the output of the CSBI topology, (see Figure 4.1), generates almost a constant reactive power, . This can also be seen in the experimental results, where the generated reactive power by the ac capacitors is almost 600 VAR in the test setup.

Table 6.2: The specifications of the experimental setup

			IGBT	Diode
20 mH	3 mH	15 F	IRG7PH30K	DSEP 30-12

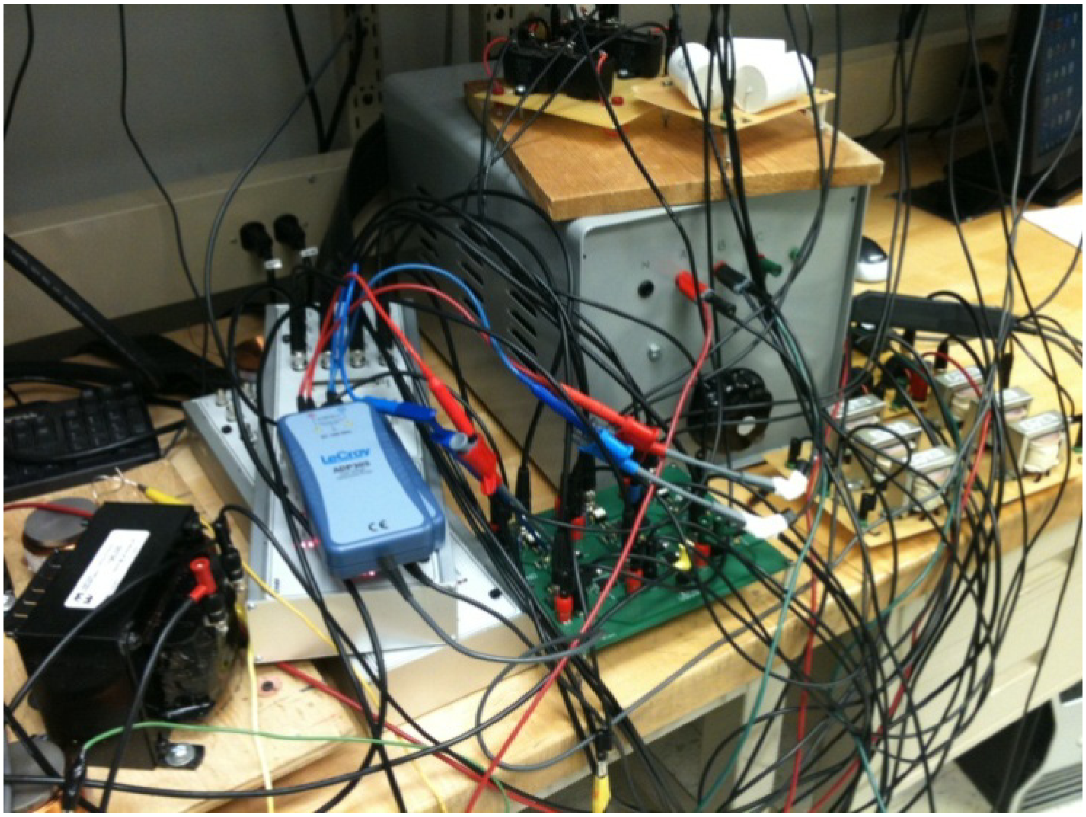

Figure 6.14: Experimental prototype for the grid-connected case

6.2.1 Active Power Control

In this test, the initial values of the active and reactive power are W and VAR over seconds. At seconds, the reference signal of the active power is changed to W, while the reference signal of the reactive power stays the same. The experimental results are demonstrated in Figures 6.15 through 6.20.

The input dc voltage and the grid line-line voltage are 50 Vdc, and 200 Vrms, respectively.

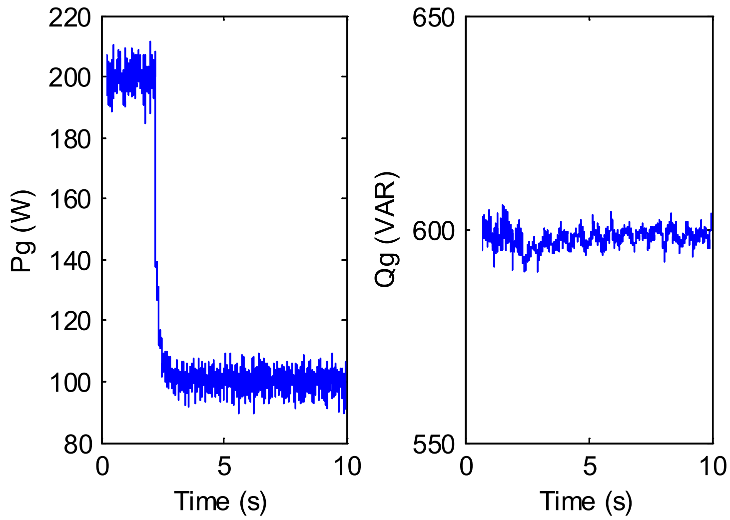

Figure 6.15: The output active power (left), and the output reactive power (right) when a step change of 100 W in the output active power is applied at t=2 sec.

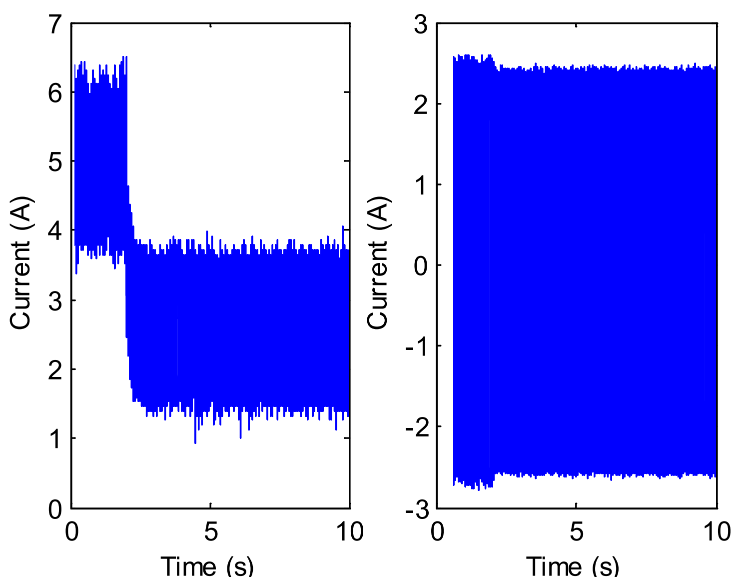

Figure 6.16: The input dc current (left), and the output ac current (right) when a step change of 100 W in the output active power is applied at t=2 sec.

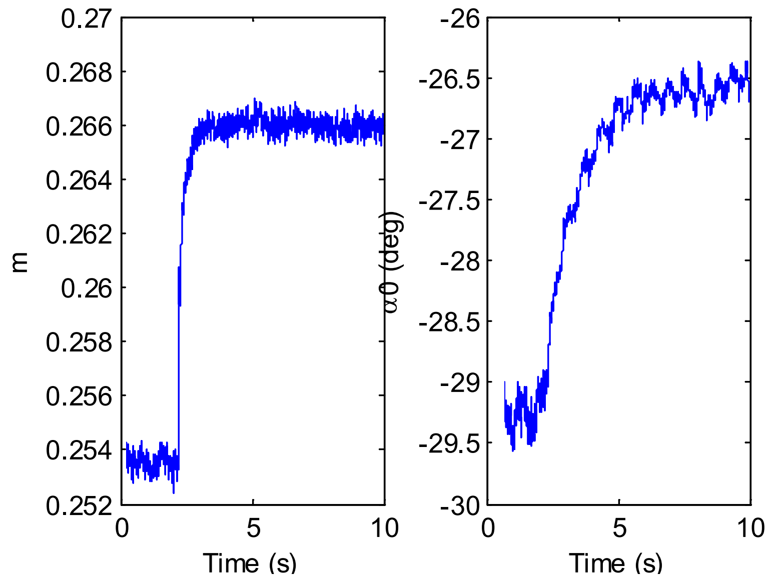

Figure 6.17: The variations of *m* (left), and (right) when a step change of 100 W in the output active power is applied at t=2 sec.

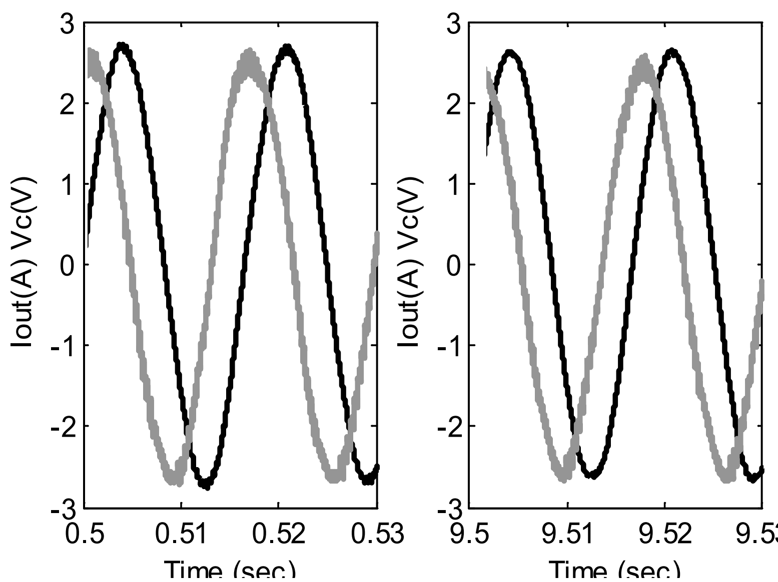

Figure 6.18: The line-line voltage of the ac caps (in black), and the output current (in gray) when P=200 W (left), and P=100 W (right).

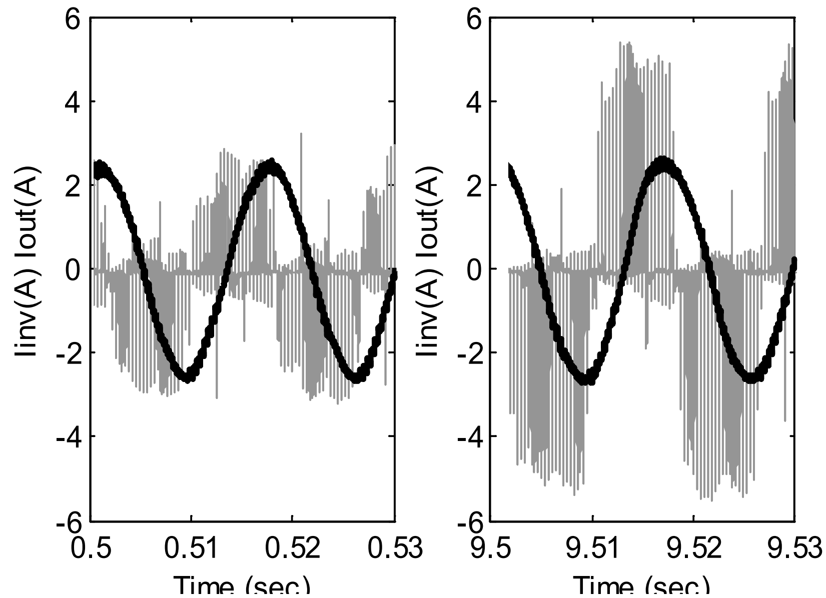

Figure 6.19: The output current (in black), and the inverter current (in gray) of phase “A” when P=200 W (left), and P=100 W (right).

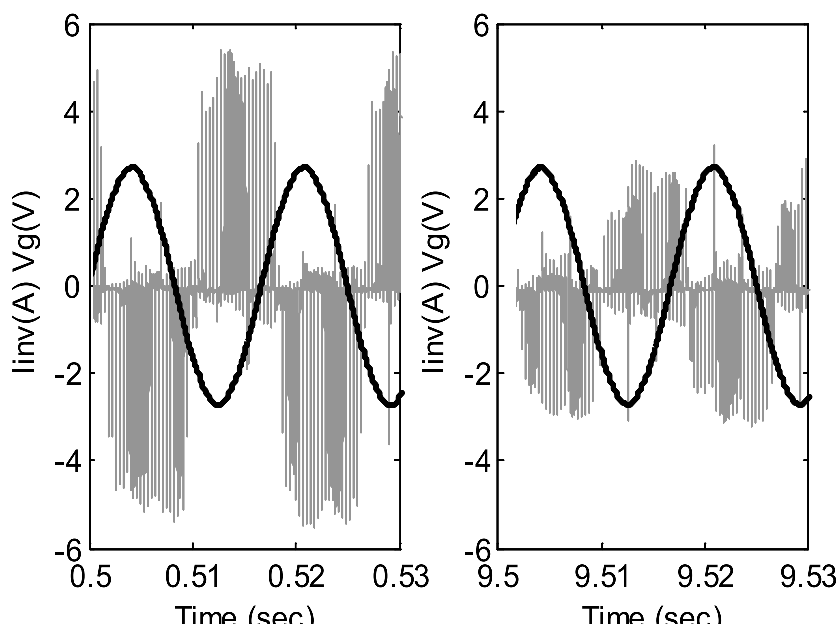

Figure 6.20: The line-line grid voltage (in black), and the inverter current (in gray) when P=200 W (left), and P=100 W (right).

6.2.2 Reactive Power Control

In this test, the initial values of the active and reactive power are W and VAR over seconds. At seconds, the reference signal of the reactive power is changed to VAR, while the reference signal of the active power stays the same. The experimental results are demonstrated in Figure 6.21 through 6.26.

In Figure 6.21, the injected active and reactive powers to the grid are shown, i.e., and . As can be seen in Figure 6.22, the average value of the inverter dc-link current remains constant, since the commanded active power does not change during the test. However, the amplitude of the injected current to the grid decreases, since the generated reactive power is commanded to change from 800 to 600 VAR (i.e., from 200 to 0 VAR). The variations of the two modulation indices, and , are also demonstrated in Figure 6.23. As expected, decreases by ~40 degrees in order to reduce the generated reactive power, while changes slightly in order to keep the active power at the same level, i.e., W.

Here, a question comes to mind: Could the change in the generated reactive power be due to a change at the inverter output voltage (i.e.,)? This query is addressed in the following. Figure 6.24 demonstrates the waveforms of the grid current, , and capacitor voltage (line-line), , before and after applying the step change in the injected reactive power. As can be observed from these waveforms, the output current amplitude for VAR (i.e., A) is less than its value for VAR (i.e., A), while the capacitor voltage does not change significantly. This change in the voltage is not enough to justify the difference between the generated reactive powers in these two conditions, i.e., VAR and VAR.

In Figure 6.25, the current waveforms before and after the ac capacitors are shown, i.e., , and . As one can see, the injected current to the grid has a lower magnitude for VAR, while the peak values of the inverter current, , are almost the same for both conditions. This means that the pulse widths of the inverter output current decreases. Also, Figure 6.26 shows the inverter current and the grid voltage (line-line). As can be seen, the inverter current undergoes almost degrees change in its phase difference with respect to the grid voltage (line-line). These are in good agreements with the changes in the modulation indices shown in Figure 6.23.

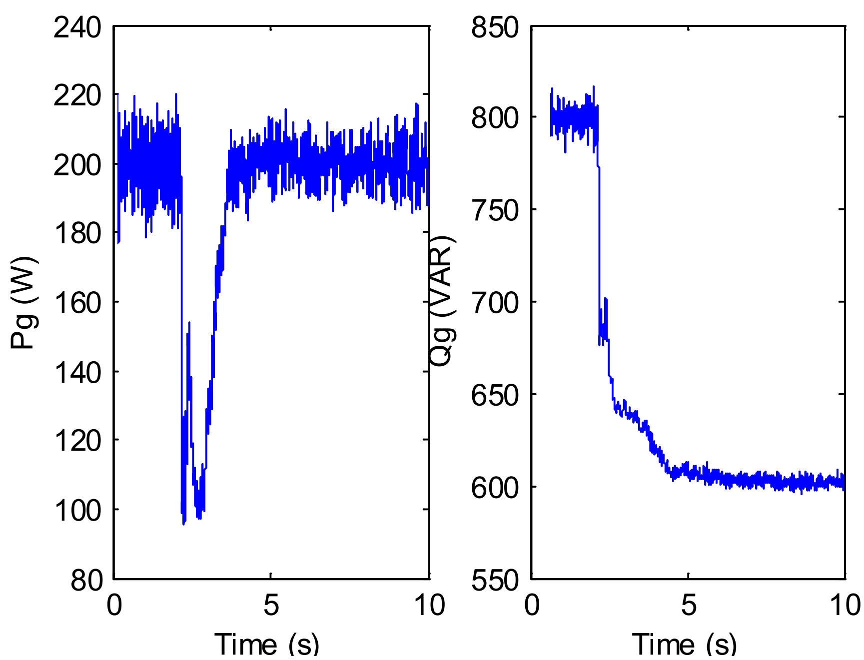

Figure 6.21: The output active power (left), and the output reactive power (right) when a step change of 200 var in the output reactive power is applied at t=2 sec.

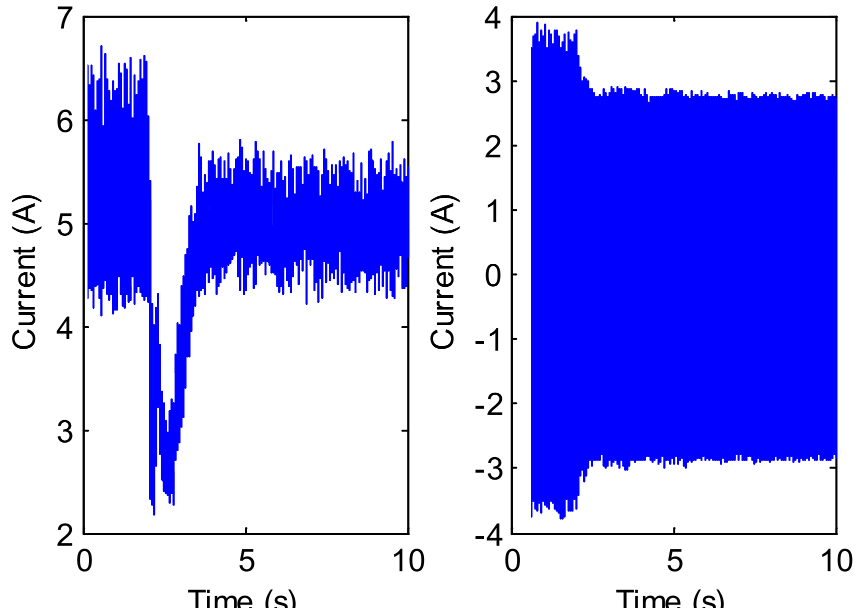

Figure 6.22: The input dc current (left), and the output ac current (right) when a step change of 200 VAR in the output reactive power is applied at t=2 sec., experimental results.

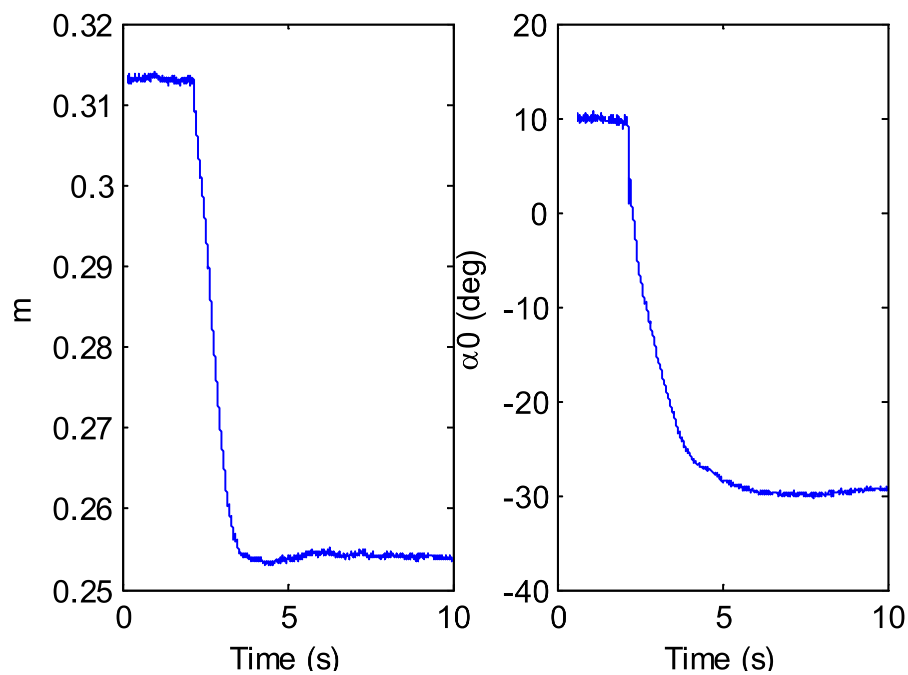

Figure 6.23: The variations of m (left), and (right) when a step change of 200 VAR in the output reactive power is applied at t=2 sec.

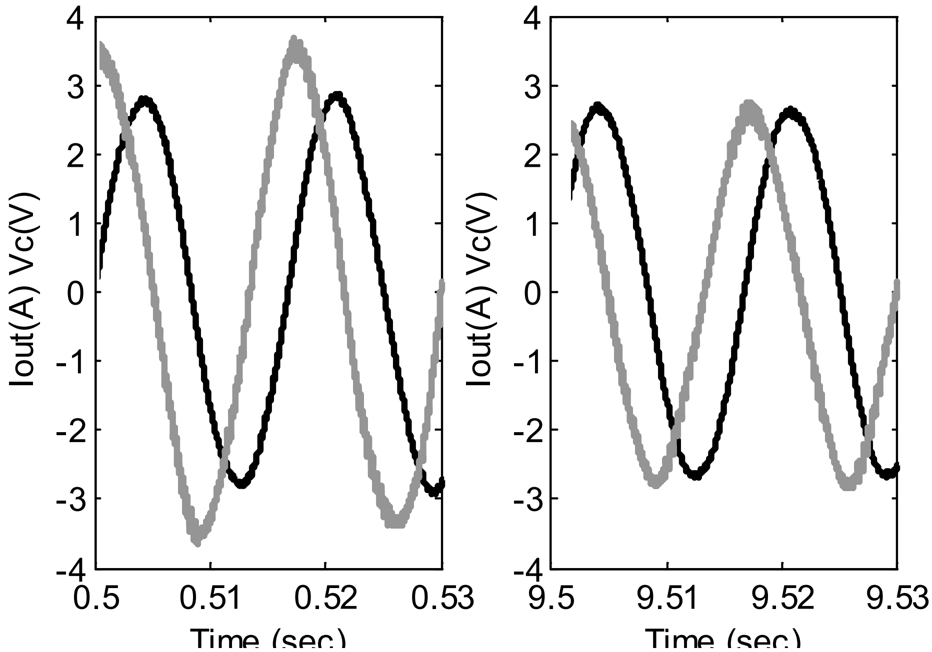

Figure 6.24: The line-line voltage of the ac caps (in black), and the output current (in gray) when Q=800 VAR (left), and Q=600 VAR (right).

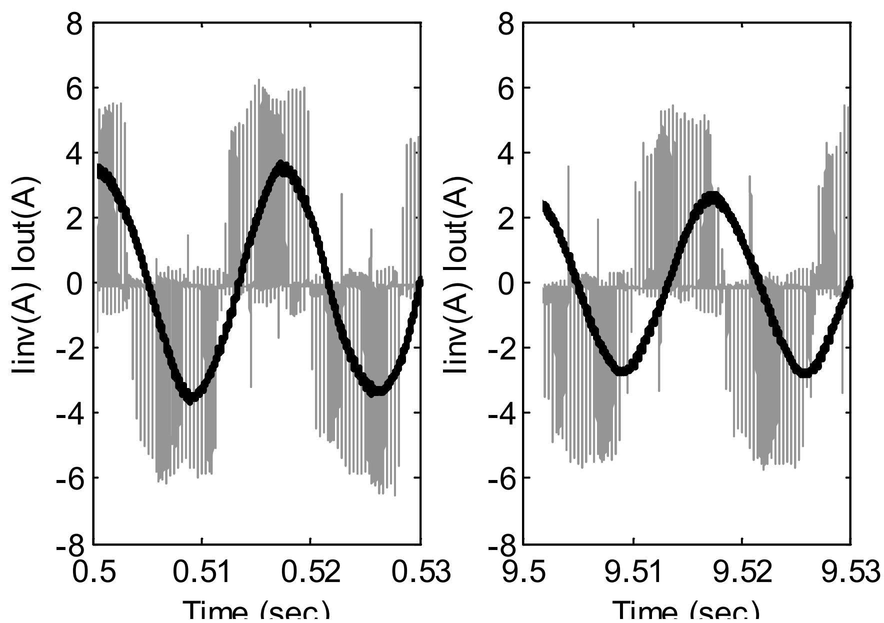

Figure 6.25: The output current (in black), and the inverter current (in gray) of phase “A” when Q=800 VAR (left), and Q=600 VAR (right).

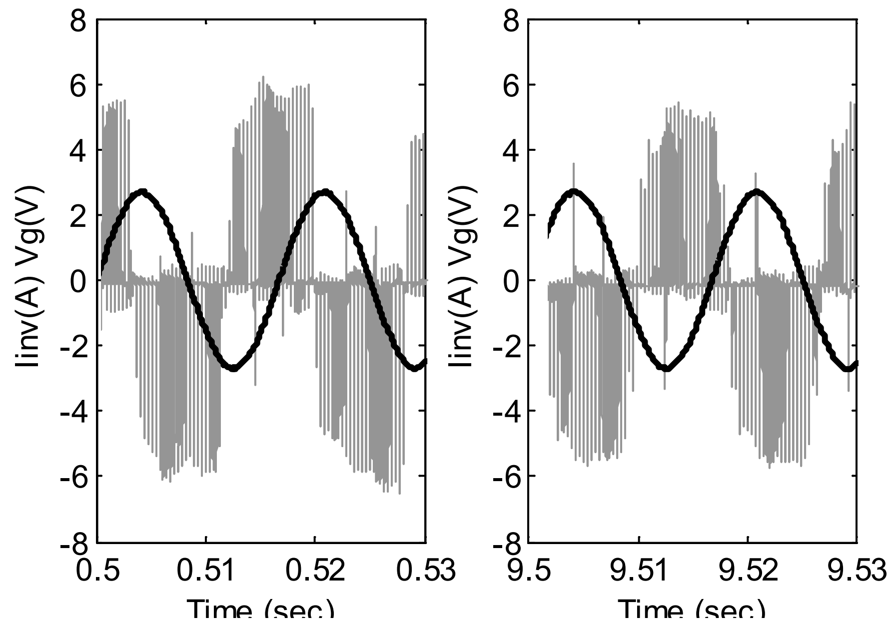

Figure 6.26: The line-line grid voltage (in black), and the inverter current (in gray) when Q=800 VAR (left), and Q=600 VAR (right)

6.3 Summary

In this chapter, the obtained results in the previous chapters were experimentally verified for both grid-connected and stand-alone cases. The capability of the CSBI in providing a regulated voltage for a stand-alone load was tested, and the results met the requirements. The performance of the proposed switching pattern in the grid-connected case was also examined, with controlling the injected active and reactive power values. Furthermore, the capability of the proposed PV inverter system in generating reactive power, and controlling the amount of the injected reactive power to the grid was fully shown.

CHAPTER 7

CONCLUSIONS AND FUTURE WORK

This chapter contains the conclusions and the possible future works for the dissertation.

7.1 Conclusions

In this dissertation, the problem of converting the variable DC output of an SE source such as a PV panel to a fixed AC voltage, either the utility grid or a stand-alone load, was introduced. A complete survey of the current technologies for the mentioned systems were performed, considering both single-phase and three-phase converters and pros and cons of each system were covered after an accurate categorization.

To overcome the defects, a micro-inverter PV module system has been proposed, in which each module can operate in its maximum power conditions and inject its own generated power to the grid, independently from the others. The benefits of such a configuration are higher efficiency (due to the single-stage power topology and also separate maximum power point tracking (MPPT) for each PV panel), as well as higher reliability (since every PV has its own inverter). The manufacturing and installation cost of the system is also decreased. The concept of plug-and-play single-stage boost inverters provides many advantages: (1) Simple control strategy unlike many other proposed control methods; (2) Capable of being applied to both stand-alone and grid-tie systems; (3) Easy implementation of MPPT by controlling two control parameters; (4) Better stability compared to the other control methods; and (5) Easy dealing with unbalanced conditions.

It was pointed out that among many conversion systems for SE sources, the single-stage boost-inverter seems to have the best efficiency and reliability, and longest life time. It is composed of a current-source inverter, associated with the proposed switching pattern that allows it to have an ac voltage at its output, larger than the input dc voltage. All the steps toward developing the switching pattern were covered with complete mathematics, for both stand-alone and grid-connected modes of operation. It was shown how the concept of the classic SVPWM is taken, and a novel switching is derived based on the same concept, but with big differences. The comparison between the classic SVPWM method for VSI, and the proposed SVPWM-based method for CSI was also performed, and various aspects of the switching pattern for the voltage and current values of the inverter system were explained.

One of the most important features of the proposed switching pattern lies in its simplicity and ease of implementation. Since it is based on the well established concept of Space Vector PWM (SVPWM), and due to the popularity of this switching pattern in industry, the proposed switching pattern can have advantages over the existing technologies.

The efficiency of a CSBI is high because it processes the energy in one single stage, while the others use multiple stages (at least two) to do the same job. Since there are losses of energy in any processing stage, the total loss will decrease if the system uses only one stage. On the other hand, CSBI eliminates the need for using electrolytic capacitors. Since electrolytic capacitors have the least life time, and reliability among all used devices in any inverter systems, the life time and reliability of the conversion system will significantly improve by eliminating these caps.

Having all the advantages of CSBI, and the concept of a micro-inverter PV module system, it makes sense to mix these two technologies, and make an efficient and reliable option for PV applications. However, according to the tasks of a conversion system for PV, the SCBI should be able to perform MPPT, boost, and dc-ac conversion at the same time. It makes it critical for a CSBI to have an advanced control strategy, capable of doing all of the tasks within the system by controlling only six switches. One of the outcomes of this dissertation is a new switching pattern for a CSBI, capable of doing the mentioned tasks.

The next step was to add more capabilities to the micro-inverter module by extracting the relationship between the control parameters, and the system components. In the stand-alone mode of operation, the relationship between the load voltage and the control parameters was derived, in order to have a voltage-regulated current-source inverter. However, in the grid-connected case, the capability of the CSBI in controlling the injected active and reactive power to the grid was shown. This was performed by deriving the equations of the dc link inductor current and the output injected current. The two dominant control parameters in the proposed switching pattern are the modulation index, and the switching angle. It was shown that the injected active and reactive power can be controlled by regulating these two parameters. The relationship between the control parameters with the output injected active and reactive power of the inverter in the grid-connected mode of operation was derived. It was shown how the desired dc current is constructed inside the dc inductor, and how the desired values of active and reactive power are injected into the grid through controlling and regulating the two major control parameters.

At the end, the experimental results for all of the previously derived equations were illustrated. In order to verify the claimed capabilities of the proposed system, a setup was built in the lab, and the real waveforms of different parts of the CSBI were illustrated in this section. Again, both grid-connected and stand-alone modes of operation were taken into account. Furthermore, the capability of the control system on regulating the amount of the active and reactive power was shown.

7.2 Future work

In this dissertation, a novel micro-inverter system was proposed for SE sources, particularly for PV applications. However, the specific conditions of a couple of potential sources such as fuel cells and batteries were not covered enough. It is a good idea to utilize the same system for the mentioned sources, applying the required changes to the components and control method. In fact, due to the differences between PV panels and fuel cells and batteries, specific factors should be taken into account for their associated converter system. For instance, the chemical process inside a fuel cell is completely different from the electricity generation process in a PV panel, that consequently leads to different MPPT methods for them.

The goal of the control design for this work was more concentrated on the simplicity, ease of implementation and applicability of the control system. These objectives lead to PI controllers for the output voltage and power regulation. However, utilizing other control methods such as sliding mode control, predictive control, adaptive and robust control may lead to optimal control performance with different objectives, faster response for instance. In the current work the application of a micro-inverter system for a building energy supply was considered, and the proposed PI controllers were able to satisfy the requirements and meet the expectations.

Although the proposed converter system was intended to be used as a low power micro-inverter system, the utilization of the same power circuit and control method may make sense to be used for large high power string PV panels too. Since the system has advantages over the current technologies, more investigations are needed to prove that whether or not the proposed converter system can be used for large string configurations of solar panels.

One important issue that needs to be considered in every residential power system is protection. Since it is intended to be used in the close proximity of human lives, the protection of such a system must be taken very seriously. Adding protection parts to the inverter system is an essential step toward making the system economic and utilizable for the industry. It needs to be considered in both the power circuit and the control system, to prevent any possible damage to both the converter system, and any human user.

BIBLIOGRAPHY

[1] R.W. Erickson, and A. P. Rogers, “A microinverter for building-integrated photovoltaics,” in Proc. *IEEE Applied Power Electronics Conference APEC’2009*, pp. 911–917.

[2] Y. Fang, and X. Ma, “A novel PV microinverter with coupled inductors and double-boost topology,” *IEEE Transactions on Power Electronics*, vol. 25, no. 12, pp. 3139–3147, Dec. 2010.

[3] F. Blaabjerg, R. Teodorescu, and M. Liserre, “Overview of control and grid synchronization for distributed power generation systems,” *IEEE Transactions on Industrial Electronics,* vol. 53, no. 5, pp. 1398–1409, Oct. 2006.

[4] Q. Li, and P. Wolfs, “A review of the single phase photovoltaic module integrated converter topologies with three different DC link configurations”, *IEEE Transactions on Power Electronics*, vol. 23, no. 3, pp. 1320–1333, May. 2008.

[5] S. Alepuz, S.B. Monge, J. Bordonau, J. Gago, D. Gonzalez, and J. Balcells, “Interfacing renewable energy sources to the utility grid using a three-level inverter,” *IEEE Transactions on Indsutrial Electronics*, vol. 53, no. 5, pp. 1504–1511, Oct. 2006.

[6] R. O. Caceres and I. Barbi, “A boost dc-ac converter: analysis, design, and experimentation,” *IEEE Trans. Power Electron*., vol. 14, no. 1, pp. 134–141, Jan. 1999.

[7] D. Schekulin, “Grid-Connected Photovoltaic System,” Germany patent DE197 32 218 Cl, Mar. 1999.

[8] N. Kasa, T. Iida, and H. Iwamoto, “Maximum power point tracking with capacitor identifier for photovoltaic power system,” in Proc. *Inst. Elect. Eng.,* vol. 147, no. 6, pp. 497–502, Nov. 2000.

[9] N. Kasa and T. Iida, “Flyback type inverter for small scale photovoltaic power system,” in Proc. *IEEE IECON*, 2002, vol. 2, pp. 1089–1094.

[10] W. Chien-Ming, “Anovel single-stage full-bridge buck-boost inverter,” *IEEE Trans. Power Electron.,* vol. 19, no. 1, pp. 150–159, Jan. 2004.

[11] Y. Xue and L. Chang, “Closed-loop SPWM control for grid-connected buck-boost inverters,” in Proc. *IEEE PESC,* 2004, vol. 5, pp. 3366–3371.

[12] W. Chien-Ming, “A novel single-stage series-resonant buck–boost inverter,” *IEEE Trans. Ind. Electron*., vol. 52, no. 4, pp. 1099–1108, Aug. 2005.

[13] S. Jain, and V. agarwal, “A single-stage grid connected inverter topology for solar pv systems with maximum power point tracking,” *IEEE Trans. Power Electron.,* vol. 22, no. 5, pp. 1928–1940, Sep. 2007.

[14] T. Chandrashekhar, and M. Veerachary, “Control of single-phase z-source inverter for a grid connected system,” in Proc. *IEEE ICPS*, 2009, vol. 5, pp. 1–6.

[15] D. Karschny, “Wechselrichter,” German Patent DE19 642 522 C1, Apr. 1998.

[16] S. Vasconcelos, P. Zacharias, and R. Mallwitz, “Highly efficient single-phase transformerless inverters for grid-connected photovoltaic systems,” *IEEE Trans. Power Electron.,* vol. 57, no. 9, pp. 3118–3128, Sep. 2010.

[17] H. Patel, and V. agarwal, “A single-stage single-phase transformer-less doubly grounded grid-connected PV interface,” *IEEE Trans. Energy Convers*., vol. 24, no. 1, pp. 93–101, Mar. 2009.

[18] T. J. Liang, W. B. Shyu, and J. F. Chen, “A novel dc/ac boost inverter,” in Proc. *Energy Conversion Engineering Conf. IECEC’02*, pp. 629–634, 2002.

[19] Y. Fang, and X. Ma, “A novel PV microinverter with coupled inductors and double-boost topology,” *IEEE Trans. Power Electron*., vol. 25, no. 12, pp. 3139–3147, Dec. 2010.

[20] F.Z. Peng, “Z-source inverter,” *IEEE Transactions on Industry Applications*, vol. 39, no. 2, pp. 504–510, Mar./Apr. 2003.

[21] B. Mirafzal, M. Saghaleini, A.K. Kaviani, “An SVPWM-based switching pattern for stand-alone and grid-connected three-phase single-stage boost-inverter,” *IEEE Transactions on Power Electronics*, vol. 26, no. 4, pp.1102-1111, Apr. 2011.

[22] G. Petrone, G. Spagnuolo, R. Teodorescu, M. Veerachary, and M. Vitelli, “Reliability issues in photovoltaic power processing systems,” *IEEE Transactions on Industrial Electronics*, vol. 55, no. 7, pp. 2569-2580, July 2008.

[23] M. Calais, J. Myrzik, T. Spooner, and V. G. Agelidis, “Inverters for single-phase grid connected photovoltaic systems-an overview,” in Proc. *IEEE 33rd Annual Power Electronics Specialists Conference*, Jun. 2002, vol. 4, no. 23–27, pp. 1995–2000.

[24] M. Calais, V.G. Agelidis, “Multilevel converters for single-phase grid connected photovoltaic systems-an overview,” *IEEE International Symposium on Industrial Electronics (ISIE ‘98)*, vol. 1, pp. 224-229, Jul. 1998.

[25] S. Alepuz, J. Bordonau, and J. Peracaula, “Dynamic analysis of three-level voltage-source inverters applied to power regulation,” *Proceedings of IEEE Power Electronics Specialist Conference*, pp. 721–726, 1999.

[26] S. Alepuz, J. Bordonau, and J. Peracaula, “A novel control approach of three-level VSIs using a LQR-based gain-scheduling technique,” *Proceedings of IEEE Power Electronics specialist Conference*, pp. 743–748, 2000.

[27] J. Rodríguez, J.S. Lai, and F.Z. Peng, “Multilevel inverters: A survey of topologies, controls, and applications,” *IEEE Transactions on Industrial Electronics*, vol. 49, no. 4, pp. 724–738, Aug. 2002.

[28] M. Mohr, W.T. Franke, B. Witting, and F.W. Fuchs, “Converter systems for fuel cells in the medium power range—a comparative study,” *IEEE Transactions on Industrial Electronics*, vol. 57, no. 6, pp. 2024–2032, Jun. 2010.

[29] Y. Huang, M. Shen, F.Z. Peng, and J. Wang, “Z-source inverter for residential photovoltaic systems,” *IEEE Transactions on Power Electronics*, vol. 21, no. 6, pp. 1776–1782, Nov. 2006.

[30] R. Badin, Y. Huang, F.Z. Peng, and H. Kim, “Grid interconnected Z-source PV system,” *Proceedings of IEEE 38th Annual Power Electronics Specialist Conference*, vol. 1, pp. 2328–2333, Jun. 2007.

[31] C.J. Gajanayake, D.M. Vilathgamuwa, P.C. Loh, R. Teodorescu, and F. Blaabjerg, “Z-source-inverter-based flexible distributed generation system solution for grid power quality improvement,” *IEEE Transactions on Energy Conversion*, vol. 24, no. 3, pp. 695–704, Sep. 2009.

[32] B. Sahan, A. Vergara, N. Henze, A. Engler, and P. Zacharias, “A single-stage PV module integrated converter based on a low-power current-source inverter,” *IEEE Transaction on Industrial Electronics*, vol. 55, no. 7, pp. 2602–2609, Jul. 2008.

[33] Y. Chen, and K. Smedley, “Three-phase boost-type grid-connected inverter,” *IEEE Transactions on Power Electronics*, vol. 23, no. 5, pp. 2301–2309, Sep. 2008.

[34] M. Kazerani, Z.C. Zhang, and B.T. Ooi, “Linearly controllable boost voltages from tri-level PWM current-source inverter,” *IEEE Transactions on Industrial Electronics*, vol. 42, no. 1, pp. 72–77, Feb. 1995.

[35] W. Libo, Z. Zhengming, and L. Jianzheng, “A single-stage three-phase grid-connected photovoltaic system with modified MPPT method and reactive power compensation,” *IEEE Transactions on Energy Conversion*, vol. 22, no. 4, pp. 881–886, Dec. 2007.

[36] Z. Qin, D. Sha, X. Liao, “A three-phase boost-type grid-connected inverter based on synchronous reference frame control,” *27th Annual IEEE Applied Power Electronics Conference & Exposition*, pp. 384-388, 2012.

[37] M. Saghaleini, B. Mirafzal, “Reactive power control in three-phase grid-connected current source boost inverter,” *27th Annual IEEE Applied Power Electronics Conference & Exposition*, pp. 904-910, 2012.

[38] R.W. Erickson, “DC-DC power converters,” *Article in Wiley Encyclopedia of Electrical and Electronics Engineering*.

[39] N. Mohan, T.M. Undeland, W.P. Robbins, *Power Electronics: Converters, Applications, and Design*, John Wiley and sons INC, Third edition, Hoboken NJ, USA, 2003

[40] J. Holts, “Pulsewidth modulation-a survey,” *IEEE Transactions on Industrial Electronics*, vol. 39, no. 5, pp. 410-420, Dec. 1992.

[41] D. G. Holmes, and T. A. Lipo, *Pulse width modulation for power converters: principles and practice*, IEEE Press, Wiley-IEEE, 2003.

[42] P. C. Krause, O. Wasynczuk, S.D. Sudhoff, *Analysis of Electric Machinery and Drive Systems*, IEEE Press, Wiley-Interscience, Second edition, 2002.

[43] V.A. Calisikan, G.C. Verghese, A.M. Stankovic, “Multifrequency averaging of dc/dc converter,” *IEEE Transactions on Power electronics*, vol. 14, no. 1, pp. 124-133, Jan. 1999.

[44] A. Davoudi, J. Jatskevich, “Parasitic realiziation in state-space average-value modeling of PWM dc-dc converters using an equal area method,” *IEEE Transactions on Circuit and Systems-1*, vol. 54, no. 9, pp. 1960-1967, Sep. 2007.

[45] V. Vorperian, R. Tymerski, F.C.Y. Lee, “Equivalent circuit models for resonant and PWM switches,” *IEEE Transactions on Power Electronics*, vol. 4, no. 2, pp. 205-214, Apr. 1989.

[46] S.R. Sanders, J.M. Noworolski, X.Z. Liu, G.C. Verghese, “Generalized averaging method for power conversion circuits,” *IEEE Transactions on Power Electronics*, vol. 6, no. 2, pp. 251-259, Apr. 1991.

[47] Z. Mihajlovic, B. Lehman, C.S. Sun, “Output ripple analysis of switching dc-dc converters,” IEEE Transaction on Circuits and Systems-1, vol. 51, no. 8, pp. 1596-1611, Aug. 2004.

[48] D. Maksimovich, S. Cuk, “A unified analysis of PWM converters in discontinuous modes,” *IEEE Transactions on Power Electronics*, vol. 6, no. 2, pp. 479-490, Jul. 1991.

[49] K.D.T, Ngo, “Low frequency characterization of PWM converters,” *IEEE Transactions on Power Electronics*, vol. PE-1, no. 4, pp. 223-230, Oct. 1986.

[50] S. Hiti, D. Boroyevich, C. Cuadros, “Small-signal modeling and control of three-phase PWM converters,” *IEEE Industry Applications Society Annual Meeting*, pp. 1143-1150, vol. 2, 1994.

[51] S. Hiti, D. Boroyevich, “Control of front-end three-phase boost rectifier,” *9th Annual IEEE Applied Power Electronics Conference & Exposition*, pp. 927-933, 1994.

[52] S. Chiniforoosh, H. Atighechi, A. Davoudi, J. Jatskevich, A. Yazdani, S. Filizadeh, M. Saeedifard, J.A. Martinez, V. Sood, K. Strunz, J. Mahseredjian, D. Dinavahi, “Dynamic average modeling of front-end diode rectifier loads considering discontinuous conduction mode and unbalanced operation,” *IEEE Transactions on Power Delivery*, vol. 27, no. 1, pp. 421-429, Jan. 2012.

[53] C.T. Rim, D.Y. Hu, G.Y. Cho, “Transformer as equivalent circuits for switches: general proofs and d-q transformation-based analyses,” *IEEE Transactions on Industry Applications*, vol. 26, no. 4, pp. 777-785, July/Aug. 1990.

[54] J. Liu, J. Hu, L. Xu, “A modified space vector PWM for Z-source inverter-modeling and design,” *Proceedings of 8th International Conference on Electrical Machines and Systems*, vol. 2, pp. 1242-1247, 2005.

[55] J. Hu, Z.Q. Zhu, “Investigation on switching patterns of direct power control strategies for grid-connected dc-ac converters based on power variation rates,” *IEEE Transactions on Power Electronics*, vol. 26, no. 12, pp. 3582-3598, Dec. 2011.

[56] N. Pogaku, M. Prodanovic, T.C. Green, “Modeling, analysis and testing of autonomous operation of an inverter-based microgrid”, *IEEE Transactions on Power electronics*, vol. 22, no. 2, pp. 613-625, Mar. 2007.

[57] www.bp.com

[58] www.bp.com/liveassets/bp_internet/solar/bp_solar_usa/STAGING/local_assets/downloads_pdfs/ BP_175B_datasheet_10_06.pdf

[59] J. Vassallo, J.C Clare, P.W. Wheeler, “A power-equalized harmonic-elimination scheme for utility-connected cascaded H-bridge multilevel converters,” *29th*

Annual IEEE Conference on Industrial Electronics Society, vol. 2, pp. 1185-1190, 2003.

[60] K. Ogata, *Modern Control Engineering*, Prentice Hall, Fourth edition, Upper Saddle River NJ, USA, 2002.

[61] K. Acharya, S.K. Mazumder, I. Basu, “Reaching criterion of a three-phase voltage-source inverter operating with passive and nonlinear loads and its impact on global stability,” *IEEE Transactions on Industrial Electronics*, vol. 55, no. 4, pp.1795-1812, Apr. 2008.

[62] F.S. Garcia, J.A. Pomilio, G.S. Deaecto, J.C. Geromel, “Analysis and control of dc-dc converters based on Lyapunov stability theory,” *IEEE Energy Conversion Congress and Exposition (ECCE 2009)*, pp. 2920-2927, 2009.

[63] F. Umbria, J. Aracil, F. Gordillo, “Singular perturbation stability analysis of three phase two-level power converters,” *18th Mediterranean Conference on Control & Automation*, pp. 123-128, 2010.

[64] J. Sun, Impedance-based stability criterion for grid-connected inverters,” *IEEE Transactions on Power Electronics*, vol. 26, no. 11, pp. 3075-3078, Nov. 2011.

[65] C. Gezgin, W.C. Bowman, V.J. Thottuvelil, “A stability assessment tool for dc-dc converters,” *17th Annual IEEE Applied Power Electronics Conference and Exposition (APEC 2002)*, vol. 1, pp. 367-373, 2002.

[66] C. Gezgin, “A transient prediction and stability analysis tool for dc-dc converters,” *18th Annual IEEE Applied Power Electronics Conference and Exposition (APEC 2003)*, vol. 2, pp. 1014-1020, 2003.

[67] J. Segundo-Ramirez, E. Barcenas, A. Medina, V. Cardenas, “Steady-state and dynamic state-space model for fast and efficient solution and stability assessment of ASD,” *IEEE Transactions on Industrial Electronics*, vol. 58, no. 7, pp. 2836-2847, July 2011.

[68] W. Yaunbin, “Research on stability of PWM controlled dc-dc converters in CCM,” *Second International Conference on Computer Modeling and Simulation*, vol. 3, pp. 223-225, 2010.

[69] E. Figueres, G. Garcera, J. Sandia, F. Gonzalez-Espin, J.C. Rubio, “Sensitivity study of the dynamics of three-phase photovoltaic inverters with and LCL grid filter,” *IEEE Transactions on Inductrial Electronics*, vol. 56, no. 3, pp. 706-717, Mar. 2009.

[70] http://ixdev.ixys.com/DataSheet/l185.pdf

[71] Z. Yu, A. Mohammed, and I. Panahi, “A review of three PWM techniques,” *Proceedings of American Control Conference*, pp. 257-261, Jun. 1997.

[72] A. Hava, R. Kerkman, and T.A. Lipo, “Carrier-based PWM-VSI overmodulation strategies: analysis, comparison, and design,” *IEEE Transactions on Power Electronics*, vol. 13, no. 4, pp. 674-689, Jul. 1998.

[73] D. G. Holmes and T. A. Lipo, *Pulse Width Modulation for Power Converters*, Principles and Practice. Hoboken, NJ: IEEE Press, 2003.

[74] J. R.Wells, B. M. Nee, P. L. Chapman, and P. T. Krein, “Selective harmonic control: a general problem formulation and selected solutions,” *IEEE Transactions on Power Electronics*, vol. 20, no. 6, pp. 1337–1345, Nov. 2005.

[75] Mohammed H. Rashid, *Power Electronics*, Prentice-Hall of India Private Limited, Second Edition, 1994(Book).

[76] Bimal K. Bose, *Modern Power Electronics and AC Drives*, Pearson education, Second Edition, 2003 (Book).

[77] H.W. van der Broek, H.C. Skudelny, G. Stanke, “Analysis and realization of a pulsewidth modulator based on voltage space vectors”, *IEEE Transactions on Industry Applications*, vol. 24, no. 1, pp. 142-150, Jan./Feb. 1988.

[78] F.Z. Peng, J.S. Lai, “Multilevel converters-a new breed of power converters,” *IEEE Transactions on Industry Applications*, vol. 32, no. 3, pp. 509-517, May/Jun. 1966.

[79] A. Nabae, I. Takahashi, H. Akagi, “A new neutral-point-clamped PWM inverter,” *IEEE Transactions on Industry Applications*, vol. IA-17, no. 5, pp. 518-523, Sep./Oct. 1981.

[80] P.M. Bhagwat, V.R. Stefanovic, “Generalized structure of a multilevel PWM inverter,” *IEEE Transactions on Inductry Applications*, vol. IA-17, no. 6, pp. 1057-1069, Nov./Dec. 1983.

[81] T.A. Meynard, H. Foch, “Multi-level conversion: high voltage choppers and voltage-source inverters,” *23rd Annual IEEE Power Electronics Specialists Conference*, vol. 1, pp. 397-403, 1992.

[82] J. Rodriguez, J.S. Lai, F.Z. Peng, “Multilevel inverters: survey of topologies, control, and applications,” *IEEE Transactions on Industry Applications*, vol. 49, no. 4, pp. 724-738, Aug. 2002.

[83] L.M. Tolbert, F.Z. Peng, T. Habetler, “Multilevel converters for large electric drives,” *IEEE Transactions on Industry Applications*, vol. 35, pp. 36-44, Jan./Feb. 1999.

APPENDIX

SINGLE-PHASE INVERTER SYSTEMS TOPOLOGIES

In this appendix, all of the mentioned topologies for the single-phase inverter systems in chapter two are shown and covered with more details. There are various configurations for the power conditioning systems that connect PV arrays to the grid. They are supposed to do these three tasks: 1-converting the output dc voltage of PV arrays to the grid ac voltage, 2- performing the MPPT in order to extract as much power as possible from the source, and 3- controlling the injected ac current into the grid, i.e., the injected active and reactive power into the grid. In this section, the concentration is on the single-phase inverters which have the capability of boosting the low amplitude voltage of a PV panel (array) to a voltage as high as the grid voltage, while they are doing the dc to ac conversion as well as controlling the injected current to the grid, all in a single power stage.

In [6], a configuration composed of two boost converters has been proposed (see Figure A1(a)). As illustrated in Table A.1, this topology uses 4 switches, all of them work at high frequency (HF) at any time. This is the main drawback for this configuration, as the rest of the topologies try to have less switches, particularly for HF usage. It should be noted that more HF switches leads to more EMI which is an important concern in every power electronic system. Another drawback is the utilization of two electrolytic capacitors, along with two large inductors in the topology. The values for these parts have been reported as 40 uF and 800 uH, respectively.

In [7], a single-stage topology based on the buck-boost configuration has been proposed (see Figure A.1(b)). It utilizes four switches, two of which work at HF (one at any half cycle), and the other two work at low-frequency (either 50 or 60 Hz). The main drawback of this topology lies in its asymmetrical operation during the positive and negative half-cycle of the grid voltage. This may lead to a complex control system for this circuit [8]. The advantages of this topology are avoiding of electrolytic capacitor, and also low switching losses. Since it is a German patent, there is no information available about its implementation.

Kasa [8] has introduced another topology based on the half-bridge buck-boost configuration (see Figure A.1(c)). The number of switches used in this topology is the same as the previous one; however, this topology does not have the drawback of asymmetrical operation. The main disadvantage of this configuration is that it uses a pair of PV sources only one of which is utilized in a given half cycle of the grid voltage [13]. In addition to this, high-value dc capacitors are needed to be placed in parallel with the two PV panels.

In [9], a topology is introduced which contains a HF transformer based on the fly-back converter topology (see Figure A.1(d)). The advantage of utilizing such a transformer is the isolation that can be achieved between the input and output of the converter, while it has the disadvantage of adding to the losses, and consequently lowering the efficiency of the system. However, this configuration uses only three switches, which lowers the cost of this circuit. Another drawback is using a very large electrolytic capacitor at the input stage of the converter, e.g., 4700 uF for the 300 W experimental setup of this work [9].

A single-stage full-bridge series-resonant buck-boost inverter (FB-SRBBI) has been proposed in [10], which again utilizes 4 switches (see Figure A.1(e)), 2 for HF and 2 for low-frequency (LF). The proposed inverter only includes a full-bridge topology and an LC resonant tank without auxiliary switches, and provides the main switch for turn-on at ZCS by the resonant tank. This configuration has a large number of devices conducting at a given instant resulting in higher conduction losses. On the other hand, the circuit does not need an electrolytic capacitor at the input stage, and it is a symmetrical topology, which is a benefit for it [13]. On top of that, the total number of components and their size (e.g., input inductors) are less comparing with other topologies.

Another asymmetrical operation converter has been proposed by [11] which is again based on the buck-boost principle (see Figure A.1(f)). This topology utilizes 4 switches, two of which for HF usage, and the rest for LF. The main feature of this topology is utilizing mutually coupled coils that will cause a limitation on its application for high-power cases. Also, it does not need high value electrolytic capacitors at the input stage.

Chien-Ming [12] has introduced a topology based on the half-bridge series-resonant buck-boost inverter which utilizes 5 switches, 3 of which for HF and 2 for LF (see Figure A.1(g)). The proposed inverter circuit topology provides the main switch for turn-on at zero-current-switching (ZCS) by an auxiliary resonant cell built before the output choke. The main drawback of this topology is the high number of utilized switches, 3 of which are for high-frequency use.

Other than the first topology, all of the mentioned topologies are applicable for low or medium power cases (i.e., power<3 kW). In [13], a high-power topology has been proposed that utilizes 4 switches, 2 of which for HF (see Figure A.1(h)). A drawback of this converter is that it requires large electrolytic capacitors, as they have used a 2000 uF capacitor in their 500 W experimental setup.

In [14], the application of single-phase z-source converter has been proposed for grid-connected PV systems (see Figure A.1(i)). This topology uses 2 switches for HF (one at each half cycle) and two for LF. It can have symmetrical operation with simple control scheme. The drawback of this topology is that it needs two large electrolytic capacitors (e.g., 1000 uF for this reference) as well as two large inductors (e.g., 1 mH for the same reference). This increases the size and cost of the system. On top of that, this circuit imposes high ripple on the input current drawn from the source.

Karschny [15] has proposed another configuration based on the buck-boost inverter which utilizes 5 switches (see Figure A.1(j)). This topology suffers from low efficiency (because of large number of switches) and also high cost and size [16].

In [17], a single-phase, single-stage, doubly grounded, transformer-less PV interface, based on the buck–boost principle, is presented (see Figure A.1(k)). The configuration is compact and uses fewer components. Only one (undivided) PV source and one buck–boost inductor are used and shared between the two half cycles, which prevents asymmetrical operation and parameter mismatch problems. However, it utilized an electrolytic capacitor at the input stage.

A current-source single-stage inverter has been proposed by [18] based on the DC/DC boost converter topology (see Figure A.1(l)). In this topology, only 2 switches are utilized for HF, and 2 more for LF.

A coupled-inductor double-boost inverter (CIDBI) has been proposed in [19] (see Figure A.1(m)). The main attribute of the CIDBI topology is the fact that it generates an ac output voltage larger than the dc input one, depending on the instantaneous duty cycle and turns ratio of the coupled inductor as well. This topology uses 4 switches, all for HF.

Table A.1: Specifications of the mentioned topologies

topology	SW (HF ,LF)								
a	4,0	2x0.8	40	-	-	100	127	30	500
b	2,2	-	-	-	-	-	-	-	-
c	2,2	2x0.026	2x1000	-	12	60	100	9.6	500
d	3	2x0.118	4700	-	12	30	100	9.6	327
e	2,2	2x0.011	5.58	1	4.7	75	110	40	500
f	4	1	2.2	1	10	160	200	20	500
g	4	0.011	-	-	5.5	120	110	40	500
h	2,2	0.220	2000	3.25	4.4	85	110	10	500
i	2,2	2x1	2x1360	1	-	60	68	15	200
j	5	-	-	-	-	-	-	-	-
k	4					92	100		200
l	2,2	0.7	-	-	2x220	60	110	-	300
m	4,0	-	-			35	220	50	200

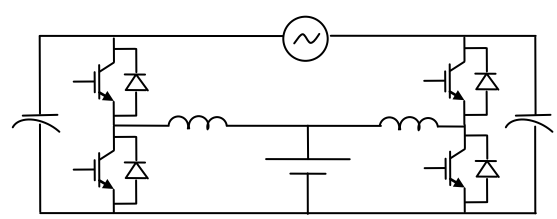

(a)

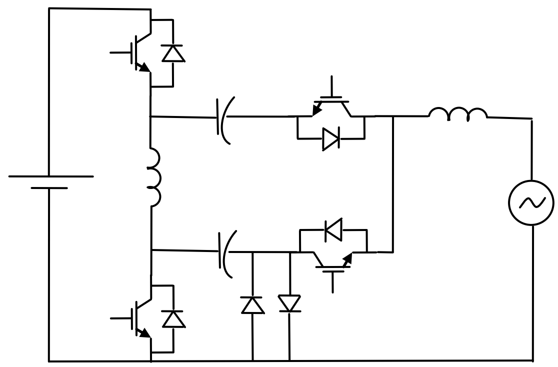

(b)

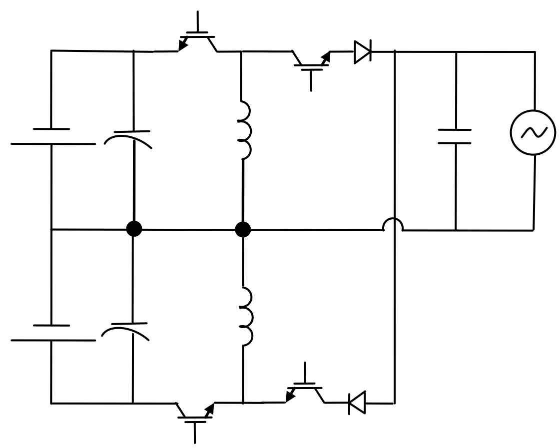

(c)

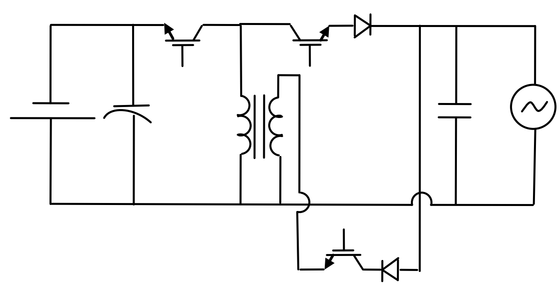

(d)

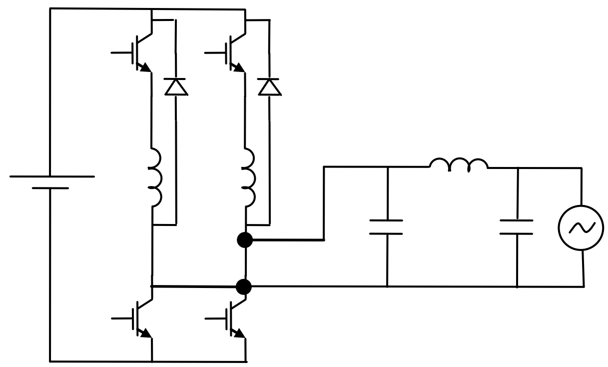

(e)

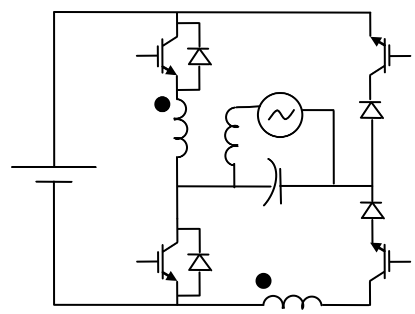

(f)

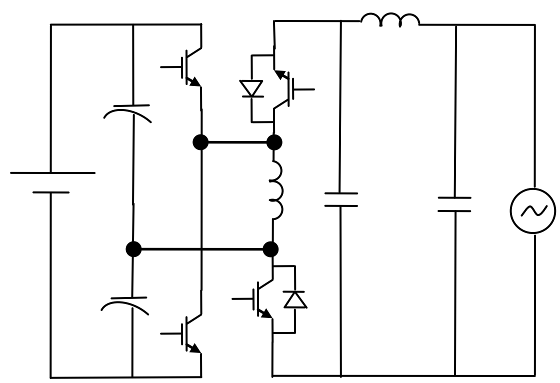

(g)

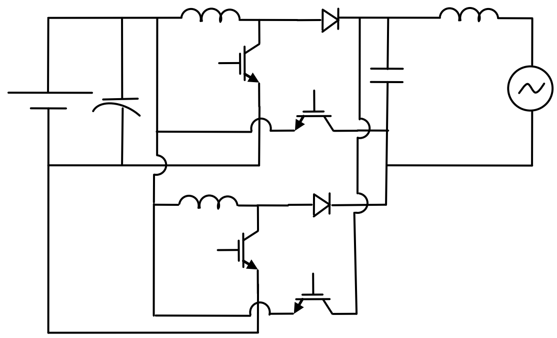

(h)

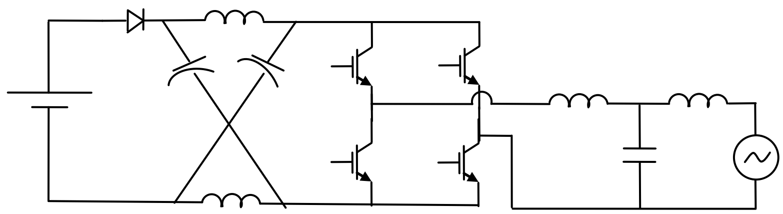

(i)

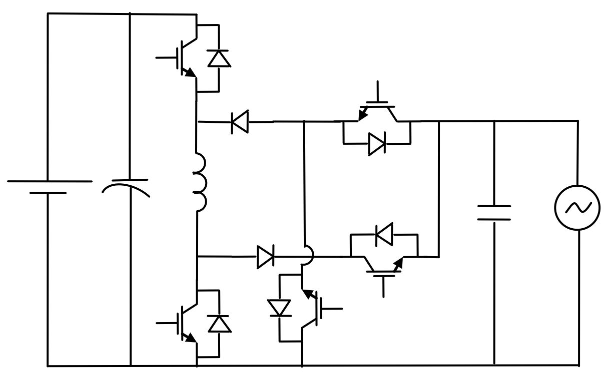

(j)

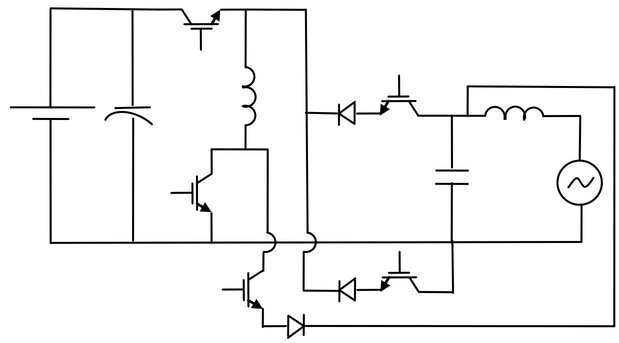

(k)

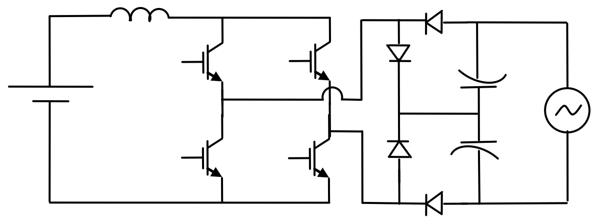

(l)

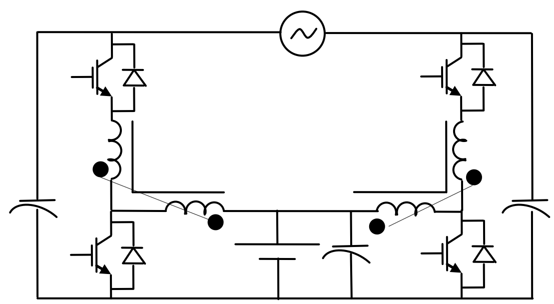

(m)

Figure A.1: The single-phase inverter system topologies

VITA

MAHDI SAGHALEINI

March 21, 1982	Born, Boroujerd, Iran
2000-2005	B.Sc., Electrical Engineering Sharif University of Technology Tehran, Iran
2005-2008	M.Sc., Electrical Engineering University of Tehran Tehran, Iran
2009-2012	PH.D. Candidate, Electrical Engineering Florida International University Miami, Florida

PUBLICATIONS AND PRESENTATIONS

[1] **M. Saghaleini,** B. Mirafzal, and K. Yen, "Active and reactive power control in a three-phase grid-connected PV-based boost inverter," to be submitted to *IEEE Trans. Power Electron.*

[2] B. Mirafzal, A.K. Kaviani, and **M. Saghaleini**, "A single-phase grid-connected boost inverter for photovoltaic applications," submitted to *IEEE Trans. Industry App*.

[3] B. Mirafzal, **M. Saghaleini**, and A.K. Kaviani, "An SVPWM-based switching pattern for stand-alone and grid-connected three-phase single-stage boost-inverter," IEEE Trans. Power Electron., Special Issue on Power Electronics for Microgrids, vol. 26, no. 4, pp. 1102-1111, April 2011.

[4] **M. Saghaleini**, and B. Mirafzal, "A control scheme of reactive power in a PV-based single-stage three-phase boost-inverter," in Proc. *The 27th IEEE Applied Power Electronics Conference and Exposition*, APEC-2012, USA, February 2012.

[5] **M. Saghaleini**, and B. Mirafzal, "Power control in three-phase grid-connected boost inverter," in Proc. *The 3rd IEEE Energy Conversion Congress and Exposition*, ECCE-2011, USA, September 2011.

[6] H. Afshari, **M. Saghaleini**, B. Hadley, S. Henry, B. Mirafzal, and C. Edrington, "A time-coordination approach for compensating pulse-load using flywheel," in Proc.

The 3rd IEEE Energy Conversion Congress and Exposition, ECCE-2011, USA, September 2011.

[7] **M. Saghaleini**, A.K. Kaviani, B. Hadley, and B. Mirafzal, "New trends in photovoltaic energy systems," in Proc. *The 10th International Conference on Environment and Electrical Engineering*, EEEIC-2011, Italy, May 2011.

[8] **M. Saghaleini**, and A. Mazloomzadeh, "Agent based control scheme for a smart power system including renewable energy sources," in Proc. *The 10th International Conference on Environment and Electrical Engineering*, EEEIC-2011, Italy, May 2011.

[9] **M. Saghaleini**, B. Mirafzal, and C. Edrington, "Regenerative energy management for pulse-loads in dual DC-AC micro-grids," in Proc. *36th* ***Annual Conference of the IEEE Industrial Electronics Society*****,** IECON-2010, USA, pp. 674-679, November 2010.

[10] **M. Saghaleini**, A. Hekmati, and S. Farhangi, "An advanced distributed power supply for a power electronic transformer," in Proc. *33rd* ***Annual Conference of the IEEE Industrial Electronics Society*****,** IECON-2007, Taiwan, pp. 2038-2043, November 2007.

[11] **M. Saghaleini**, and S. Farhangi, "Distributed power supply with power factor correction: a solution to feed all modules in power electronic transformers," in Proc. *7th IEEE International Conference on Power Electronics*, ICPE-2007, South Korea, pp. 1225-1229, October 2007.

[12] **M. Saghaleini**, A. Hekmati, M. Rezaei and S. Afsharnia, "Application of advanced SVC incase of reactive power and unbalancy compensation of a locomotive," in Proc. *IEEE International Conference on Industrial Technologies*, ICIT-2006, India, pp. 1897-1902, December 2006.

AWARDS AND ACHIEVEMENTS

- Recipient of Doctoral Evidence Acquisition Fellowship Award, 2011
  University Graduate School, Florida Int. University

- Elite Graduate Member of National Elite Organization of Iran, since 2008

- Honored as the best BSc. final project amongst 120 Undergraduate Students, 2005
  Department of Electrical Engineering, Sharif University of Technology